



**Politecnico
di Torino**

Politecnico di Torino

Corso di Laurea Magistrale in Ingegneria Edile

A.a. 2020/2021

Sessione di Laurea Novembre/Dicembre 2021

Seismic vulnerability of building aggregates

Study and analysis of interactions with adjacent buildings

Relatore:

Prof. Gian Paolo Cimellaro

Co-relatore:

Prof. Sebastiano Marasco

Candidato:

Alessandro Di Iorio

Abstract

This thesis deals with the study and analysis of adjacent buildings interaction and their seismic vulnerability assessment. In particular, it deals with the analysis of the pounding effect and the torsional effect to which the reference building may be subject due to the presence of adjacent buildings in case of an earthquake.

Based on the existing methodologies, the appropriate methods and models may be addressed in assessing the seismic vulnerability of a building aggregates by reducing the computational effort, while providing a satisfying accuracy. To consider the torsional effect of the structure the N2 extended method proposed by Fajfar, Marušić et al. (2005) is used, while the pounding effects are taken into account through a load distribution along the height of the structure. These forces are calculated with elastic linear model proposed by Maison and Kasai (1990) (1992).

A four story masonry building located in L'Aquila, Italy, has been adopted as case study to evaluate the accuracy of the proposed methods.

The results show how the application of the proposed method involves a reduction of the vulnerability index of the structure of approximately 40% for the case study.

Contents

| | |
|--|-------------|
| Abstract | iii |
| Contents..... | iv |
| List of figures | vi |
| List of tables | viii |
| 1. Introduction | 1 |
| 1.1. Building aggregates | 2 |
| 1.2. Behaviour of building aggregates | 4 |
| 1.3. Structural Units (US) | 8 |
| 2. Legislation and seismic analysis | 10 |
| 2.1. Seismic action | 10 |
| 2.2. Current Standards for building aggregates | 15 |
| 2.3. Methods of analysis | 19 |
| 2.3.1. Linear Static Analysis..... | 21 |
| 2.3.2. Linear Dynamic Analysis | 22 |
| 2.3.3. Nonlinear Static Analysis | 23 |
| 2.3.4. Nonlinear Dynamic Analysis | 25 |
| 2.4. Masonry | 26 |
| 2.4.1. Mechanical characterization | 27 |
| 3. State of art..... | 30 |
| 3.1. Torsional effect | 30 |
| 3.2. Pounding effect | 33 |
| 3.3. Estimation of maximum displacement | 41 |
| 4. Case study..... | 47 |
| 4.1. Territorial organization | 47 |
| 4.2. Historical-critical analysis | 50 |
| 4.3. Description of Structural Unit..... | 54 |
| 4.4. Geometrical relief | 55 |
| 4.5. Technical-constructive relief | 60 |

| | | |
|-----------|--|------------|
| 4.6. | Adjacent buildings | 64 |
| 5. | Case study model | 66 |
| 5.1. | Equivalent frame model..... | 66 |
| 5.2. | Material properties | 69 |
| 5.3. | Evaluation of actions | 70 |
| 5.3.1. | Load analysis | 70 |
| 5.3.2. | Snow action | 73 |
| 5.3.3. | Seismic action..... | 74 |
| 5.4. | Combination of actions | 77 |
| 5.5. | Hinge properties..... | 78 |
| 5.6. | Modeling “Building C”..... | 81 |
| 5.7. | Calculation of pounding effect | 82 |
| 5.8. | Calculation of torsional effect..... | 86 |
| 6. | Results and comparisons..... | 88 |
| 6.1. | Results of modal analysis | 88 |
| 6.2. | Results pushover analysis isolated building | 91 |
| 6.3. | Calculation of isolated building vulnerability index..... | 95 |
| 6.4. | Results pushover analysis building in aggregate | 96 |
| 6.5. | Calculation of building in aggregate vulnerability index | 101 |
| 6.6. | Comparisons | 102 |
| 7. | Conclusions | 106 |
| 8. | References..... | 108 |

List of figures

| | |
|--|----|
| Figure 1. Example of cadastral plans dating back to 1500 - 1858..... | 3 |
| Figure 2. Growth mechanisms of aggregates (Donà and De Maria 2011)..... | 4 |
| Figure 3. Typical planimetric scheme of a terraced aggregate..... | 5 |
| Figure 4. Actions acting on an intermediate cell..... | 5 |
| Figure 5. Rotation and translation mechanisms (Donà and De Maria 2011)..... | 6 |
| Figure 6. Scheme of mechanisms in global terms (Donà and De Maria 2011)..... | 7 |
| Figure 7. Torsional effect on a corner cell..... | 7 |
| Figure 8. Limit States against seismic actions..... | 11 |
| Figure 9. Example of an elastic response spectrum in acceleration..... | 15 |
| Figure 10. Distribution of equivalent static forces..... | 22 |
| Figure 11. Example of modes of vibration..... | 23 |
| Figure 12. Distribution of lateral forces in Pushover Analysis..... | 23 |
| Figure 13. Equivalent bilinear system and diagram..... | 24 |
| Figure 14. Performance Point (PP)..... | 24 |
| Figure 15. Example of construction of a masonry..... | 26 |
| Figure 16. Graph stress-strain of the masonry and its constituent materials..... | 27 |
| Figure 17. Seismic behaviour of adjacent buildings..... | 34 |
| Figure 18. Pounding categories (Cole, Dhakal et al. 2010)..... | 34 |
| Figure 19. Pounding scenarios (Cole, Dhakal et al. 2010)..... | 35 |
| Figure 20. Linear elastic model..... | 36 |
| Figure 21. Linear viscoelastic model (Kelvin-Voigt model)..... | 37 |
| Figure 22. Hertz model..... | 38 |
| Figure 23. Hertz damp model..... | 39 |
| Figure 24. Nonlinear viscoelastic model..... | 40 |
| Figure 25. Case study..... | 47 |
| Figure 26. Extract of cadastral plan..... | 48 |
| Figure 27. Extract of PRG..... | 48 |
| Figure 28. History of earthquakes in L'Aquila area..... | 49 |
| Figure 29. Extract of MOPS..... | 49 |
| Figure 30. "Carta dell'Antonelli", 1622..... | 51 |
| Figure 31. Vandi, 1753..... | 51 |
| Figure 32. Relief of Italian Army..... | 52 |
| Figure 33. Construction phases of the aggregate..... | 53 |
| Figure 34. Geometric relief - Floor plans..... | 58 |
| Figure 35. Geometrical relief - Prospectus..... | 59 |
| Figure 36. Geometrical relief - Section..... | 59 |
| Figure 37. Technical-constructive relief - Abacus..... | 60 |
| Figure 38. Technical-constructive relief - Floor plans..... | 63 |
| Figure 39. Facade "Via Tempera" with Building C..... | 64 |
| Figure 40. Facade "Via Verdi" with Building D..... | 65 |
| Figure 41. 3D Model..... | 66 |

| | |
|--|-----|
| Figure 42. SAM Method..... | 67 |
| Figure 43. Theory of Dolce | 67 |
| Figure 44. Example of equivalent frame | 68 |
| Figure 45. Equivalent frame model | 69 |
| Figure 46. Design Spectrum SLO | 75 |
| Figure 47. Design Spectrum SLD | 76 |
| Figure 48. Design Spectrum SLV | 76 |
| Figure 49. Design Spectrum SLC..... | 77 |
| Figure 50. Design Spectrum | 77 |
| Figure 51. Bilinear shear-displacement model | 79 |
| Figure 52. Pier | 80 |
| Figure 53. Spandrel | 80 |
| Figure 54. Define Hinge Properties SAP2000 | 81 |
| Figure 55. Lateral displacements "Building D" | 83 |
| Figure 56. Lateral displacements "Building A" | 84 |
| Figure 57. Lateral displacements "Building A" and "Building D" | 85 |
| Figure 58. Modal periods and frequencies | 88 |
| Figure 59. Modal participation factors..... | 89 |
| Figure 60. Modal participating mass ratios | 89 |
| Figure 61. Deformed shape Mode 1 | 90 |
| Figure 62. Deformed shape Mode 2 | 91 |
| Figure 63. Capacity curve Pushover_X..... | 92 |
| Figure 64. Capacity curve Pushover_Y | 92 |
| Figure 65. Hinge analysis Pushover_X | 93 |
| Figure 66. Hinge analysis Pushover_Y | 94 |
| Figure 67. Equivalent elasto-plastic SDOF_X | 94 |
| Figure 68. Equivalent elasto-plastic SDOF_Y | 95 |
| Figure 69. Capacity curve Pushover_X..... | 97 |
| Figure 70. Capacity curve Pushover_Y | 98 |
| Figure 71. Hinge analysis Pushover_X | 99 |
| Figure 72. Hinge analysis Pushover_Y | 99 |
| Figure 73. Equivalent elasto-plastic SDOF_X | 100 |
| Figure 74. Equivalent elasto-plastic SDOF_Y | 101 |
| Figure 75. Comparison capacity curves_X..... | 102 |
| Figure 76. Comparison capacity curves_Y..... | 103 |
| Figure 77. Variation of vulnerability indices_X..... | 104 |
| Figure 78. Variation of vulnerability indices_Y..... | 104 |

List of tables

| | |
|--|-----|
| Table 1. Material properties..... | 69 |
| Table 2. Mechanical characteristics of masonry | 69 |
| Table 3. Load analysis SO1 | 70 |
| Table 4. Load analysis SO2..... | 71 |
| Table 5. Load analysis SO3 | 71 |
| Table 6. Load analysis SO5..... | 72 |
| Table 7. Load analysis SO6..... | 72 |
| Table 8. Load analysis SO7..... | 72 |
| Table 9. Load analysis SO8..... | 73 |
| Table 10. Load analysis SO9..... | 73 |
| Table 11. Seismic parameters for each Limit State..... | 75 |
| Table 12. Additional masses "Building C"..... | 82 |
| Table 13. Lateral displacements "Building D" | 83 |
| Table 14. Lateral displacements "Building A" | 84 |
| Table 15. Lateral displacements "Building A" | 85 |
| Table 16. Maximum impact forces..... | 86 |
| Table 17. Characteristics of equivalent elasto-plastic SDOF_X..... | 94 |
| Table 18. Performance checks_X..... | 95 |
| Table 19. Characteristics of equivalent elasto-plastic SDOF_Y..... | 95 |
| Table 20. Performance checks_Y | 95 |
| Table 21. Isolated building vulnerability index_X..... | 96 |
| Table 22. Isolated building vulnerability index_Y..... | 96 |
| Table 23. Normalised displacements..... | 97 |
| Table 24. Corrective coefficients torsional effects..... | 97 |
| Table 25. Characteristics of equivalent elasto-plastic SDOF_X..... | 100 |
| Table 26. Performance checks_X..... | 100 |
| Table 27. Characteristics of equivalent elasto-plastic SDOF_Y..... | 100 |
| Table 28. Performance check_Y | 101 |
| Table 29. Building in aggregate vulnerability index_X..... | 101 |
| Table 30. Building in aggregate vulnerability index_Y | 102 |
| Table 31. Percentage variation of vulnerability indices_X..... | 103 |
| Table 32. Percentage variation of vulnerability indices_Y | 104 |

1. Introduction

The aim of this paper is to study the seismic vulnerability of buildings aggregates and to analyze the effects of their interactions. The interactions among adjacent buildings can drastically modify the seismic response of each single structural entity that constitutes the aggregate. Nonlinear dynamic analyses are required to capture the inherent dynamic effects (e.g. pounding). Moreover, due to their complexity and high computational load they are unsuitable to be applied by practitioners. For this reason, the aim of this thesis is to develop a simplified nonlinear static-based method capable of effectively capture the buildings aggregate effects on the single structure. On the other hand, the proposed method allow to reduce the required computational effort. The proposed method offers new insight into building aggregates effects assessment and aims at overcoming the existing lacks in practical and current regulations.

In the first part of this thesis, the existing body of literature about the methods and models to estimate the pounding and the torsional effects on building aggregates are described. In the second part the proposed method is presented. The structure is modelled as an equivalent frame consisting of horizontal and vertical one-dimensional elements (spandrels and piers, respectively). These elements are connected each other through infinitely rigid elements. The pounding effects are simulated by a load distribution along the height of the structure calculated using the linear elastic model proposed by Maison and Kasai (1990) (1992). which introduces a spring with a stiffness that simulates the impact stiffness of colliding structures. Then, a non-linear static analysis (pushover) is performed using the extended N2 method Fajfar, Marušić et al. (2005) to consider the torsional effects.

Later, this method is applied to an existing masonry building located in L'Aquila, Italy. The building has experienced moderate damage during the L'Aquila earthquake in 2009.

The results show how the application of the proposed method involves a reduction of the vulnerability index of the structure of approximately 40% for the case study.

1.1. Building aggregates

A building aggregate is a set of buildings built in different eras and arranged in succession seamlessly. The different buildings are adjacent to each other and under the effect of seismic action interact with each other.

Before the expansion of the suburbs occurred in the twentieth century there was a process of building expansion of the historic centres that led to a gradual clogging of all the free spaces adjacent the existing buildings. This type of historical evolution was a direct consequence of the need for a contrast action able to balance the structure hit by the earthquake. In this way, therefore, the creation of connections with detached cells and the reciprocal interactions between them favored the stability of all structures. The most obvious example of this prevention technique diffused in the past is the realization of the "archi a sbatacchio" between two distinct cells. This technique offers the possibility of solving many problems if carried out with the right criteria, but, at the same time, poses many others if performed in an approximate way. Hence the importance of a study of the seismic vulnerability of a building present within a building aggregate also considering the interactions with adjacent buildings.

Because of this evolutionary process of building, the wall boxes are not always "closed", that is with the four perimeter walls well connected between them. In fact, in terraced construction the housing cell at the head has only three sides built together, or only two corner if it comes from the clogging of a courtyard. In order to realize the walls at a later moment, therefore, usually were left on the edges of the buildings some "waiting posts", i.e. some protruding

stones. Although the connection was made according appropriate design criteria, it represents a weak constraint and therefore the walls are not well connected. It is crucial to understand the growth mechanisms of the aggregate, in order to figure out how it evolved over time, which cells were created first and which subsequently, and extract information on buildings connections. For this purpose it is useful to find the available cadastral and historical cartography of the aggregate.

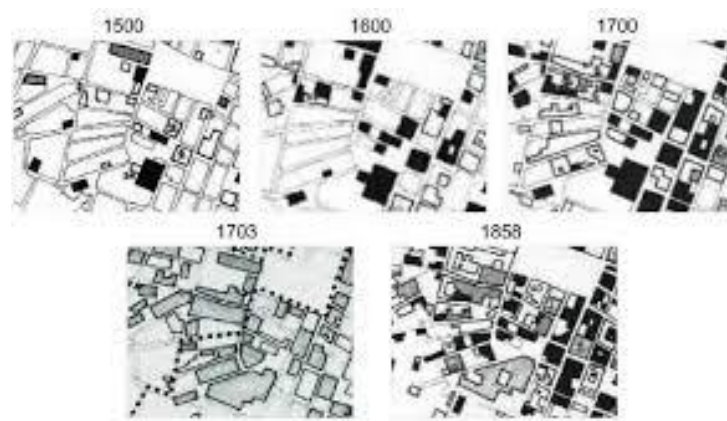


Figure 1. Example of cadastral plans dating back to 1500 - 1858

It is possible to recognize inside the building aggregate the primitive cells (A), that is the buildings built first and therefore more dated, the clogging cells (B), that is environments isolated from the outside through the construction of a wall to connect two cells already existing and whose walls are, usually, without connections with the original cells, and growth cells (C, D), that is environments isolated from the outside through the construction of two or three walls that can be connected between them but, usually, without connections with the original cells (Donà and De Maria 2011).

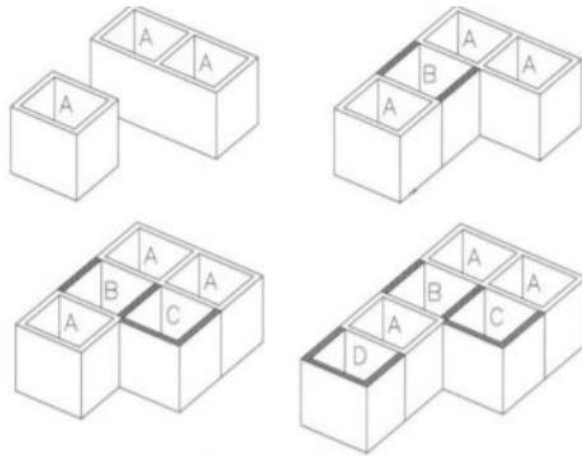


Figure 2. Growth mechanisms of aggregates (Donà and De Maria 2011).

1.2. Behaviour of building aggregates

For an isolated building there are usually no substantial differences in behaviour in the two main directions as the planimetric scheme is fairly homogeneous and the only element that involves this difference in behaviour is represented by the warping of the floors. This argument, however, is not true for aggregate buildings.

In fact, there is a substantial difference in the behaviour of the building of interest in the two main directions for various reasons. The first reason is represented by the typical planar layout of a terraced aggregate. It includes transverse walls (windward walls), which are generally intact, a longitudinal spinal wall that offers the main bearing capacity while separates the building cells, and longitudinal perimeter walls which are prepared for the openings of windows and doors.

Therefore, we can see how the walls have a different stiffness that determines a different response and a different behaviour in the two main directions.

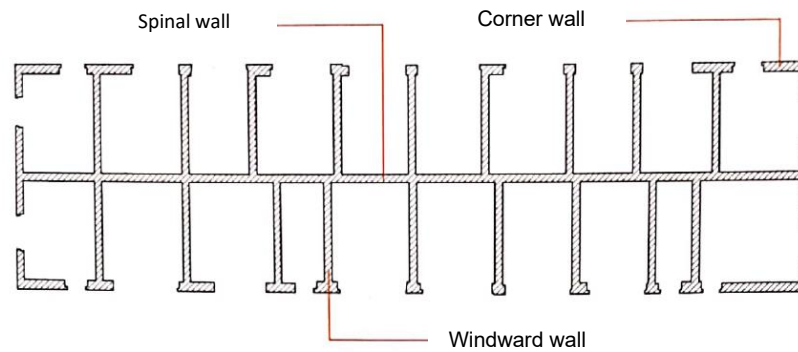


Figure 3. Typical planimetric scheme of a terraced aggregate

In addition, mutual support between cells is a key issue in terraced construction. In fact, each cell subject to the earthquake relies on the stabilizing effect of the adjacent cell. Each cell tends to absorb the actions transmitted by the “prior” structure. Instead, the next building produce a buttress effect on the analyzed cell.

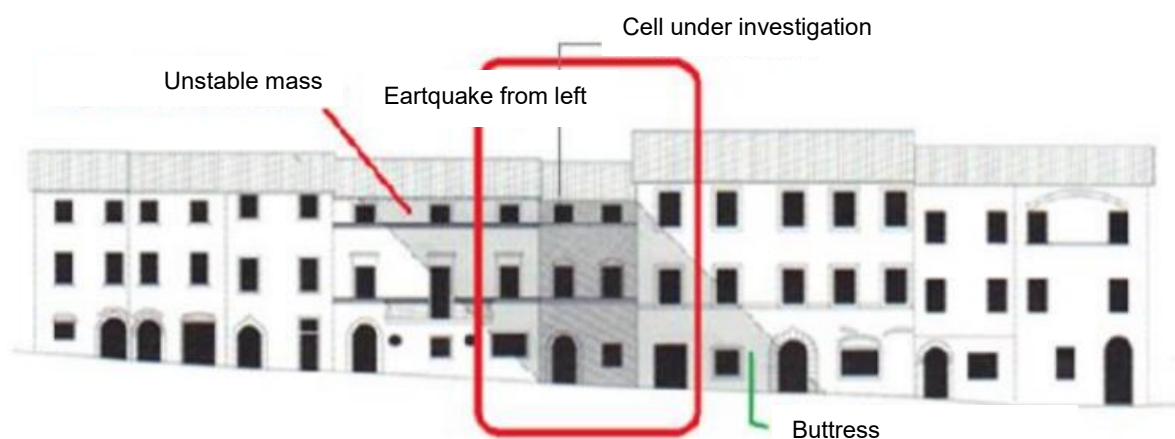


Figure 4. Actions acting on an intermediate cell

It is possible to notice how the mechanism of tilt of the facades, which can involve both the entire wall and only a portion of it, is one of the most probable collapse mechanisms toccuring within an aggregate.

The extreme cells do not have adjacent structures that offers a buttress effect; therefore they are more subjected to rotation and translation mechanisms.

The rotation mechanisms are activated by minor horizontal stresses that tend to isolate a portion of the wedge of the wall from the remaining and that tends to rotate around a hinge produced

by special conditions of constraint, such as the presence of chains or contrast elements. This wedge is referred to by the term "rotation sector" or simply "sector A". The translation mechanisms are activated by greater horizontal stresses and involve a wedge ("sliding sector" or simply "sector B"), which has a greater angle than the "sector A".

These mechanisms are prevented by seismic retrofit actions such as the "archi a sbatacchio" commonly used in the past or tie rods.

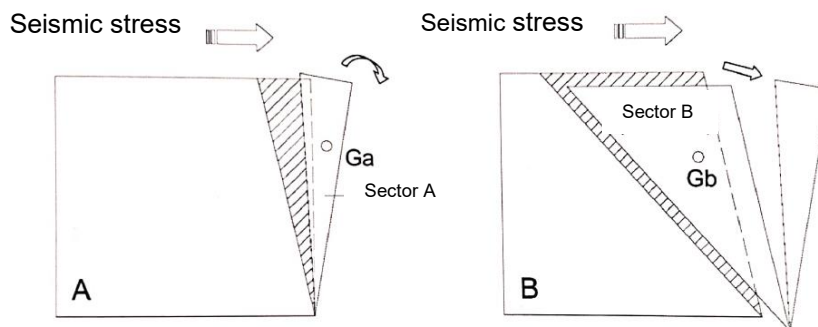


Figure 5. Rotation and translation mechanisms (Donà and De Maria 2011).

Therefore, if we consider the aggregate in global terms, it is possible to conduct two half-lines of about 45° from the extreme bases of the block inwards that enclose the portions of the wall that may be subject to the mechanisms just described. Instead, the portion below the "critical line" identified by the tangents to the half-lines represents the most stable portion in which the static compression flows, diverted by the seismic action, can be transferred until the foundation (Donà and De Maria 2011).

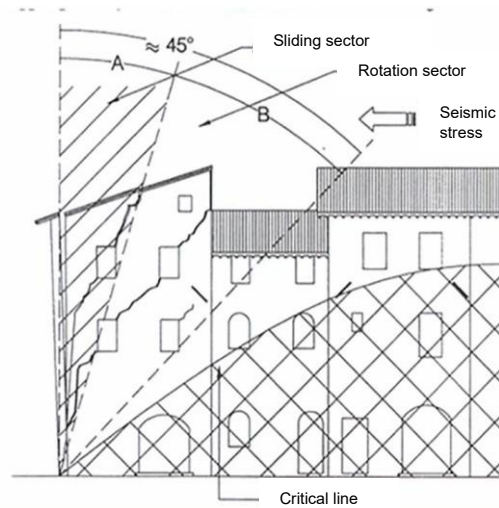


Figure 6. Scheme of mechanisms in global terms (Donà and De Maria 2011).

The corner cells can be thought as the header cells in both directions. In addition to the mechanisms of tipping and sliding they are also subject to a torsional effect due to the presence of unstable forces in both directions.

The national design regulation (8.7.1 of NTC18 (trasporti 2018)) states that for corner or header structural units the analyses cannot be carried out neglecting the torsional effects.

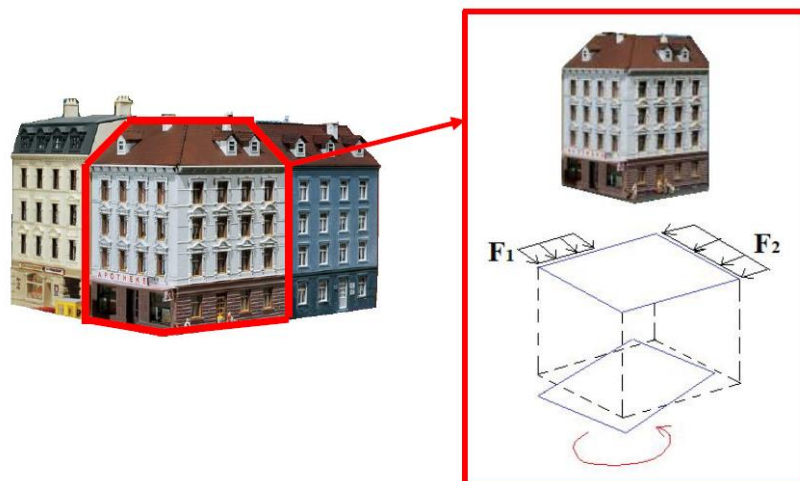


Figure 7. Torsional effect on a corner cell

1.3. Structural Units (US)

In the analysis of aggregates, the concept of building is preferred to replace the concept of Structural Unit (US). A Structural Unit is characterized by the following properties:

- Continuity from sky to ground, as regards the flow of vertical loads;
- Delimited by open spaces or by technical joints or adjacent buildings built with different construction and structural types;
- Built in the same era.

Therefore it is necessary to identify the different Structural Units and highlight the structural interactions with the adjacent buildings, including:

- Actions (both vertical and horizontal) from adjacent US slabs or walls;
- The thrusts of arcs and vaults from adjacent US;
- The thrusts from contrast arches or tie rods anchored on other buildings;
- The pounding between adjacent US;
- The thrusts caused by offset horizons on the walls in common with the adjacent US;
- The local effects caused by misalignments of the elevations, differences in heights or stiffnesses between adjacent US;
- The tilting and translation actions in the header US.

In addition to the identification of the Structural Unit prescribed by the 2019 Circular, the "Guidelines for the analysis of masonry buildings in aggregate" issued by the ReLUIIS and the Civil Protection Department in October 2010 following the seismic event that occurred in Abruzzo in April 2009, suggest to identify two other elements within the building aggregate:

- The Minimum Intervention Unit (UMI);
- The Minimum Unit of Analysis (UMA).

In particular, the Minimum Intervention Unit is configured as a portion of aggregate, consisting of one or more Structural Units, which will be subject to a single intervention, in accordance with a correct modelling of the aspects of structural interaction. The optimal choice of the UMI will be such as to minimize the mutual interactions under the effect of the seismic action.

Instead, the Minimum Unit of Analysis is the portion of aggregate, generally larger than the UMI, to require for evaluating any structural interactions, such as the thrust of vaulted systems, the loads (vertical or horizontal) coming from slabs or walls of structural units adjacent to the UMI and the pounding caused by adjacent buildings.

2. Legislation and seismic analysis

2.1. Seismic action

The design seismic actions are calculated based on the seismic hazard of the site provided by INGV (National Institute of Geophysics and Volcanology). Seismic hazard parameters are a function of the morphological and stratigraphic characteristics that determine the local seismic response. The Legislation prescribes two different methods for the assessment of seismic action:

- By using elastic acceleration response spectra according to the seismic hazard;
- Through the use of acceleration time histories compatible with a predefined target spectrum that is consistent with the local seismic hazard.

The first method of analyses is widely adopted for its simplicity and effectiveness.

Four Limit States (LS) are defined: two as Serviceability LS and two as Ultimate LS. Each Limit State is associated with a certain probability of exceedance of P_{VR} in the reference period of construction. In particular, the Service Limit States are:

- Operating Limit State (SLO) with a probability of exceeding 81%: following the earthquake the construction does not suffer significant damage and interruptions of use;
- Damage Limit State (SLD) with a probability of exceeding 63%: as a result of the earthquake the construction as a whole suffers damage such as not to put at risk users and not to compromise the ability to resist and stiffness.

Instead, the Ultimate Limit States are:

- Life Safety Limit State (SLV) probability of exceeding 10%: as a result of the earthquake, the construction suffers damage to the structural components associated with a significant loss of stiffness against horizontal actions;
- Collapse Limit State (SLC) probability of exceeding 5%: as a result of the earthquake the construction suffers very serious damage to the structural components.

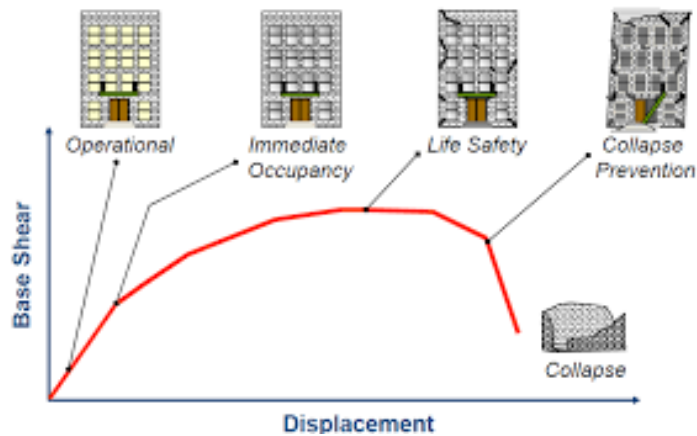


Figure 8. Limit States against seismic actions

To evaluate the seismic action the first step is to define the following parameters:

- Nominal design life, V_N , defined as the number of years in which the building is expected to maintain specific performance levels. The minimum values of V_N to be adopted for the different types of construction are reported in Tab. 2.4.I of the NTC18.

Tab. 2.4.I – Valori minimi della Vita nominale V_N di progetto per i diversi tipi di costruzioni

| TIPI DI COSTRUZIONI | | Valori minimi di V_N (anni) |
|---------------------|---|-------------------------------|
| 1 | Costruzioni temporanee e provvisorie | 10 |
| 2 | Costruzioni con livelli di prestazioni ordinari | 50 |
| 3 | Costruzioni con livelli di prestazioni elevati | 100 |

- Coefficient of use, C_U , defined according to the class of use of the construction and that depends on the function that carries out the building and the consequences that would result from its interruption. The value of the coefficient of use C_U is defined, to varying of the class of use, like shown in Tab. 2.4.II of the NTC18:

Tab. 2.4.II – Valori del coefficiente d'uso C_U

| CLASSE D'USO | I | II | III | IV |
|--------------------|-----|-----|-----|-----|
| COEFFICIENTE C_U | 0,7 | 1,0 | 1,5 | 2,0 |

- Reference period of seismic action, V_R , obtained by multiplying the nominal life V_N of the construction by the coefficient of use C_U .

$$V_R = V_N \cdot C_U \quad (2.1)$$

Once these parameters have been defined, the following parameters can be determined and identified:

- Probability of exceedance of ground acceleration, P_{VR} , as defined above;
- Seismic return period, T_R , defined as the mean time between occurrence of two seismic events equal to or greater than an assigned intensity value. This parameter is a function of the V_R reference period and the probability of P_{VR} exceedance through the following formula:

$$T_R = -V_R / \ln(1 - P_{VR}) = -C_U \cdot V_N / \ln(1 - P_{VR}) \quad (2.2)$$

- Soil category, based on stratigraphic description and values of shear wave propagation rate V_S . The Legislation defines 5 categories of subsoil, as reported in Tab. 3.2.II of NTC18, to which corresponds a stratigraphic amplification coefficient, S_S , which takes into account the amplification of the signal linked to the stratigraphy of the soil. The values of this coefficient as a function of the soil category are defined in Tab. 3.2.IV of NTC18;

Tab. 3.2.II – Categorie di sottosuolo che permettono l'utilizzo dell'approccio semplificato.

| Categoria | Caratteristiche della superficie topografica |
|-----------|--|
| A | Ammassi rocciosi affioranti o terreni molto rigidi caratterizzati da valori di velocità delle onde di taglio superiori a 800 m/s, eventualmente comprendenti in superficie terreni di caratteristiche meccaniche più scadenti con spessore massimo pari a 3 m. |
| B | Rocce tenere e depositi di terreni a grana grossa molto addensati o terreni a grana fina molto consistenti, caratterizzati da un miglioramento delle proprietà meccaniche con la profondità e da valori di velocità equivalente compresi tra 360 m/s e 800 m/s. |
| C | Depositi di terreni a grana grossa mediamente addensati o terreni a grana fina mediamente consistenti con profondità del substrato superiori a 30 m, caratterizzati da un miglioramento delle proprietà meccaniche con la profondità e da valori di velocità equivalente compresi tra 180 m/s e 360 m/s. |
| D | Depositi di terreni a grana grossa scarsamente addensati o di terreni a grana fina scarsamente consistenti, con profondità del substrato superiori a 30 m, caratterizzati da un miglioramento delle proprietà meccaniche con la profondità e da valori di velocità equivalente compresi tra 100 e 180 m/s. |
| E | Terreni con caratteristiche e valori di velocità equivalente riconducibili a quelle definite per le categorie C o D, con profondità del substrato non superiore a 30 m. |

Tab. 3.2.IV – Espressioni di S_b e di C_c

| Categoria sottosuolo | S_b | C_c |
|----------------------|---|------------------------------|
| A | 1,00 | 1,00 |
| B | $1,00 \leq 1,40 - 0,40 \cdot F_0 \cdot \frac{a_g}{g} \leq 1,20$ | $1,10 \cdot (T_C^*)^{-0,20}$ |
| C | $1,00 \leq 1,70 - 0,60 \cdot F_0 \cdot \frac{a_g}{g} \leq 1,50$ | $1,05 \cdot (T_C^*)^{-0,33}$ |
| D | $0,90 \leq 2,40 - 1,50 \cdot F_0 \cdot \frac{a_g}{g} \leq 1,80$ | $1,25 \cdot (T_C^*)^{-0,50}$ |
| E | $1,00 \leq 2,00 - 1,10 \cdot F_0 \cdot \frac{a_g}{g} \leq 1,60$ | $1,15 \cdot (T_C^*)^{-0,40}$ |

- Topographical condition distinct in 4 categories, as reported in Tab. 3.2.III of NTC18, to which corresponds a topographical amplification coefficient, S_T , which takes into account the amplification of the signal related to the topography of the ground. The values of this coefficient as a function of the soil category are defined in Tab. 3.2.V of NTC18;

Tab. 3.2.III – Categorie topografiche

| Categoria | Caratteristiche della superficie topografica |
|-----------|---|
| T1 | Superficie pianeggiante, pendii e rilievi isolati con inclinazione media $i \leq 15^\circ$ |
| T2 | Pendii con inclinazione media $i > 15^\circ$ |
| T3 | Rilievi con larghezza in cresta molto minore che alla base e inclinazione media $15^\circ \leq i \leq 30^\circ$ |
| T4 | Rilievi con larghezza in cresta molto minore che alla base e inclinazione media $i > 30^\circ$ |

Tab. 3.2.V – Valori massimi del coefficiente di amplificazione topografica S_T

| Categoria topografica | Ubicazione dell'opera o dell'intervento | S_T |
|-----------------------|--|-------|
| T1 | - | 1,0 |
| T2 | In corrispondenza della sommità del pendio | 1,2 |
| T3 | In corrispondenza della cresta di un rilievo con pendenza media minore o uguale a 30° | 1,2 |
| T4 | In corrispondenza della cresta di un rilievo con pendenza media maggiore di 30° | 1,4 |

- Amplification coefficient, S , defined as the product between the stratigraphic amplification coefficient S_S and the topographical amplification coefficient S_T .

$$S = S_S \cdot S_T \quad (2.3)$$

At this point must be defined the following parameters that define the basic seismic hazard:

- Maximum horizontal site acceleration, a_g ;
- Maximum value of spectrum amplification factor in horizontal acceleration, F_0 ;
- Reference value for determining the start period of the section at constant velocity of the spectrum in horizontal acceleration, T_C^* .

These parameters are provided by INGV at a grid of 10751 points defined by the coordinates of latitude and longitude that covers the entire national territory. The a_g , F_0 and T_C^* parameters are also listed for all grid points in Annexes A and B of D.M. 14/01/2008.

Once these parameters are obtained, it is possible to determine the spectral form to be used in seismic combination calculations. In fact, the Legislation provides the formulas necessary to determine the elastic response spectrum in acceleration according to the parameters described above. This spectrum provides, depending on the period of vibration, the maximum acceleration response of the generic elementary dynamic system, that is the simple oscillator. For the construction of this spectrum the Legislation defines three periods of vibration:

- T_B : start of the section with constant acceleration;
- T_C : start of steady-speed section;
- T_D : start of the constant displacement section;

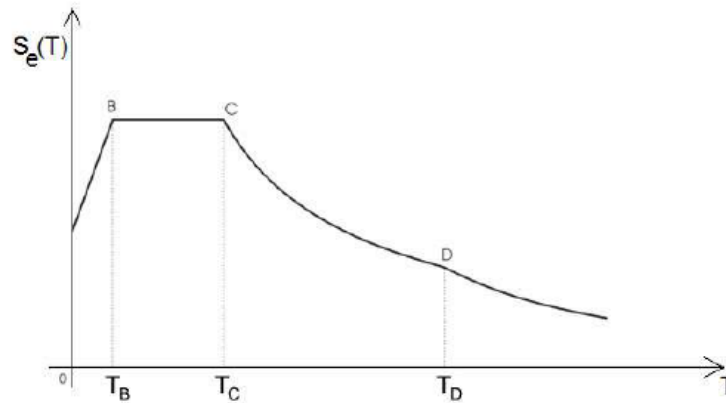


Figure 9. Example of an elastic response spectrum in acceleration

To switch from the elastic response spectrum to the design spectrum that takes into account the inelastic dissipative capacities of the structure, spectrum ordinates will be reduced by using the behaviour factor, q .

2.2. Current Standards for building aggregates

In 2018, the new Technical Legislations for Construction (NTC18) come into force, which in Chapter 8 deal with the subject of existing buildings and establish the general criteria for safety assessment and design, the execution and testing of interventions on existing buildings. These interventions are divided into three categories:

- Repair or local operations: operations involving individual structural elements and which do not reduce pre-existing safety conditions;
- Improvement interventions: interventions to increase the pre-existing structural safety without necessarily reaching the safety levels set by Legislation;
- Adjustment interventions: interventions to increase the pre-existing structural safety, reaching the levels of structural safety set by Legislation.

The safety assessment is defined in sub-chapter 8.3 as a quantitative procedure to determine the extent of the actions that the structure is able to support with the minimum level of safety required. This assessment shall be made in relation to that required for a new building. For this reason the NTC18 introduce a new parameter, called vulnerability index ζ_E , defined as the relationship between the maximum seismic action bearable by the structure and the maximum seismic action that would be used in the design of a new construction on the same soil and with the same characteristics. This value may be determined as follows:

$$\zeta_E = \frac{S_a}{S_d} \quad (2.4)$$

In which S_a represents the ground spectral acceleration of the existing structure at the reference period, while S_d represents the design ground spectral acceleration for a new construction with the same characteristics and on the same site as the existing building. The vulnerability index can also be determined with the following formula:

$$\zeta_E = \frac{F_{collapse}^*}{F_{max}^*} \quad (2.5)$$

Where $F_{collapse}^*$ represents the maximum tolerable base shear of the existing building, while F_{max}^* represents the maximum seismic force required to design a new construction.

The reference model for analyses is defined in sub-chapter 8.5. The definition of reference models describing the behaviour of the building is one of the most complex phases of the entire analysis procedure. Indeed, considering the wide variety of existing constructions, it is not possible to indicate effective modelling procedures.

The first essential step for a correct modelling turns out to be the historical-critical analysis of the construction and a correct operation of geometric-structural relief. In fact, knowledge of the history of a building is indispensable both for the assessment of safety, both for the definition of interventions and the prediction of their effectiveness, while the relief has to identify the

resistant organism of the construction also considering the quality and the state of conservation of the materials and the constituent elements. If the building is inserted inside a building aggregate it is advisable not to dwell exclusively on the single Structural Unit (US), but to verify the constructive characteristics that can influence the seismic behaviour of the entire aggregate.

In particular, it is essential to verify:

- The historical and constructive evolution of the entire building aggregate;
- The main events that have influenced the morphological aspects of the urban fabric;
- The structural typology of the Structural Unit and the adjacent buildings;
- Possible alteration of the wall boxes and effective connections of facade walls between adjacent buildings and perimeter walls with those orthogonal;
- The alignment of perimeter walls and interior spinal walls;
- The shape and position of openings in walls: their axially, symmetry and repetition;
- The misalignments and tapering of the walls, the walls laid "in false" on the floors below and the differences in altitude between adjacent floors;
- The presence of effective contrast devices such as tie rods or "archi a sbatacchio".

In addition to a correct historical and geometric-constructive knowledge of the building aggregate and of the specific structural unit, of fundamental importance is an adequate knowledge of the characteristics of the materials and their degradation acquired through documentation available, in situ visual checks and experimental investigations. This topic will be dealt with more specifically in Sub-Chapter 2.4. Masonry.

The sub-chapter 8.7 of NTC18 contains information about the verification methods and about the characteristics of the main interventions to be applied to existing buildings, depending on the specific construction types. These indications are also useful for assessing the safety of buildings on actual state.

Both local and global mechanisms can be manifested in existing masonry constructions. The local mechanisms affect individual wall panels or larger portions of the building and engage the wall panels mainly outside their medium plan. They are disadvantaged by the absence or lack of effectiveness of the connections, both between walls and horizons, and at intersections between walls. However, the global mechanisms are those that affect the entire building and engage the wall panels mainly in their medium plan.

The safety of the construction shall be assessed against both types of mechanism.

Limit analysis methods may be used for seismic analysis of local mechanisms. With such methods it is possible to evaluate the seismic capacity in terms of both resistance and displacement.

The overall seismic analysis shall consider, as far as possible, the real structural system, with particular attention to the stiffness and resistance of the horizons and the effectiveness of the connections of the structural elements with the horizons and with each other. In particular, due to the rigidity of the slabs, three possible situations can be referred to:

- Slabs which can be modelled as infinitely rigid;
- Slabs with finite stiffness (able to constrain walls and to distribute seismic stresses);
- Slabs with negligible stiffness (inadequate to redistribute horizontal actions between walls).

In the case of slabs infinitely rigid and well connected to the walls, the horizontal actions can be divided according to the strength, stiffness and the position of the various walls.

In the case of slabs of negligible stiffness each wall can be checked for actions that compete directly for areas of influence of the slabs bound to them.

In the case of slabs with finished stiffness, the response can be obtained by inserting into the construction model the mechanical characteristics of each slab.

In the analysis of a building that are part of a building aggregate, possible interactions that derive from adjacent buildings shall be taken into account. The verification of a US that presents infinitely rigid slabs or with significant stiffness can be carried out by non-linear static analysis, with checks in terms of both forces and displacements. In the case of corner or header US, the analysis cannot be carried out neglecting torsional effects. However, the verification of a US that presents slabs with negligible stiffness can be done by analysing the individual walls of the US because each wall is subject to vertical loads of competence and the corresponding actions of the earthquake in the direction parallel to the wall.

2.3. Methods of analysis

The aim of seismic analysis is to determine the demand to be compared with the capacity of the structure. Demand means the magnitude of the stresses, deformations and displacements of structural elements caused by seismic action to be compared with the capacity of the structure in terms of strength, ductility and displacement.

The analytical methods are linear and non-linear, depending on the characteristics of the structure and the behaviour model adopted. In particular, it shall:

- **Linear Analysis:** Linear analysis involves the use of linear elastic laws for materials and can be used to calculate seismic demand in the case of both non-dissipative and dissipative structural behaviour. In both cases the seismic demand is calculated by reference to the design spectrum. In order to model the dissipative capacity of the structure a behaviour factor q will be adopted, which depends on the structural typology, its degree of hyperstaticity and the design criteria adopted and takes into account the dissipative capacities of the material. Where geometric non-linearities cannot be neglected, they may be taken into account by amplifying the effects of seismic action by applying an appropriate amplification factor;

- Nonlinear Analysis: Nonlinear analysis can be used for both non-dissipative behaviour structural systems and dissipative behaviour structural systems and takes into account non-linearities of material and geometry. In addition, it may be used for these purposes and in the following cases:
 - To identify the distribution of inelastic demand in buildings designed with the behaviour factor q ;
 - Evaluate the over-resistance ratios α_u/α_1 ;
 - As a design method for new buildings as an alternative to linear analysis methods;
 - As a method for evaluating the capacity of existing buildings.

The methods are also classified in relation to the fact that equilibrium is treated statically or dynamically. In particular:

- Dynamic Analysis: in this type of analysis equilibrium is treated dynamically. An example is the modal analysis that calculates the modes of vibration of a structural system or numerical integration methods that solve instant by instant the equations of motion;
- Static Analysis: in this type of analysis the equilibrium is treated statically. Assigned a system of distributed or concentrated static loads it is possible to obtain the displacements and stresses.

The four types of analysis described above can be combined in order to obtain 4 different methods of analysis:

- Linear Static Analysis;
- Linear Dynamic Analysis;
- Nonlinear Static Analysis;
- Nonlinear Dynamic Analysis.

2.3.1. Linear Static Analysis

Linear Static Analysis consists in the application of static forces equivalent to the inertia forces induced by seismic action. It can be carried out for regular constructions in height and with period of the main vibrating mode (T_1) not exceeding $2.5T_C$ or T_D . For the calculation of the principal T_1 period, the following formula may be used as a first approximation:

$$T_1 = C_1 \cdot H^{3/4} \quad (2.6)$$

Where:

- H = height of the construction from the foundation plane;
- $C_1 = 0.05$ for masonry constructions.

Alternatively, for civil or industrial constructions not exceeding 40m in height and whose mass is evenly distributed along the height, T_1 may be estimated using the following formula:

$$T_1 = 2\sqrt{d} \quad (2.7)$$

Where d is the elastic lateral displacement of the highest point of the building due to the combination of loads $G_1 + G_2 + \sum_j \Psi_{2j} Q_{kj}$ applied in the horizontal direction.

Therefore, with this method the seismic action is represented as a system of static forces applied in proximity to the individual decks where the masses of the building are admitted concentrated. The magnitude of these forces is obtained from the ordinate of the design spectrum corresponding to the T_1 period and their distribution on the structure follows the form of the main mode of vibration in the direction under consideration, estimated approximately.

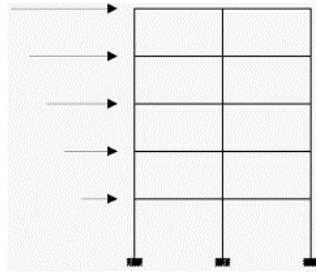


Figure 10. Distribution of equivalent static forces

Therefore, Linear Static Analysis essentially consists of a simplified Linear Dynamic Analysis in which:

- Instead of carrying out the dynamic analysis of the construction, a fundamental mode is assumed with a T_1 period calculated in an approximate way and linearly increasing displacements with the height of the foundation plane;
- The effects of seismic action, represented by the design response spectrum, shall be calculated for the fundamental mode considered;
- No combination of effects is performed because other modes of vibration are not considered.

2.3.2. Linear Dynamic Analysis

Linear Dynamic Analysis consists:

- In determining the vibration modes of the construction (modal analysis);
- In calculating the effects of seismic action, represented by the design response spectrum, for each of the vibration modes identified;
- In the combination of these effects.

The modal analysis consists of solving the equations of the motion of the linear structure in the steady state condition.

Only the modes of vibration with significant participating mass, i.e. all modes with a participating mass exceeding 5% and a number of modes with a total participating mass exceeding 85% are considered.

The effects of the selected modes are combined by the CQC rule (Complete Quadratic Combination) or the SRSS rule (Square Roof of Sum of Squares).

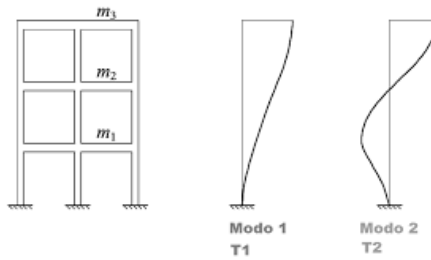


Figure 11. Example of modes of vibration

2.3.3. Nonlinear Static Analysis

The Nonlinear Static Analysis, also called Pushover Analysis, aims at obtaining the capacity curve of the structure, expressed by the function F_b-d_c , where F_b is the base shear and d_c is the displacement of a control point which for buildings is usually represented by the mass centre of the last horizontal. To obtain the capacity curve, vertical loads and a distribution of horizontal loads applied in the center of the mass at all building levels are assumed. This distribution of forces is monotonically increasing until collapse.

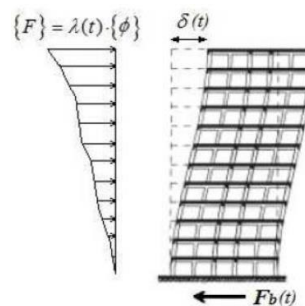


Figure 12. Distribution of lateral forces in Pushover Analysis

At least two distributions of inertia forces should be considered, one falling within the main distributions (Group 1) and the other in the secondary distributions (Group 2). The most frequently used load distributions in technical practice are as follows:

- From Group 1: a distribution of forces similar to that obtained by modal analysis with response spectrum;
- From Group 2: a uniform distribution of inertia forces along the height of the construction.

For each considered LS, the comparison between the capacity curve and the demand for displacement allows to determine the level of performance achieved. For this purpose, the real structural system is associated with a structural system equivalent to a single degree of freedom, that is, a simple oscillator with elasto-plastic behavior. In this way the capacity curve can be adjusted so as to obtain an elastic-perfectly plastic curve by adopting the principle of energy equivalence.

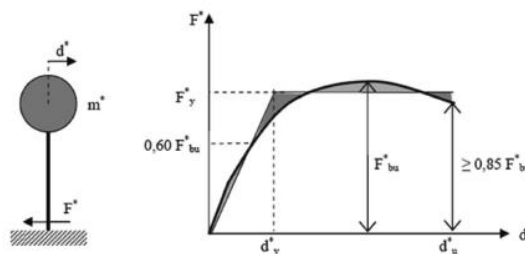


Figure 13. Equivalent bilinear system and diagram

Based on the seismic demand (design spectrum) and the building capacity (capacity curve), it is possible to define the Performance Point that determines the level of performance achieved.

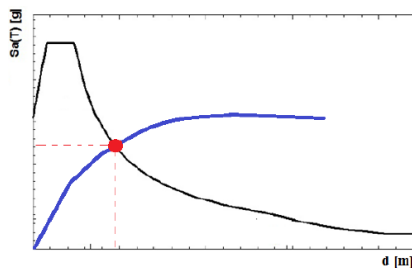


Figure 14. Performance Point (PP)

For the evaluation of the Performance Point (PP) it is possible to follow one of the following methods:

- Method A, based on the evaluation of inelastic demand through the principle of equal displacement or equal energy;
- Method B, based on the estimation of the inelastic demand through an equivalent viscous damping model.

2.3.4. Nonlinear Dynamic Analysis

Nonlinear Dynamic Analysis consists in the calculation of the seismic response of the structure by integration of the equations of motion using a non-linear model of the structure and subjected to temporal histories of the soil motion, i.e. accelerograms spectrum-compatible with the elastic response spectrum. It aims to assess the dynamic behaviour of the structure in the non-linear field, allowing the comparison between the ductility required and ductility available to the SLC and the related verifications, and to verify the integrity of structural elements against possible fragile behaviours.

To perform this type of analysis it is necessary to use non-linear models able to reproduce the post-elastic behaviour of the structural elements in order to correctly represent the dissipative capacity for hysteresis.

Usually the response of the accelerogram oscillator is calculated by applying the Newmark numerical integration method.

In addition, the results of the Nonlinear Dynamic Analysis must be compared with the results of a modal analysis with a design response spectrum in order to control the differences in terms of global stresses at the base of the structure.

This is certainly the most complete procedure but at the same time it is also the most complex type of analysis.

2.4. Masonry

Masonry was the main building material in the world until at least 1920 and the existing masonry buildings represent a consistent building heritage and often are characterized by historical-architectural values.

Masonry is a material composed of two elements: blocks and mortar. As for the blocks, there are numerous types because they can vary in shape, size and in origin. In fact, they can be artificial, such as brick blocks, or natural made from stone material, such as rocks and stones. Instead, the mortar has the function of joining these blocks and redistributing the load. They have different characteristics depending on the components which form it, such as the type of sand or lime used in the dough.



Figure 15. Example of construction of a masonry

These two materials with different characteristics work together by mediating their properties and make masonry a material with good characteristics to be applied in constructions. In particular, it has a good compressive strength and a low or negligible tensile strength. This is due to the different behaviour of the constituent elements. In fact, the results of an experimental monoaxial tensile-compression test of a brick masonry show that:

- Both components have a very low tensile strength compared to compression;

- Bricks have higher modulus of elasticity than mortar;
- The mortar has a wider field of deformation than the brick: therefore, it has a ductile breaking behaviour, unlike the brick that has fragile breaking behaviour.

These results are shown in the following graph:

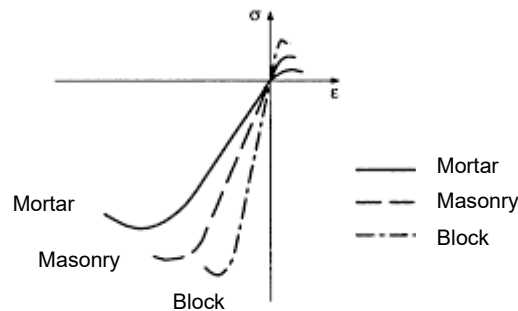


Figure 16. Graph stress-strain of the masonry and its constituent materials

Although masonry is an inhomogeneous material due to the presence of blocks and mortar, the material is assumed as homogeneous continuous macroscopically equivalent to the composite material.

2.4.1. Mechanical characterization

Chapter 8 of NTC18 deals with existing buildings and, in particular, section 8.5 defines the reference model for analyses.

In addition to a correct historical and geometric-constructive knowledge of the building aggregate and the specific Structural Unit, of fundamental importance is an adequate knowledge of the mechanical characteristics of materials and their degradation.

The direct measurement of the mechanical characteristics of the masonry is carried out by in situ tests on portions of masonry or laboratory tests on undisturbed elements taken in situ. Based on their degree of deepening, 3 test levels can be distinguished:

- Limited tests;
- Extended tests;
- Exhaustive texts.

Additional information may be obtained from non-destructive test methods or available documentation.

Table C.8.5.I of NTC18 provides information on the possible values of the mechanical parameters for the behaviour of the most recurrent types of masonry and relative to precise conditions:

Tabella C8.5.I -Valori di riferimento dei parametri meccanici della muratura, da usarsi nei criteri di resistenza di seguito specificati (comportamento a tempi brevi), e peso specifico medio per diverse tipologie di muratura. I valori si riferiscono a: f = resistenza media a compressione, τ_0 = resistenza media a taglio in assenza di tensioni normali (con riferimento alla formula riportata, a proposito dei modelli di capacità, nel §C8.7.1.3), f_{v0} = resistenza media a taglio in assenza di tensioni normali (con riferimento alla formula riportata, a proposito dei modelli di capacità, nel §C8.7.1.3), E = valore medio del modulo di elasticità normale, G = valore medio del modulo di elasticità tangenziale, w = peso specifico medio.

| Tipologia di muratura | f (N/mm ²) | τ_0 (N/mm ²) | f_{v0} (N/mm ²) | E (N/mm ²) | G (N/mm ²) | w (kN/m ³) |
|--|-----------------------------|----------------------------------|----------------------------------|-----------------------------|-----------------------------|-----------------------------|
| | min-max | min-max | | min-max | min-max | |
| Muratura in pietrame disordinata (ciottoli, pietre erratiche e irregolari) | 1,0-2,0 | 0,018-0,032 | - - | 690-1050 | 230-350 | 19 |
| Muratura a conci sbozzati, con paramenti di spessore disomogeneo (*) | 2,0 | 0,035-0,051 | - - | 1020-1440 | 340-480 | 20 |
| Muratura in pietre a spacco con buona tessitura | 2,6-3,8 | 0,056-0,074 | - - | 1500-1980 | 500-660 | 21 |
| Muratura irregolare di pietra tenera (tufo, calcarenite, ecc.,) | 1,4-2,2 | 0,028-0,042 | - - | 900-1260 | 300-420 | 13 ÷ 16(**) |
| Muratura a conci regolari di pietra tenera (tufo, calcarenite, ecc.,) (**) | 2,0-3,2 | 0,04-0,08 | 0,10-0,19 | 1200-1620 | 400-500 | |
| Muratura a blocchi lapidei squadri | 5,8-8,2 | 0,09-0,12 | 0,18-0,28 | 2400-3300 | 800-1100 | 22 |
| Muratura in mattoni pieni e malta di calce (***) | 2,6-4,3 | 0,05-0,13 | 0,13-0,27 | 1200-1800 | 400-600 | 18 |
| Muratura in mattoni semipieni con malta cementizia (es.: doppio UNI foratura ≤40%) | 5,0-8,0 | 0,08-0,17 | 0,20-0,36 | 3500-5600 | 875-1400 | 15 |

(*) Nella muratura a conci sbozzati i valori di resistenza tabellati si possono incrementare se si riscontra la sistematica presenza di zeppe profonde in pietra che migliorano i contatti e aumentano l'ammorsamento tra gli elementi lapidei; in assenza di valutazioni più precise, si utilizzi un coefficiente pari a 1,2.

(**) Data la varietà litologica della pietra tenera, il peso specifico è molto variabile ma può essere facilmente stimato con prove dirette. Nel caso di muratura a conci regolari di pietra tenera, in presenza di una caratterizzazione diretta della resistenza a compressione degli elementi costituenti, la resistenza a compressione f_{pu} essere valutata attraverso le indicazioni del § 11.10 delle NTC.

(***) Nella muratura a mattoni pieni è opportuno ridurre i valori tabellati nel caso di giunti con spessore superiore a 13 mm; in assenza di valutazioni più precise, si utilizzi un coefficiente riduttivo pari a 0,7 per le resistenze e 0,8 per i moduli elastici.

The mechanical characteristics can be multiplied by corrective coefficients based on some improvements in masonry characteristics (Table C.8.5.II, NTC18):

Tabella C8.5.II -Coefficienti correttivi massimi da applicarsi in presenza di: malta di caratteristiche buone; ricorsi o listature; sistematiche connessioni trasversali; consolidamento con iniezioni di malta; consolidamento con intonaco armato; ristilatura armata con connessione dei paramenti.

| Tipologia di muratura | Stato di fatto | | | Interventi di consolidamento | | | |
|--|----------------|---------------------|-------------------------|----------------------------------|---------------------|---|----------------------------------|
| | Malta buona | Ricorsi o listature | Connessione trasversale | Iniezione di miscele leganti (*) | Intonacoarmato (**) | Ristilatura armata con connessione dei paramenti (**) | Massimo coefficiente complessivo |
| Muratura in pietrame disordinata (ciottoli, pietre erratiche e irregolari) | 1,5 | 1,3 | 1,5 | 2 | 2,5 | 1,6 | 3,5 |
| Muratura a conci sbozzati, con paramenti di spessore disomogeneo | 1,4 | 1,2 | 1,5 | 1,7 | 2,0 | 1,5 | 3,0 |
| Muratura in pietre a spacco con buona tessitura | 1,3 | 1,1 | 1,3 | 1,5 | 1,5 | 1,4 | 2,4 |
| Muratura irregolare di pietra tenera (tufo, calcarenite, ecc.,) | 1,5 | 1,2 | 1,3 | 1,4 | 1,7 | 1,1 | 2,0 |
| Muratura a conci regolari di pietra tenera (tufo, calcarenite, ecc.,) | 1,6 | - | 1,2 | 1,2 | 1,5 | 1,2 | 1,8 |
| Muratura a blocchi lapidei squadriati | 1,2 | - | 1,2 | 1,2 | 1,2 | - | 1,4 |
| Muratura in mattoni pieni e malta di calce | (***) | - | 1,3 (***) | 1,2 | 1,5 | 1,2 | 1,8 |
| Muratura in mattoni semipieni con malta cementizia (es.: doppio UNI foratura ≤40%) | 1,2 | - | - | - | 1,3 | - | 1,3 |

(*) I coefficienti correttivi relativi alle iniezioni di miscele leganti devono essere commisurati all'effettivo beneficio apportato alla muratura, riscontrabile con verifiche sia nella fase di esecuzione (iniettabilità) sia a-posteriori (riscontri sperimentali attraverso prove soniche o similari).

(**) Valori da ridurre convenientemente nel caso di pareti di notevole spessore (p.es. > 70 cm).

(***) Nel caso di muratura di mattoni si intende come "malta buona" una malta con resistenza media a compressione f_m superiore a 2 N/mm². In tal caso il coefficiente correttivo può essere posto pari a $f_m^{0,25}$ (f_m in N/mm²).

(****) Nel caso di muratura di mattoni si intende come muratura trasversalmente connessa quella apparecchiata a regola d'arte.

These coefficients may be applied in combination in multiplicative form.

In addition, these mechanical parameters are reduced by a Confidence Factor (FC) defined according to the Knowledge Level (LC). In particular:

- LC1: when limited investigations have been carried out on the construction details and limited tests have been carried out on the mechanical characteristics of the materials. This LC corresponds to an FC = 1,35;
- LC2: when extensive investigations have been carried out on the construction details and extensive tests have been carried out on the mechanical characteristics of the materials. This LC corresponds to an FC = 1,2;
- LC3: when exhaustive investigations have been carried out on the constructive details and exhaustive tests have been carried out on the mechanical characteristics of the materials. To this LC corresponds an FC = 1;

3. State of art

The modelling and the relative analysis of a building aggregate involves a detailed study of the effects that a single Structural Unit can cause on adjacent Units.

In particular, we remember the torsional effect that the adjacent US cause on an angle US and the pounding effect due to the presence of adjacent US even at different heights.

Both effects have been the subject of study and research for many years and a short summary is presented below.

3.1. Torsional effect

Torsional effects may significantly modify the seismic response of buildings and they can cause severe damage of structures. Indeed the presence of adjacent buildings and the inherent geometrical irregularities amplify the torsional effects. Irregularities are classified into two types: irregularities in plan and irregularities along the height. The first type is related to offset between center of the mass and stiffness which result in a substantial increase in torsional effects when the structure is subjected to lateral forces. The second involves changes in geometric and/or structural properties along the height of the building, which generally result in increased seismic demand in specific planes.

In the case of irregular structures, Nonlinear Static Analysis procedures may be not suitable since they assumes force distribution along with the two principal building directions. Irregular

structures, on the other hand, have a significant participating mass for one or more modes of vibration. Therefore, the dynamic behaviour of these structures cannot be evaluated by considering only one translational mode. For this reason, several extensions of Nonlinear Static Analysis for irregular building structures have been studied.

These extensions are mainly based on two approaches: the first takes into account the contribution of more eigenmodes; Paret, Sasaki et al. (1996) developed the so-called Multi-Modal Pushover (MMP) which involves performing different pushover analyses using different lateral load distributions based on different elastic modal forms. In this way, it is possible to obtain capacity curves for each mode and compare them with seismic demand using the CSM method. Once the comparison is made it is possible to obtain a value, called Modal Criticality Index (MCI), that identifies the critical vibrating mode. With a similar approach, Chopra and Goel (2002), (2004) defined the Modal Pushover Analysis (MPA) for symmetrical and asymmetrical structures. With this procedure several pushover analyses are performed considering different lateral load distributions based on different modal shapes. In particular, for asymmetrical structures it involves the application of both lateral forces and a torque at each level of the building. Then, the results are combined through the SRSS rule (Square Root of Sum of Squares) or the CQC rule (Complete Quadratic Combination) to obtain an estimate of seismic demand for inelastic systems. Subsequently, Chopra and Goel (2004) developed the Modified MPA (MMPA) procedure, in which the contribution of higher vibrating modes is calculated by assuming linearly elastic system. The contribution of higher modes is combined with the inelastic response associated with the first mode. In this way, the computational effort decreases and turns out to be a valid alternative for practical applications because it leads to a better estimation of seismic demand. Reyes and Chopra (2011), (2011) developed a variant of this method, called Practical Modal Pushover Analysis (PMPA), which estimates seismic demands directly from the response (and design) spectrum. In this procedure, the structure is

treated in a linear elastic way in the estimation of the contributions of the higher modes of seismic demand.

The second approach is based on the first modal shape considering that the target displacement of a single control point cannot be representative of the dynamic behaviour of irregular buildings because torsional effects entail reductions and amplifications of the displacement demand at the two opposite ends of the storey. Following this approach, (Moghadam and Tso 2000, Moghadam and Tso 2000) defined a method consisting in determining target displacements, one for each resistant element, performing an elastic spectral analysis and assuming a certain lateral load distribution. Then, a series of pushover analyses are carried out for different resistant elements pushing these elements until the displacement at the top does not reach the previously determined target displacement. The same approach is used in Fajfar, Marušić et al. (2005) to extend the N2 method to irregular structures in plan. The modified N2 method is based on the combination of the results of a pushover analysis carried out on a 3D model that aims to control the distribution of the target displacement along the height of the structure with the results of a dynamic modal analysis that control the distribution of lateral displacements caused by the torsional effect. In particular, the displacements obtained from the pushover analysis are amplified by a correction coefficient determined by the ratio of the normalized displacement obtained by modal analysis, i.e. the displacement of a specific point in the plane divided by the displacement of the center of mass, and that obtained by the analysis pushover. This method results to be clear and easy to achieve.

A further method has been developed by Bosco, Ghersi et al. (2012) and is based on the concept that the distribution of the maximum dynamic displacements of the plane can be determined by two pushovers carried out by applying the lateral forces with two eccentricities, called "corrective eccentricities", compared to the center of mass of the plane.

All these methods have been evaluated and compared. In particular, Azizi-Bondarabadi, Mendes et al. (2021) and Nakamura, Derakhshan et al. (2017) evaluate the extended N2 method for irregular buildings in unreinforced masonry. The results show that this method is capable of correctly simulating the seismic response of masonry structures. Bento, Bhatt et al. (2010) and Bosco and Bento (2012) evaluate the results obtained by applying the extended N2 method and the MPA on simple multi-storey buildings. The results show that both methods result in more conservative results. The extended N2 method better predicts torsional effects. Instead, Bosco, Ghersi et al. (2013) compares the results obtained from 3 methods: original N2 method, extended N2 method and method of "corrective eccentricities". The results showed that:

- a) the original N2 method is capable of predicting the response only for rigid torsional structures;
- b) the extended N2 method is always conservative and simple to be performed;
- c) the "corrective eccentricities" method results close to those obtained with non-linear dynamic analysis, but requires a greater computational effort than the extended N2 method.

3.2. Pounding effect

Structural pounding phenomenon occurs when two or more adjacent buildings strike under the effect of dynamic horizontal actions. The collision between the structures can generate impact forces that can cause further local and global damage. The impact force and the number of collisions between structures depends on multiple factors such as the mutual distance and the fundamental period of the structures. In fact, the pounding phenomenon is amplified when adjacent structures vibrate out of phase due to the difference in their periods.

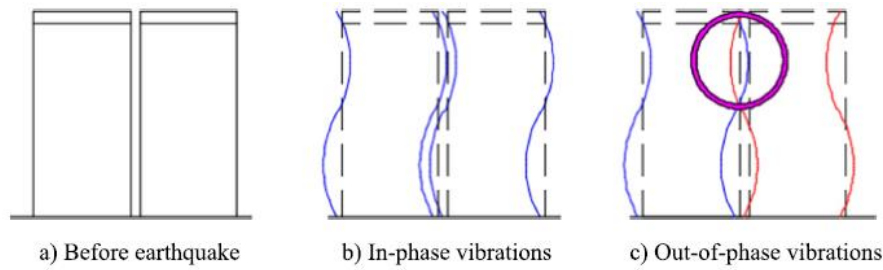


Figure 17. Seismic behaviour of adjacent buildings

In addition, the pounding scenarios of buildings can generally be divided into two categories: floor-to-floor pounding, when the colliding structures have the same story height, and floor-to-column pounding, when the structures have different story heights. The latter category is indeed the worst because the potential points of impact are not at the floor level, but along the height of the vertical structural members (Cole, Dhakal et al. 2010).

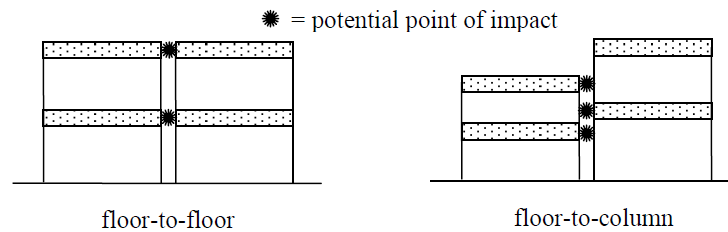


Figure 18. Pounding categories (Cole, Dhakal et al. 2010).

The pounding scenarios can also be classified into 6 categories (Jeng and Tzeng 2000, Cole, Dhakal et al. 2010). :

1. Floor-to-column pounding;
2. Pounding of heavier structures with lighter adjacent structures;
3. Pounding of higher structures with lower adjacent structures;
4. Torsional pounding;
5. Pounding of the structure at the end of terraced buildings;
6. Pounding of structures with fragile materials such as unarmred masonry.

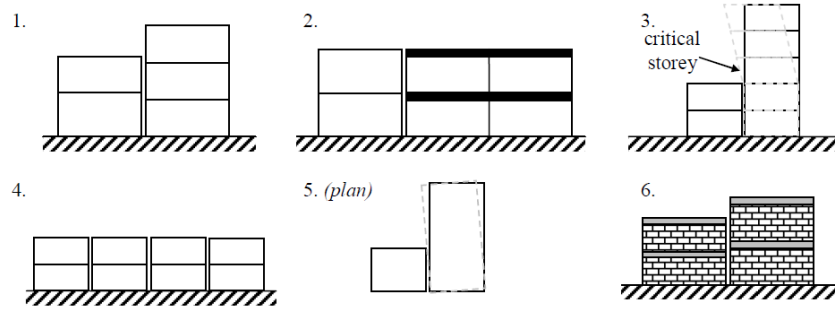


Figure 19. Pounding scenarios (Cole, Dhakal et al. 2010).

The assessment of the impact forces can be performed by applying two approaches: the stereomechanical approach and the force-based approach (or also known as the penalty approach). The stereomechanical approach exploits the law of the conservation of momentum and energy and relates the impact velocities with the coefficient of restitution according to the following expressions (Goldsmith 2001):

$$v_1' = v_1 - (1 + e) \frac{m_2 v_1 - m_2 v_2}{m_1 + m_2} \quad (3.1)$$

$$v_2' = v_2 + (1 + e) \frac{m_1 v_1 - m_1 v_2}{m_1 + m_2} \quad (3.2)$$

Where e represents the coefficient of restitution and simulates the dissipation of energy during the impact. In fact, it represents the level of plasticity and the loss of energy during the impact and is between 0 and 1; 0 means that the impact is completely plastic, while 1 means that the impact is completely elastic. This coefficient of restitution may be calculated in accordance with the following relationship:

$$e = \frac{v_2' - v_1'}{v_1 - v_2} \quad (3.3)$$

Anagnostopoulos and Spiliopoulos (1992) estimated the coefficient of restitution between 0.5 and 0.75. In many studies general coefficient of restitution equal to 0.65 was chosen for concrete structures (Anagnostopoulos 1988, Anagnostopoulos and Spiliopoulos 1992, Jankowski 2005,

Jankowski 2008, Mahmoud and Jankowski 2011). Jankowski (2010) showed how the value of the coefficient of restitution depends on the relative pre-impact speed and the material used. In any case, a constant value of 0.69 may be used.

This stereomechanical approach is very rarely used because it does not consider the impact period and does not directly assess the impact force during contact.

As an alternative, the approach based on the assessment of contact forces involves the use of interposed elements between colliding bodies. Maison and Kasai (1990) (1992) created a linear elastic model that introduces a spring with a stiffness that simulates the impact stiffness of the colliding structures. This spring is activated only when contact between structures occurs:

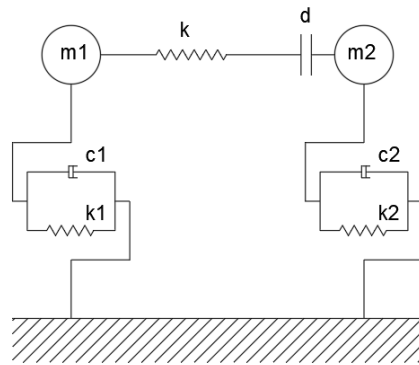


Figure 20. Linear elastic model

$$F(t) = \begin{cases} k\delta(t) & \delta(t) > 0 \\ 0 & \delta(t) \leq 0 \end{cases} \quad (3.4)$$

$$\delta(t) = u_1(t) - u_2(t) - d$$

Where $u_1(t)$ and $u_2(t)$ are the displacements of the two structures and d is the initial distance between the structures. Instead, k is the stiffness of the spring and is assumed equal to the stiffness of the impacting element according to the following basic formula:

$$k = \frac{EA}{L} \quad (3.5)$$

Where E , A and L are respectively the elastic modulus, the area and the length of the impacting element.

Cole, Dhakal et al. (2011) defined a new formula based on the duration of the t_c impact:

$$k = \frac{\left(\frac{m_1 m_2}{m_1 + m_2} \right) \left(\frac{\pi}{t_c} \right)^2}{1 - \left(\frac{-\ln e}{\sqrt{\pi^2 + (\ln e)^2}} \right)^2} \quad (3.6)$$

Xu, Xu et al. (2016) developed a further formula according to the fundamental periods of the two collident structures:

$$k = \frac{m_2}{m_1 + m_2} k_1 e^{\frac{2(\ln e)}{\pi} \arcsin \frac{\pi}{\sqrt{\pi^2 + (\ln e)^2}}} \quad T_1 \leq T_2$$

$$k = \frac{m_1}{m_1 + m_2} k_2 e^{\frac{2(\ln e)}{\pi} \arcsin \frac{\pi}{\sqrt{\pi^2 + (\ln e)^2}}} \quad T_1 > T_2 \quad (3.7)$$

In addition, Jankowski (2005) used predefined spring stiffness values depending on the type of structure and material. In particular, for buildings with steel-to-steel impact it used $k = 2,07 \cdot 10^7$ N/m, while for buildings with concrete-to-concrete impact it used $k = 9,35 \cdot 10^7$ N/m.

In order to consider the plastic behaviour and energy dissipation during the collision, Anagnostopoulos (1988) adopted a Kelvin-Voigt model where the damping coefficient was estimated as reported by the following equation:

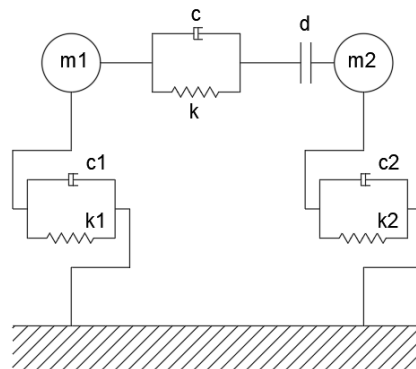


Figure 21. Linear viscoelastic model (Kelvin-Voigt model)

$$F(t) = \begin{cases} k\delta(t) + c\dot{\delta}(t) & \delta(t) > 0 \\ 0 & \delta(t) \leq 0 \end{cases}$$

$$c = 2\xi \sqrt{k \frac{m_1 m_2}{m_1 + m_2}} \quad (3.8)$$

$$\xi = -\frac{\ln e}{\sqrt{\pi^2 + (\ln e)^2}}$$

Where $\dot{\delta}(t)$ is the relative velocity between the two colliding elements, c is the impact damping coefficient and ξ is the impact damping ratio.

However, this model considers uniform energy dissipation in the pre-contact and post-contact phase. For this reason tensile actions are considered. To overcome this situation, modifications to the model were made in order to omit these tensile forces. In particular, Ye, Li et al. (2009) proposed the so-called Modified Kelvin Model (MK), Pant, Wijeyewickrema et al. (2010) adopted the so-called Modified Kelvin-Voigt Model (MVK) and Mahmoud and Jankowski (2011) modified the model accordingly.

A further model consisting in the introduction of a spring with non-uniform stiffness was proposed by Davis (1992) based on the following Hertz model:

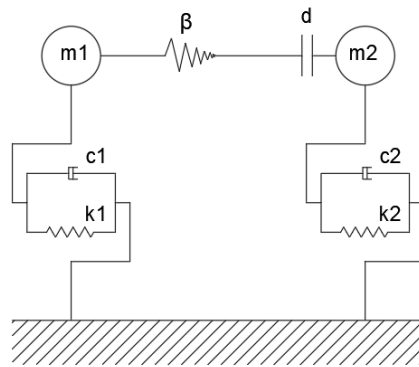


Figure 22. Hertz model

$$F(t) = \begin{cases} \beta\delta^{1.5}(t) & \delta(t) > 0 \\ 0 & \delta(t) \leq 0 \end{cases} \quad (3.9)$$

Where β is the impact stiffness parameter. Jankowski (2005) used default values of this parameter depending on the type of structure and material. In particular, for buildings with steel-to-steel impact it used $\beta = 4,66 \cdot 10^9 \text{ N/m}^{1.5}$, while for buildings with concrete-to-concrete impact it used $\beta = 1,13 \cdot 10^9 \text{ N/m}^{1.5}$.

This model does not consider the plastic behaviour and energy dissipation during the collision. For this reason, Muthukumar and DesRoches (2006) proposed an Hertz-based model in order to also consider the de-spatter energy dissipated during contact. This model, also known as the Hertzdamp model, introduces a non-linear damper in combination with the non-uniform stiffness spring:

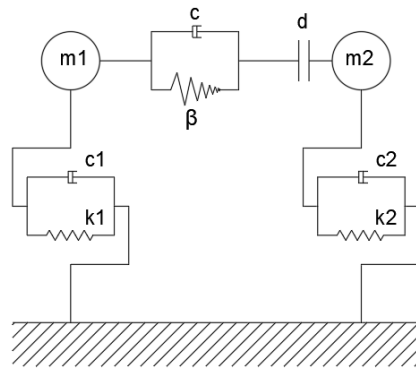


Figure 23. Hertzdamp model

$$F(t) = \begin{cases} \beta \delta^{1.5}(t) + C(t) \dot{\delta}(t) & \delta(t) > 0 \\ 0 & \delta(t) \leq 0 \end{cases}$$

$$C(t) = \xi \delta^{1.5}(t) \tag{3.10}$$

$$\xi = \frac{3\beta(1-e^2)}{5e(v_1 - v_2)}$$

Where $C(t)$ is the impact damping parameter.

This model was later modified by Ye, Li et al. (2009) defining a new value for the impact damping ratio.

A nonlinear viscoelastic model was developed by Jankowski (2005). In this model a non-linear spring following the Hertz law and a non-linear damper are applied to simulate the energy dissipation process:

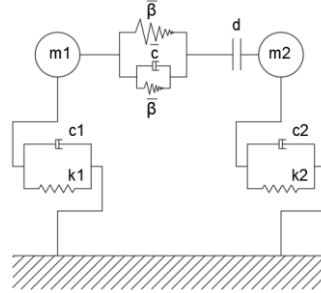


Figure 24. Nonlinear viscoelastic model

$$F(t) = \begin{cases} \bar{\beta}\delta^{1.5}(t) + \bar{c}(t)\dot{\delta}(t) & \delta(t) > 0; \dot{\delta}(t) > 0 \\ \bar{\beta}\delta^{1.5}(t) & \delta(t) > 0; \dot{\delta}(t) \leq 0 \\ 0 & \delta(t) \leq 0 \end{cases}$$

$$\bar{c}(t) = 2\bar{\xi} \sqrt{\bar{\beta} \sqrt{\delta(t)} \frac{m_1 m_2}{m_1 + m_2}} \quad (3.11)$$

$$\bar{\xi} = \frac{9\sqrt{5}}{2} \frac{1 - e^2}{e(e(9\pi - 16) + 16)}$$

Where $\bar{\beta}$ and $\bar{c}(t)$ are respectively the impact stiffness parameter and the impact damping parameter. In addition, Jankowski (2005) used default values of the impact stiffness parameter depending on the type of structure and the material. In particular, for buildings with steel-to-steel impact it used $\bar{\beta} = 1,03 \cdot 10^{10} \text{ N/m}^{1.5}$, while for buildings with concrete-to-concrete impact it used $\bar{\beta} = 2,75 \cdot 10^9 \text{ N/m}^{1.5}$.

Finally, Khatiwada, Chouw et al. (2011) proposed a viscous elastoplastic model that takes into account elastoplastic behaviour:

$$\begin{aligned}
F(t) &= \begin{cases} \bar{\beta}\delta^{1.5}(t) + \bar{c}(t)\dot{\delta}(t) & \bar{\beta}\delta^{1.5}(t) + \bar{c}(t)\dot{\delta}(t) < F_E; \dot{\delta}(t) > 0 \\ F_E & \bar{\beta}\delta^{1.5}(t) + \bar{c}(t)\dot{\delta}(t) \geq F_E; \dot{\delta}(t) > 0 \\ \bar{\beta}\delta^{1.5}(t) & \bar{\beta}\delta^{1.5}(t) < F_E; \dot{\delta}(t) \leq 0 \\ F_E & \bar{\beta}\delta^{1.5}(t) \geq F_E; \dot{\delta}(t) \leq 0 \end{cases} \\
\bar{c}(t) &= 2\bar{\xi} \sqrt{\bar{\beta}\sqrt{\delta(t)} \frac{m_1 m_2}{m_1 + m_2}} \\
\bar{\xi} &= \frac{9\sqrt{5}}{2} \frac{1 - e^2}{e(e(9\pi - 16) + 16)}
\end{aligned} \tag{3.12}$$

Where F_E is the yield strength of the structural element at the point of contact.

In addition, Polycarpou, Papaloizou et al. (2014) proposed a model for 3D MDOF systems to also take into account friction forces, structural eccentricity, irregularity in plan but also the effective impact area.

3.3. Estimation of maximum displacement

Approximated methods for estimating maximum displacements are commonly used for building vulnerability assessment.

The assessment of maximum displacements using approximated methods allows to easily evaluate the impact force due to the pounding effects, while reduce the computational workload.

The methods used to estimate the maximum displacement response in MDOF system are classified into 3 groups (Yaghmaei-Sabegh, Neekmanesh et al. 2017):

1. Methods based on equivalent SDOF systems, such as RA00 and LM10;
2. Methods based on displacement amplification factors, such as ASCE 41-06 and M99;
3. Methods based on equivalent linearization, such as BWML08 and YNL14.

The RA00 method proposed by Requena and Ayala (2000) is a variation of the CSM method, but differs from the latter in determining the Performance Point. In fact, a non-linear static

analysis is used in this method to determine the capacity curve of the structure. Subsequently, the original structure represented by an MDOF system is transformed into an equivalent SDOF system. The SDOF system is subject to one or more seismic excitations, while the maximum displacement is estimated by assess the Performance Point of the SDOF system. This displacement is then converted into the corresponding maximum top displacement of the MDOF system according to the following relationship:

$$u_{top} = S_d PF_1 \quad (3.13)$$

Where u_{roof} is the maximum top displacement of the structure, S_d is the spectral displacement corresponding to the fundamental mode of the structure and PF_1 is the first-mode modal participation factor.

A further method based on equivalent SDOF systems is the LM10 method proposed by Lin and Miranda (2010). This method is similar to RA00 because it uses the displacement response of an elastoplastic equivalent SDOF system to estimate the maximum top displacement of the structure. The modal analysis is conducted to obtain the fundamental period and the related modal participation factor. Then, the pushover analysis is performed to obtain the bilinear capacity curve. The yield strength of the structure V_y and the yield strength of the elastoplastic SDOF system $V_{y,SDOF}$ are evaluated by dividing the yield strength of the structure by the modal mass coefficient of the first mode. Thus, the inelastic displacement is calculated while the value of the maximum inelastic top displacement is computed as below:

$$u_{top} = PF_1 \Delta_i \quad (3.14)$$

Where PF_1 is the first modal participation factor and Δ_i is the inelastic displacement of the equivalent SDOF system.

The ASCE 41-06 (Displacement Coefficient Method DCM) is based on displacement amplification factors. In this method the target top displacement, u_{top} , can be obtained from the following expression:

$$u_{top,t} = C_0 C_1 C_2 S_a \left(\frac{T_e^2}{4\pi^2} \right) g \quad (3.15)$$

Where C_0 is a modification factor that relates the spectral displacement and the top displacement of the building, C_1 is a modification factor that relates the maximum expected inelastic displacements to the displacements calculated from a linear elastic analysis, C_2 is a modification factor that represents the effect of hysterical behaviour on the maximum displacement response, S_a is the response spectral acceleration, calculated considering the fundamental period, and T_e is the fundamental period of the building.

A further method was proposed by Miranda (1999) and is named as M99. This method is based on the elastic spectrum and use a set of corrective factors that depend on the number of stories, the distribution of lateral forces, and the proportion between flexural and shear deformations. In this method the multi-storey building is modeled as an equivalent continuous structure based on the combination of a flexible cantilevered beam and a sheared cantilevered beam. The maximum top displacement is obtained from the following equation:

$$u_{top} = \beta_1 \beta_3 S_d \quad (3.16)$$

Where S_d is the spectral displacement calculated considering the fundamental period, β_1 is an approximate participation factor representing the ratio of the maximum top displacement to the spectral displacement, while β_3 is the inelastic displacement ratio defined as the ratio of the maximum inelastic displacement and the maximum elastic displacement. Values of the aforementioned coefficients are given by the following equations:

$$\beta_1 = \frac{\sum_{j=1}^N \psi_j}{\sum_{j=1}^N \psi_j^2} \quad (3.17)$$

Where ψ_j is the assumed shape value at the j th floor level.

If a uniform story height, uniform mass distribution and triangular displacement form are assumed, this amplification factor can be calculated as follows:

$$\beta_1 = \frac{\sum_{j=1}^N \left(\frac{j}{N}\right)}{\sum_{j=1}^N \left(\frac{j}{N}\right)^2} = \frac{3N}{2N+1} \quad (3.18)$$

Where N is the number of story.

The coefficient β_3 is calculated as below:

$$\beta_3 = \frac{u_i}{u_e} = \left[1 + \left(\frac{1}{\mu} - 1 \right) \exp(-12T\mu^{-0.8}) \right]^{-1} \quad (3.19)$$

Where μ is the displacement ductility ratio.

This method allows the calculation of lateral displacements along the height through the following formula:

$$u(z) = \frac{W_{\max} H^4}{EI(1-e^{-a})} \left[C_1 \sinh \alpha \frac{z}{H} + C_2 \cosh \alpha \frac{z}{H} + C_3 e^{-\alpha z/H} + C_4 \left(\frac{z}{H} \right)^2 + C_5 \frac{z}{H} + C_6 \right] \quad (3.20)$$

Where W_{\max} is the intensity of the distributed load on the top, H is the total height, a is a dimensionless parameter that represents the shape of the lateral load and $C_1 - C_6$ are constants that depend on the constraint conditions.

The last group of approximated methods for estimating maximum displacements are methods based on equivalent linearization. Among the others, the BWML08 method proposed by

Browning, Warden et al. (2008) deals with the approximation of the maximum non-linear top displacements using the elastic response spectrum obtained considering an equivalent damping and an effective period:

$$u_{top} = PF_1 S_d(T_{eff}, 10\%) \quad (3.21)$$

Where PF_1 is the first modal participation factor and $S_d(T_{eff}, 10\%)$ is the spectral displacement considering an effective period depending on the area in which the building is located and a damping ratio of 10%.

The YNL14 method proposed by Yaghmaei-Sabegh, Neekmanesh et al. (2014) is very similar to the BWML08 method, but considers an effective period depending not only on the area, but also on the location of the earthquake compared to the building site, and a damping ratio of 9%:

$$u_{top} = PF_1 S_d(T_{eff}, 9\%) \quad (3.22)$$

All these approximated methods have been evaluated and compared by Yaghmaei-Sabegh, Neekmanesh et al. (2017).

In particular, 27 concrete models with different geometric properties were used to evaluate these methods. Obviously different modal analyses have been carried out in order to determine the dynamic characteristics of the structures, such as the fundamental period and the first modal participation factor. By comparing the results obtained using these methods with those obtained from non-linear dynamic analyses, it is possible to note that the average relative error is greater than 31% for the methods within the Group 1 and the Group 2. and less than 25,5% for the methods within the Group 3. However, the choice of the approximated method depends also on the available information about the reference structure. Although in all methods it is necessary to perform the modal analysis to obtain information on the dynamic behaviour of the structure,

some methods require the use of parameters that are obtained from pushover analysis.

Furthermore, Group 2 and 3 require only the elastic response spectrum.

4. Case study

The case study adopted to assess the accuracy of the proposed methods is an existing masonry building located within the historic center of L'Aquila, Italy. It is within a building aggregate and it represents the end of the two sides of the aggregate. For this reason, it is subject to pounding and torsional effects due to the presence of adjacent buildings.



Figure 25. Case study

4.1. Territorial organization

As previously mentioned, the building is located in the historic center of L'Aquila, Italy, precisely at the corner of Via G. Verdi and Via Tempera, and falls within the "A" area of the PRG called "Centro Storico". A few meters away there is the important crossroads called

"Quattro Cantoni" corresponding to the intersection of the two main directions on which the urban development of the city has been grafted. Due to its centrality, the area has always played an important role in urban planning. For this reason the area has been subject to significant changes over time.



Figure 26. Extract of cadastral plan



Figure 27. Extract of PRG

The building is located in an area of sub-flat morphology, located at an altitude of about 730 m a.s.l. The stratigraphy of the soil is characterized by a first layer of soil and the presence of clayey silt up to 12,50 m. Below this level there are calcareous breccias of 1-3 cm diameter in a limo-clayey matrix. So, the subsoil category is C and the topographic category is T1.

In addition, the area has been home to numerous destructive earthquakes. Among these we remember the most recent earthquake of L'Aquila in 2009. The following is also added:

- the sequence of 1703 and the earthquake of the Marsica (1915);

- some earthquakes that hit the L'Aquila area, destructive (1315, 1461 and 1762) or otherwise quite strong (1958);
- the event of 1639, which damaged the basin of Amatrice;
- the events of 1950 and 1951 in the area north of the Gran Sasso;
- the events of 1706 and 1933 in the Maiella area.

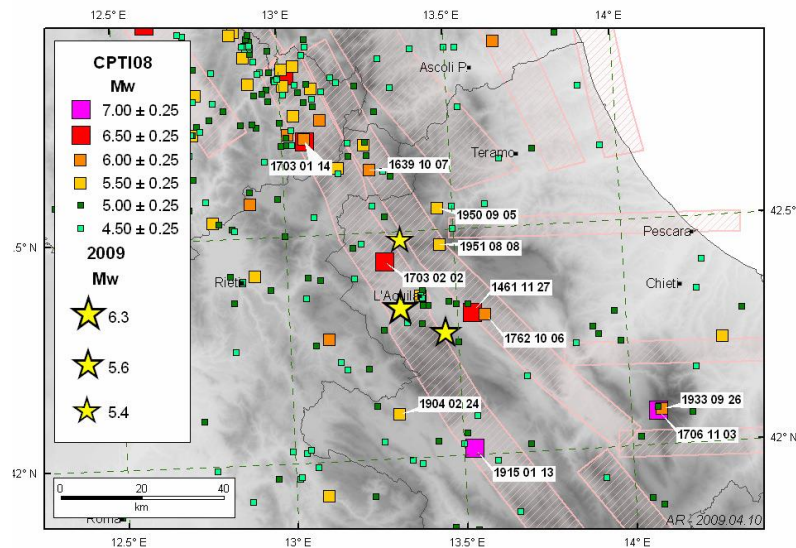


Figure 28. History of earthquakes in L'Aquila area

The area of interest is part of the “Carta delle microzone omogenee in prospettiva sismica” (MOPS) in a stable area susceptible to local amplification. Therefore, it is an area in which amplifications of seismic motion are expected, as an effect of the local litho-stratigraphic and morphological order.



Figure 29. Extract of MOPS

4.2. Historical-critical analysis

As can be seen from the previous images, the aggregate in question is part of a much larger block circumscribed by the following roads: Via G. Verdi, Via Tempera, Via San Bernardino and Via San Giovanni da Capestrano. The aforementioned block is characterized by a set of heterogeneous buildings by type, by structure and also by the time of construction. This heterogeneity is due to interventions carried out in different eras, consisting of new buildings to replace previous building organisms, or from new construction to saturation of interstitial empty spaces between the existing building. Inside the block the portion for which there is a certain structural homogeneity is evidently the part overlooking Via Tempera and part of Via Verdi and Via San Bernardino. This part is certainly the oldest part of the block and is structurally separated from the remaining part of the most recently built by means of technical joints.

Below is presented the material available that has allowed to elaborate a probable reconstruction of the constructive history of the aggregate.

The oldest representation available (Carta dell'Antonelli 1622, engraved by Lauro) shows the presence of buildings of considerable importance, such as the Basilica di San Bernardino da Siena (2), the “Ospedale Maggiore” (3) and the “Seminario” (4). The latter included the entire block under consideration. From this paper it is possible to hypothesize that the buildings on Via Tempera can all be built on a wall of a similar closed place. This hypothesis is supported by the fact that the canton between Via Tempera and Via Verdi is very late (mid-19th century), built only to compensate for the subsequent modifications of the corner building. In addition, it is possible to note that there is a small church at the intersection of Via Tempera and Via San Bernardino.



Figure 30. "Carta dell'Antonelli", 1622

In the plan of Vandi of 1753 after the disastrous earthquake of 1703, it is noted that the built on Via Tempera is not continuous, but presents a central void. The “Seminario” probably destroyed by the earthquake is no longer visible. In addition, it should be noted that the building at the corner of Via Verdi and Via Tempera (case study) presents the old alignment to the palace on the other side of Via Tempera, called “Palazzo Galeota”.



Figure 31. Vandi, 1753

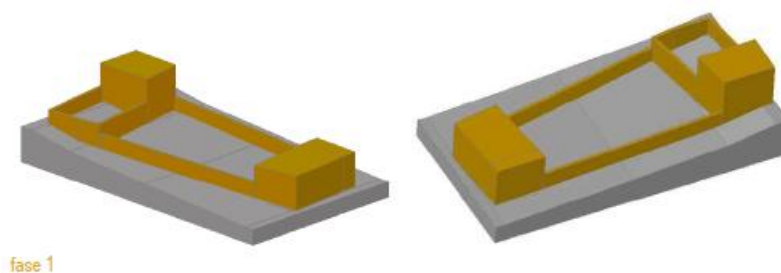
The central void on Via Tempera is also present on the “Piano di Catalani”, 1829. Instead, from the “Rilievo dell’Esercito Italiano” of 1888 it is possible to notice how this void is filled, making the built on Via Tempera continuous. For this reason, we can date the construction of this intermediate building between 1829 and 1888. It should also be noted that in the same period of time the buildings on Via Verdi have been set back losing all the premises that gave on the ancient alignment, preserving only the cellars that are still visible and almost inexplicably located below Via Verdi.



Figure 32. Relief of Italian Army

In the 1932 intervention of Eng. Valentini also the facade of “Palazzo Galeota” is set back to align with the buildings of Via Verdi. The building of the aggregate on Via Verdi was substantially what appears today, except for the portion of the building placed on the left side. This portion was demolished in the '70s to build the current reinforced concrete construction.

Below are the volumes corresponding to the phases and constructive assumptions of the aggregate:



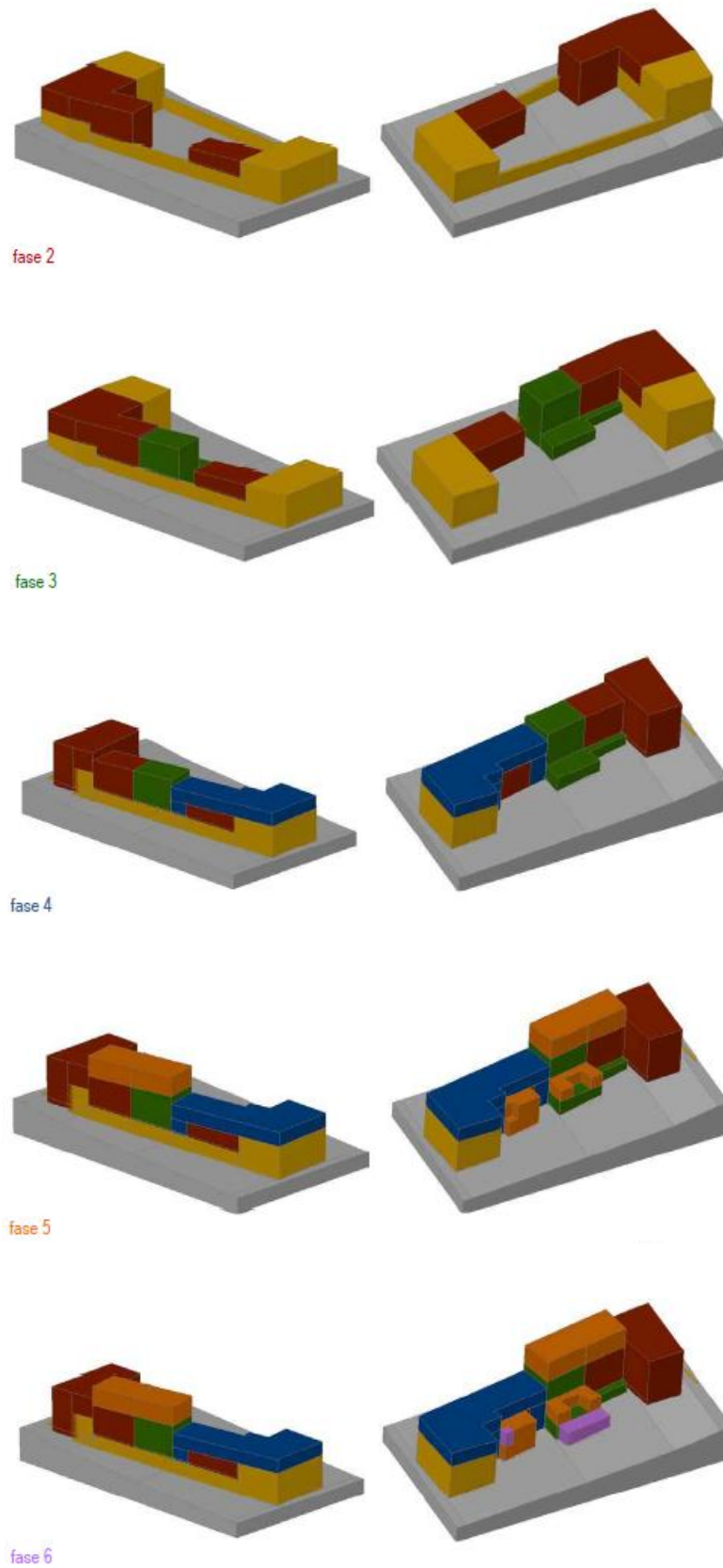


Figure 33. Construction phases of the aggregate

4.3. Description of Structural Unit

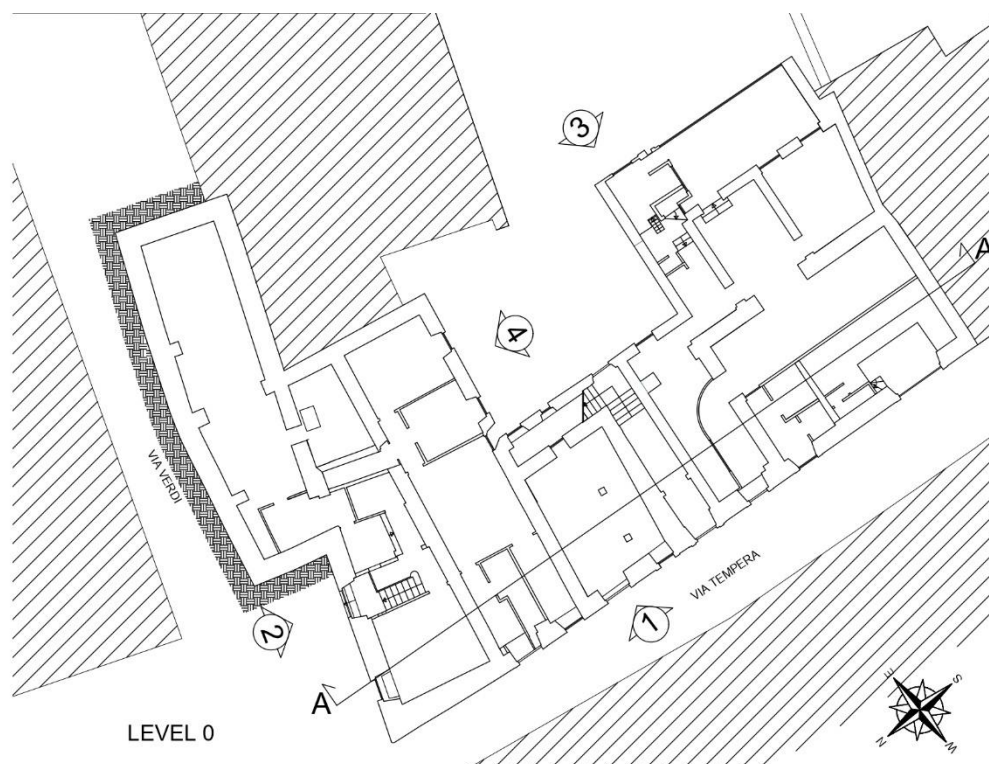
The Structural Unit is divided into two buildings (Building A and Building B):

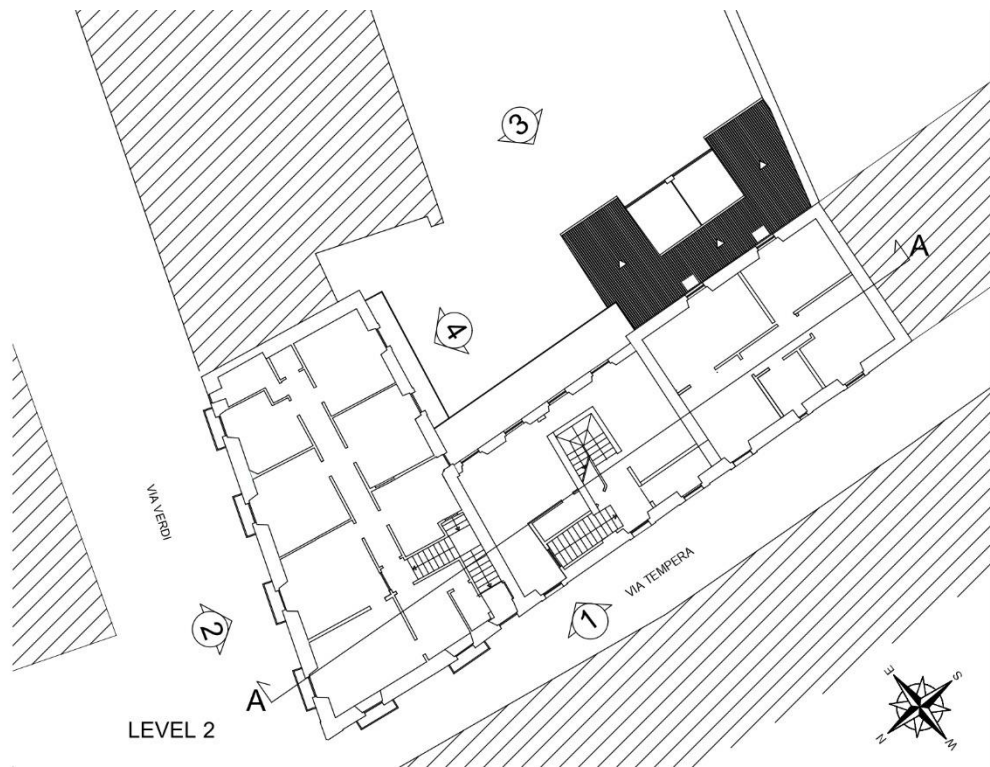
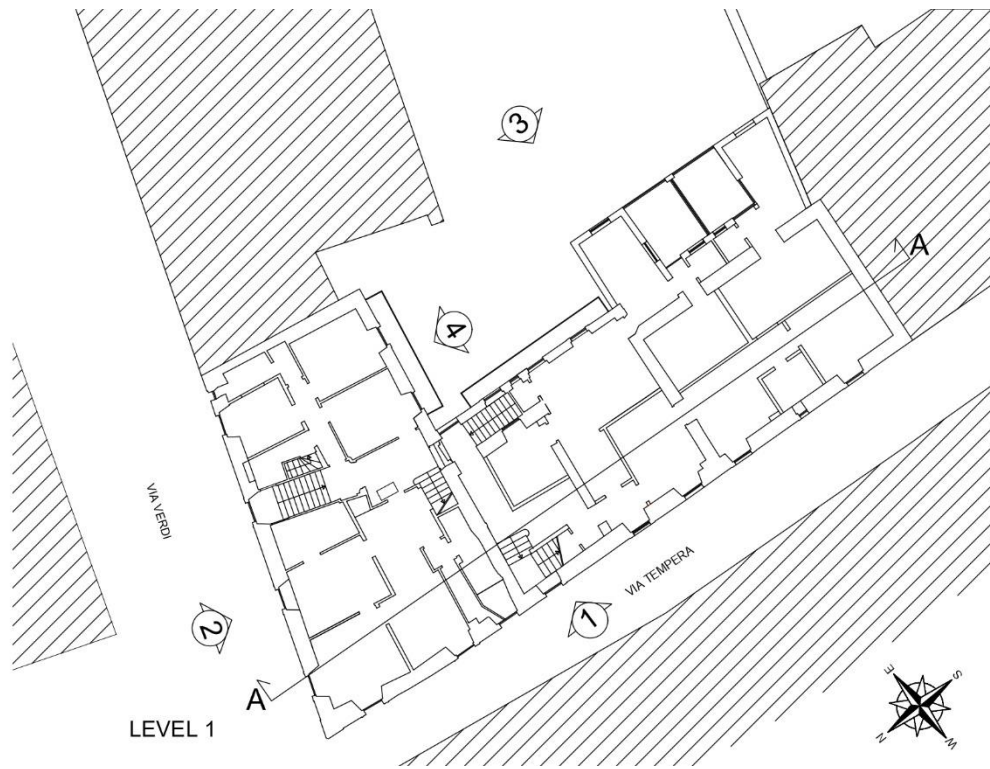
- Building A: located at the corner of Via G. Verdi and Via Tempera. The property has a mainly residential destination and is divided into n.2 housing units, n.2 professional studios and n.1 commercial activities. The period of construction of the building in its present shape can be traced back to the second half of 1800. It is divided into n.2 floors above ground and attic and a basement. Structurally the building is characterized by a vertical supporting structure in disordered stone. It should be noted that the distribution of the load-bearing walls is such as to determine a great seismic vulnerability. In fact, the load-bearing walls are distributed on the perimeter of the building while inside there are no transverse or longitudinal walls. Different types of horizontal structures can be identified. For the first deck are used ceilings in vaulted bricks and beams. For the remaining floors and the roofing are used slabs in beams and tiles. In addition, the roof is marked by a fairly recent intervention on the supporting structure with the insertion of steel trusses and the construction of a curb in c.a. All the intermediate floors are characterized by flexibility in the plan and the absence of perimeter curb or the use of chains and tie rods. In addition, due to the lack of intermediate walls, the horizons have a remarkable light because they rest on the perimeter walls;
- Building B: located in Via Tempera. The property has a predominantly residential destination with the exception of some commercial premises on the ground floor. The period of construction of the building can be traced back to the second half of 1800, but there is an elevation of about n.2 floors that can be traced back to the early years of 1900. In addition, it should be noted that the building has been the subject of various interventions that can be classified as internal works even in more recent times. To these interventions is added an intervention carried out at the beginning of 1990 to restructure the last plan and the coverage. The planimetric conformation is quite regular; it has a

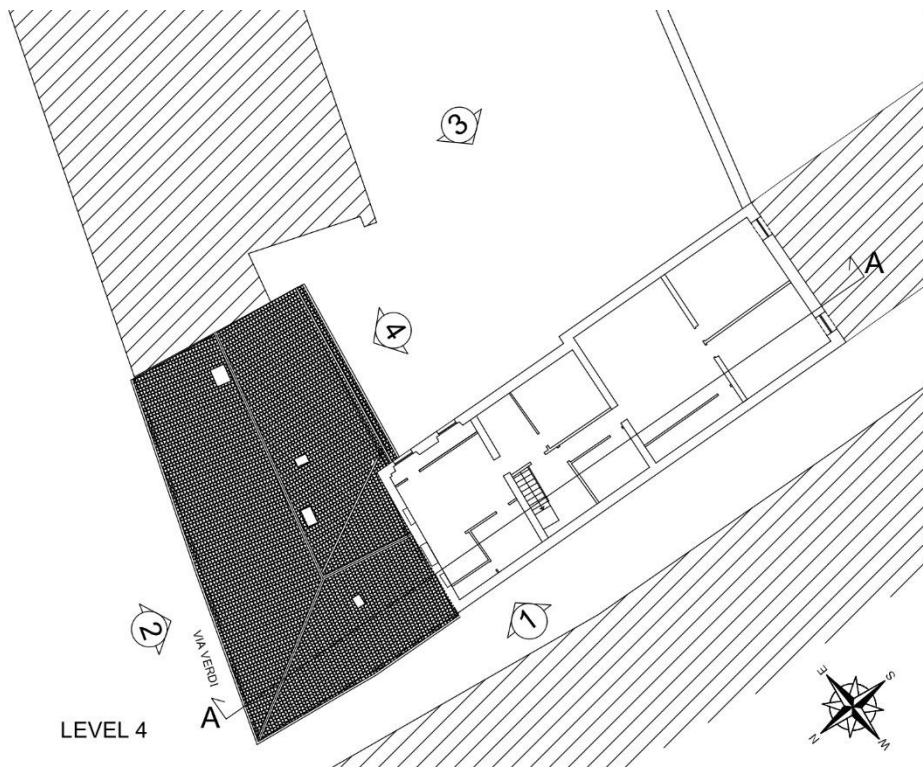
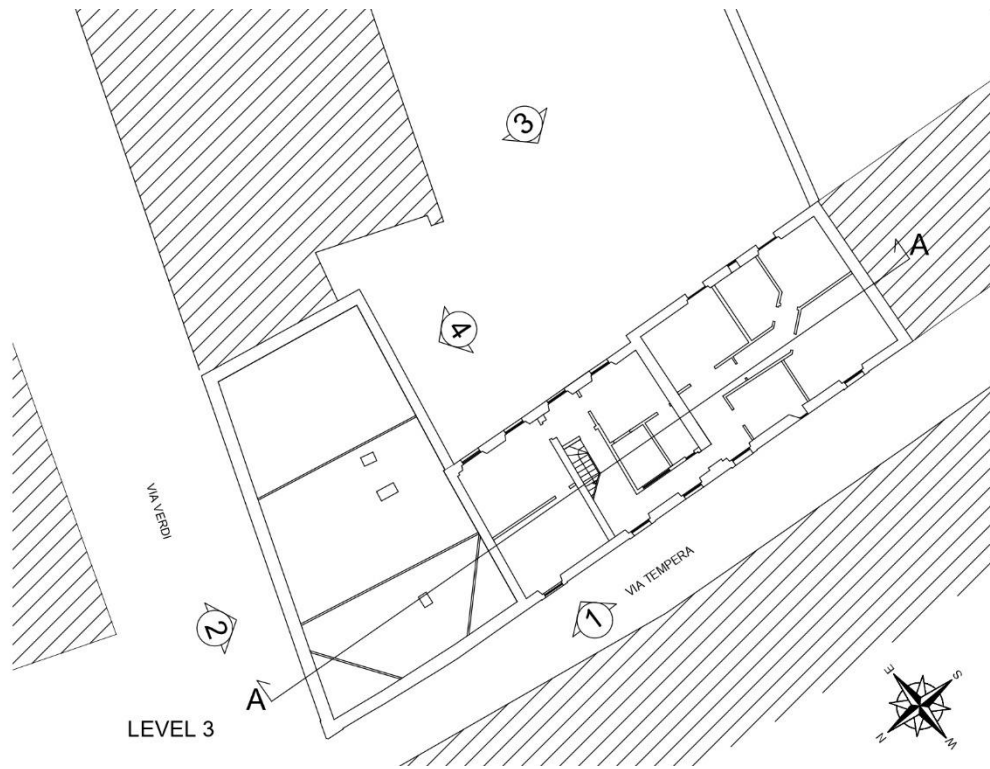
rectangular matrix plant characterized by an expansion on the inner side of the high court n.2 floors. Structurally the building is characterized by a vertical load-bearing structure that has two types of masonry equipment: for the first three levels is used a messy stone masonry, while for the last two floors a solid brick masonry is used. Also with regard to the horizontal load-bearing structures there are different types. In particular, there are stone vaults plastered with ribs and lunettes, stone barrel vaults, slabs and steel beams and slabs with supporting structure in wood and reinforced screed. The roof is made with simple warping wooden structure of the type not pushing with brick tiles. The flexibility in the horizontal structure plane is aggravated by the absence of intermediate perimeter kerbs and elements to ensure adequate box behaviour such as chains or tie rods.

4.4. Geometrical relief

Below is an extract of the geometric relief of the Structural Unit:







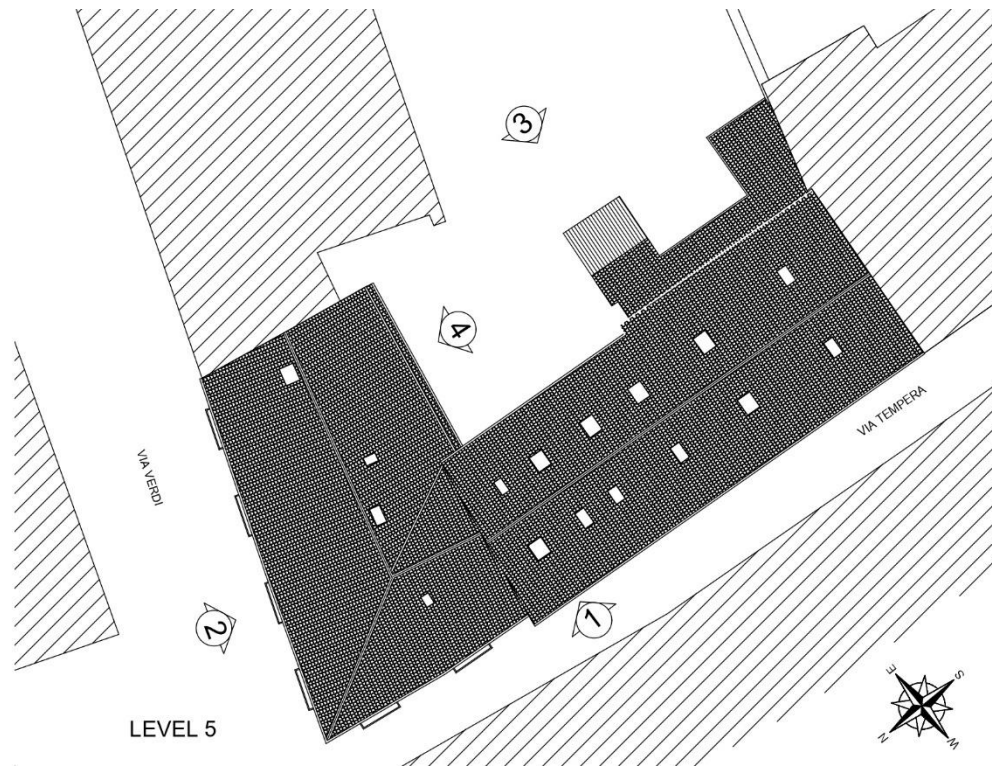
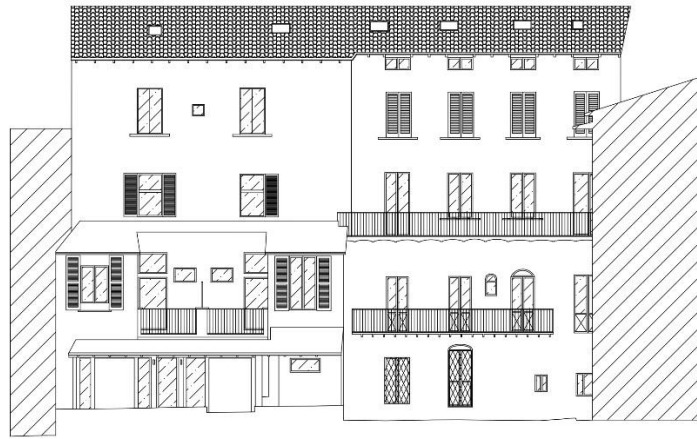


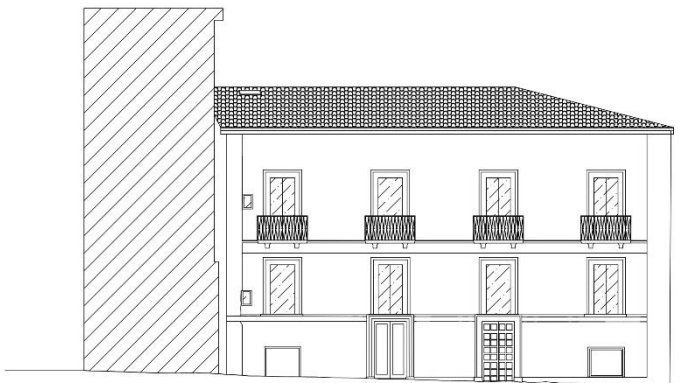
Figure 34. Geometric relief - Floor plans



02 internal Via Tempera



03 Via Verdi



04 internal Via Verdi

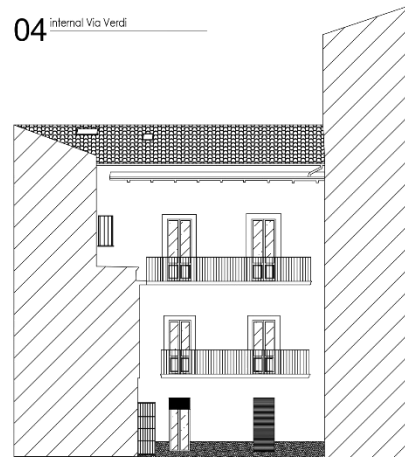


Figure 35. Geometrical relief - Prospectus

SECTION A-A

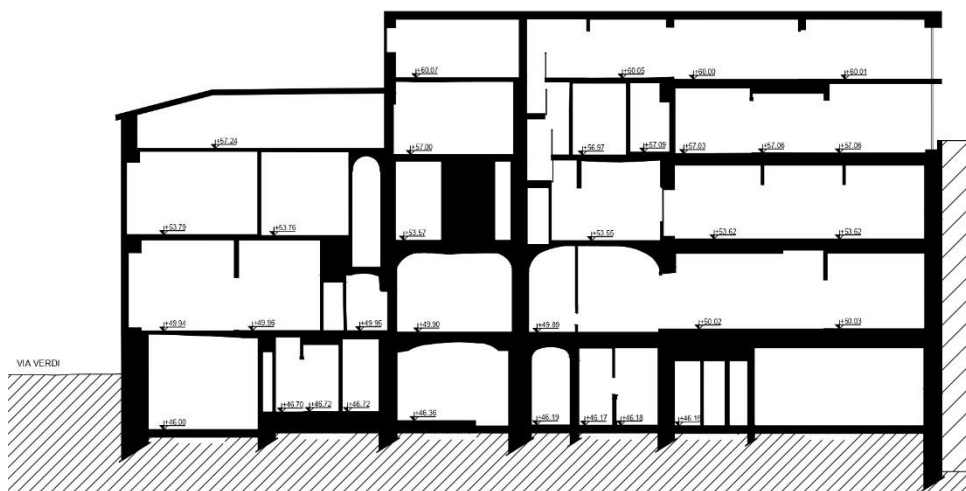


Figure 36. Geometrical relief - Section

4.5. Technical-constructive relief

Below is an extract of the technical-constructive relief of the Structural Unit identifying the different structural types for vertical and horizontal structures:

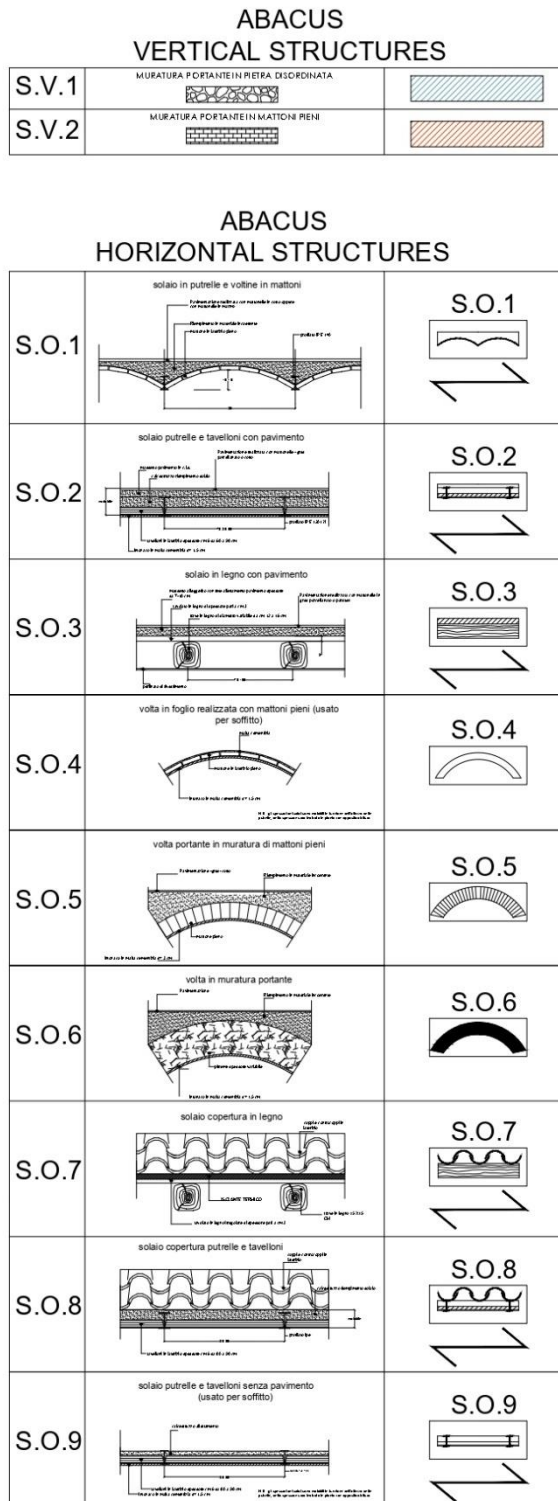
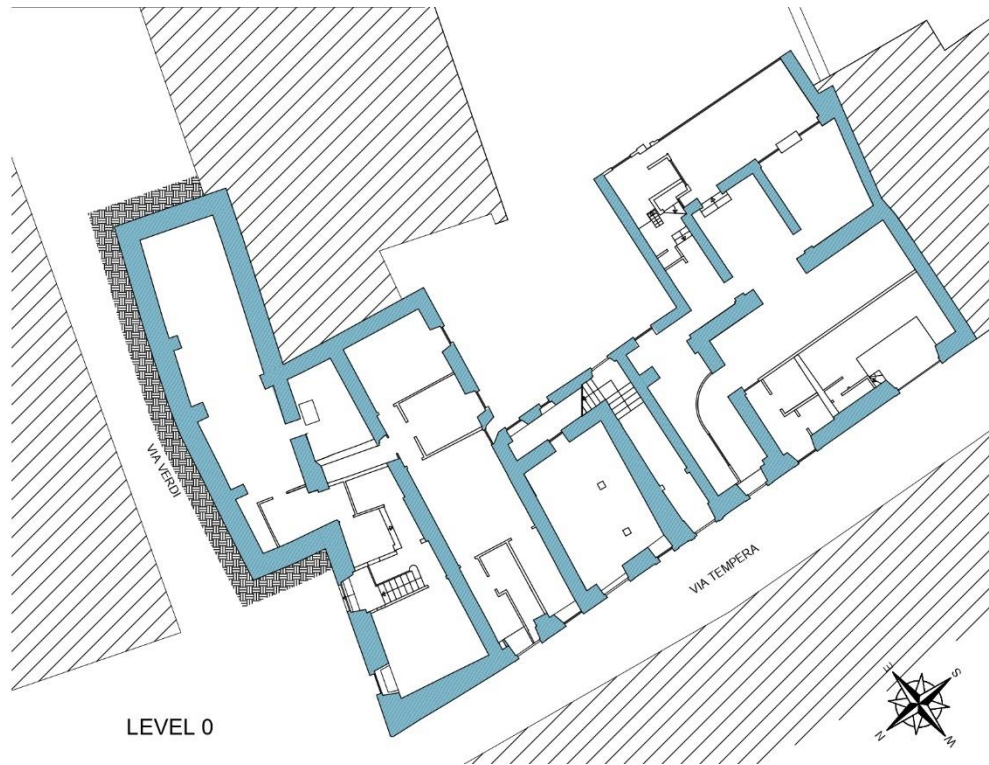


Figure 37. Technical-constructive relief - Abacus





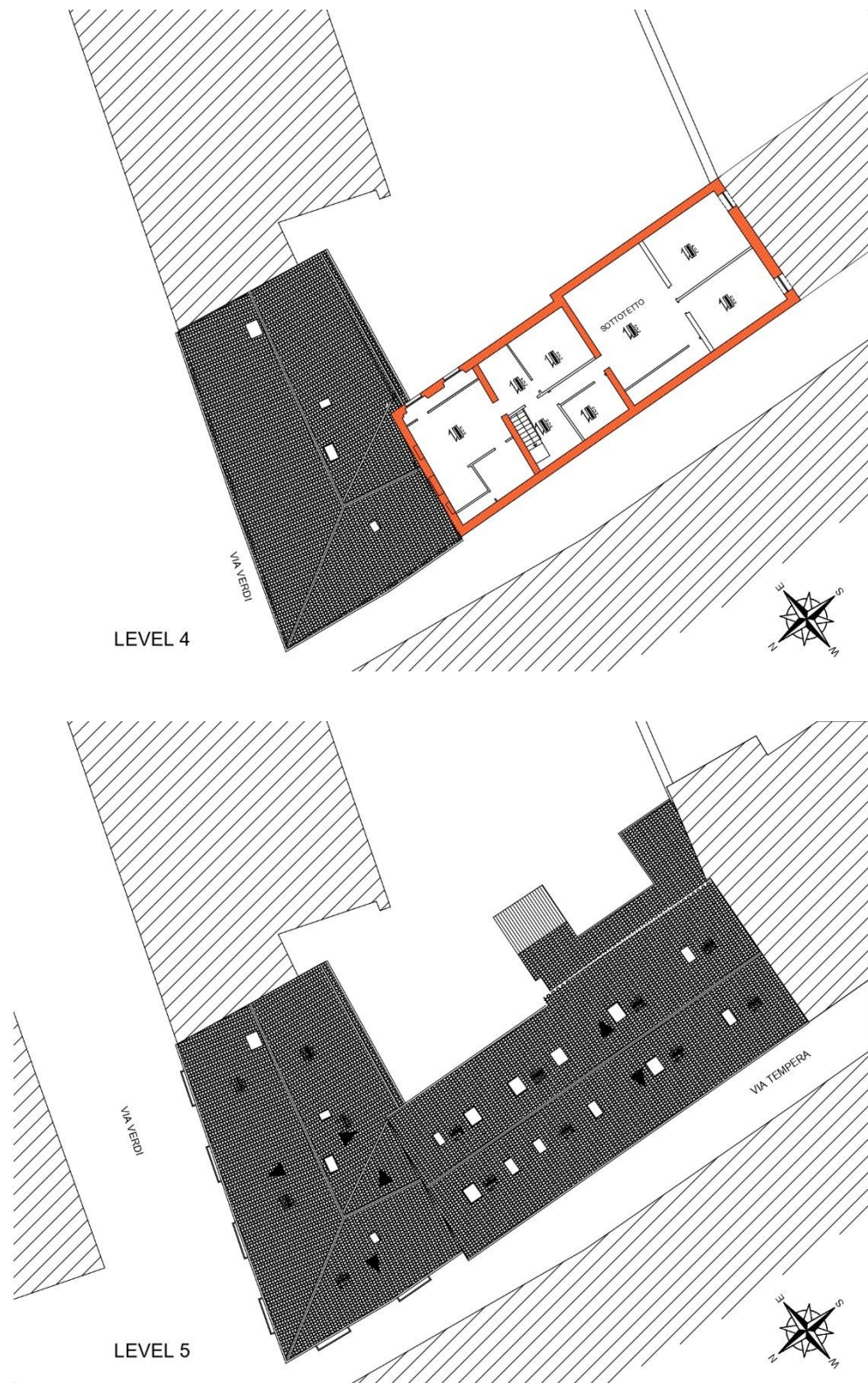


Figure 38. Technical-constructive relief - Floor plans

4.6. Adjacent buildings

The following paragraph describes the buildings adjacent to the case study building in order to study the possible interaction between them. The buildings considered are Building C and Building D:

- Building C: located at the corner of Via Tempera and Via S. Bernardino. The property is divided into n.8 units of which n.3 intended for housing, n.1 for use as a laboratory on the first floor, n.3 commercial premises on the ground floor and n.1 storage room on the ground floor. This building has a structure and technological-constructive characterization similar to the Structural Unit being studied. As there is no information about the roof, it is assumed that a roof with simple warped wooden structure of the type not pushing with brick roof tiles, such as Building B. There is a common boundary wall between Building C and Building B. In addition, As can also be seen from the facades, the floors of Building C are offset by half a floor compared to the floors of Building B due to the slope of Via Tempera.

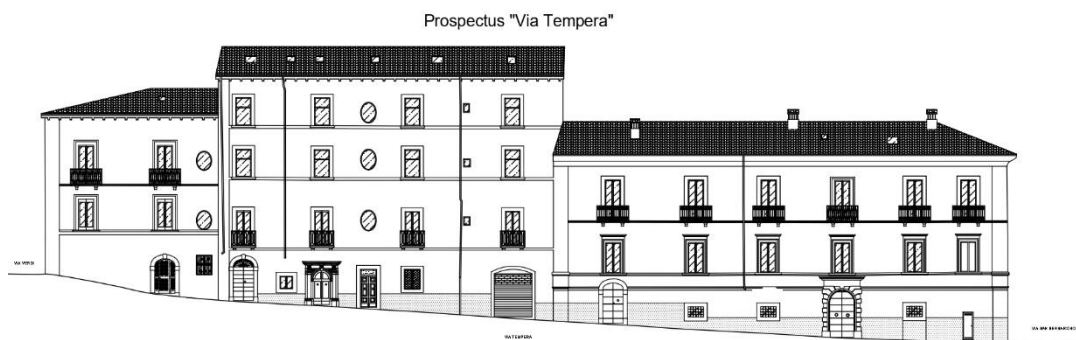


Figure 39. Facade "Via Tempera" with Building C

- Building D: located in Via Verdi. The building, as previously described, was demolished during the 70s to realize the current construction in c.a. There is no technical separation joint between Building D and Building A. Moreover, it was not possible to obtain detailed information about the geometric relief and construction techniques, but, from the analysis of the elevations, it is possible to notice that the floors of the two buildings are offset by half a floor.

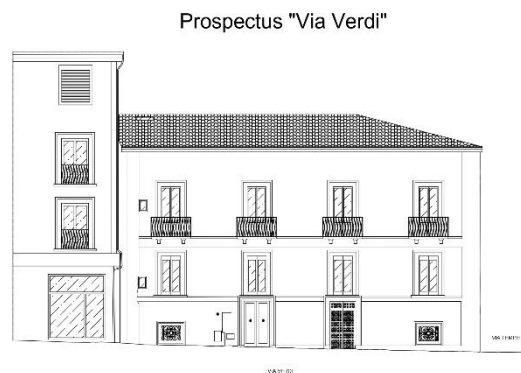


Figure 40. Facade "Via Verdi" with Building D

5. Case study model

This section describes the case study modeling with the SAP2000 program.

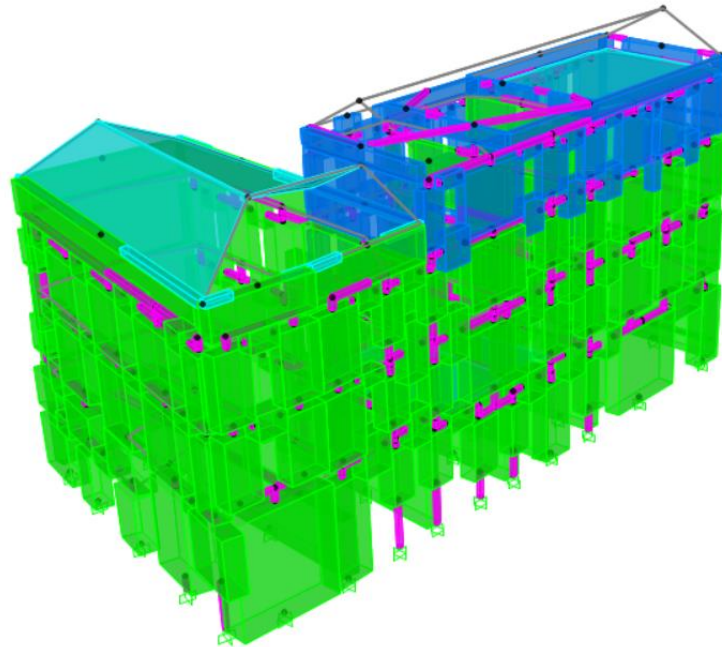


Figure 41. 3D Model

5.1. Equivalent frame model

Equivalent frame modeling allows the analysis of three-dimensional buildings with an acceptable computational effort compared to non-linear FEM modeling.

The modeling of the structure adopted in this work is based on the Simplified Analysis Method (SAM) proposed by Magenes (2000). The SAM method allows the modeling of masonry walls as an equivalent 2D frame. The frame is composed of vertical and horizontal one-dimensional

elements (piers and spandrels, respectively) deformable axially and shear. These elements are connected to each other at the end by rigid offsets.

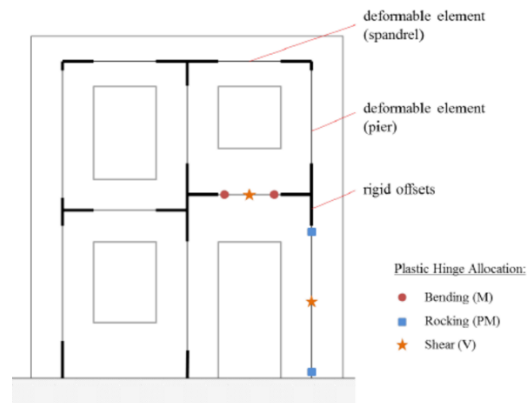


Figure 42. SAM Method

The piers are defined excluding the spandrels affected by the openings. Each element is represented by its barycentric axis and consists of a deformable part with finite resistance and infinitely rigid parts at the end. The deformable height of the piers is calculated according to the theory of Dolce (1989) by the following relation:

$$H_{eff} = h' + \frac{1}{3} D \frac{(H' - h')}{h'} \quad (5.1)$$

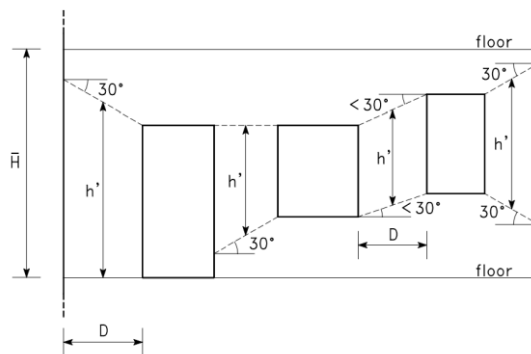


Figure 43. Theory of Dolce

The deformable part of the spandrels corresponds to the free light of the opening.

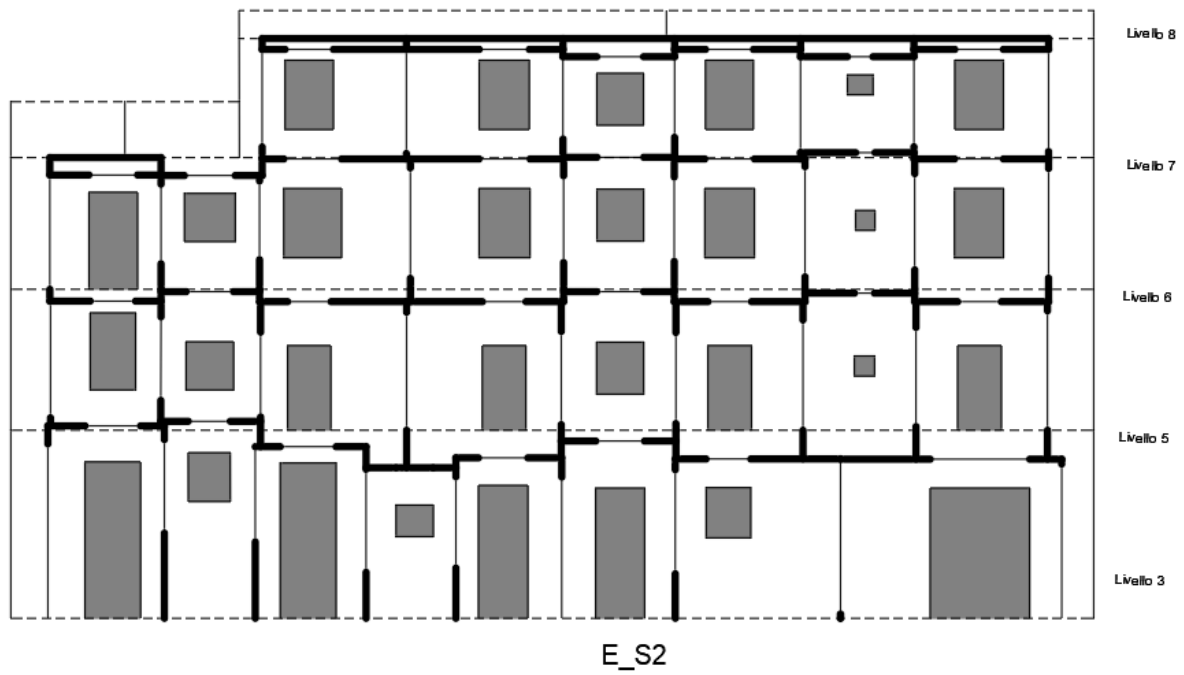


Figure 44. Example of equivalent frame

Slab modelling by assessing the appropriate degree of deformability completes the three-dimensional frame. In this work the slabs have been modeled with shell elements in order to correctly define the stiffness and thickness.

In addition, the foundations are built by means of the wall padding for at least one metre from the ground floor. For this reason, joints were inserted at the base of the individual vertical elements.

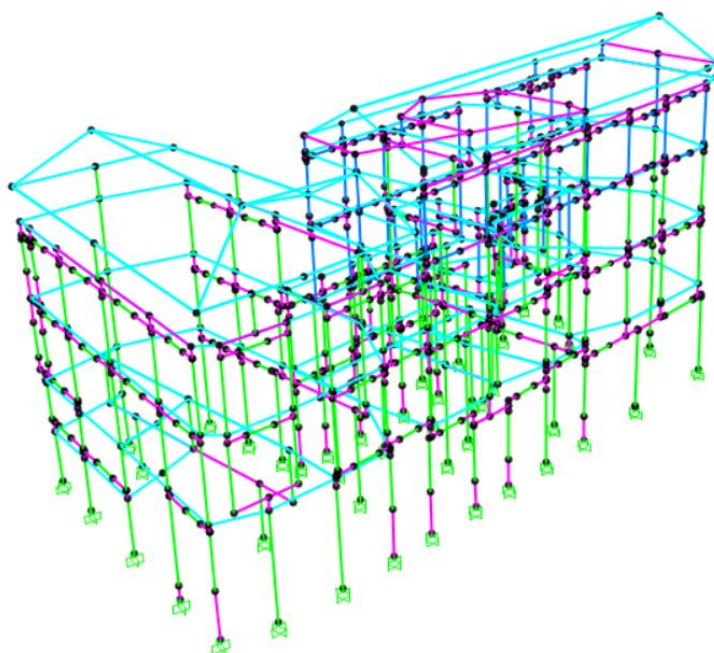


Figure 45. Equivalent frame model

5.2. Material properties

The mechanical characteristics of the materials of which they are made have been defined for each element constituting the model.

Below is a table with the mechanical characteristics of each material:

| Material | w [kN/m ³] | E [N/mm ²] |
|---------------------|------------------------|------------------------|
| Stone walls | 19 | 870 |
| Solid brick masonry | 18 | 1500 |
| Rigid Link Material | 0 | 2,00E+8 |
| C20/25 | 25 | 30000 |

Table 1. Material properties

In particular, for masonry materials the mechanical characteristics have been defined through table C8.5.I of the NTC18. It has been considered a Level of Knowledge LC1 and no improvements in the state of fact. The mechanical characteristics are as follows:

| Material | f [N/mm ²] | τ_0 [N/mm ²] | E [N/mm ²] | G [N/mm ²] | w [kN/m ³] |
|-------------|------------------------|-------------------------------|------------------------|------------------------|------------------------|
| Stone | 1 | 0,018 | 870 | 290 | 19 |
| Solid brick | 2,6 | 0,05 | 1500 | 500 | 18 |

Table 2. Mechanical characteristics of masonry

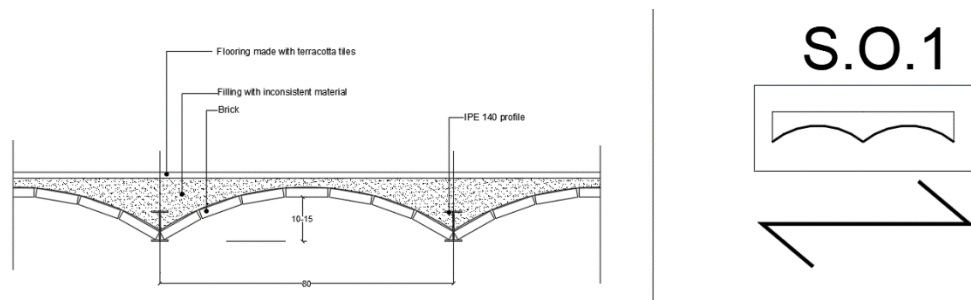
5.3. Evaluation of actions

The following paragraph describes the actions acting on the structure. The classification and determination of these actions was made according to the indications of NTC18.

5.3.1. Load analysis

Permanent structural (G1), permanent non-structural (G2) and variable loads (Q) have been determined for each type of slab:

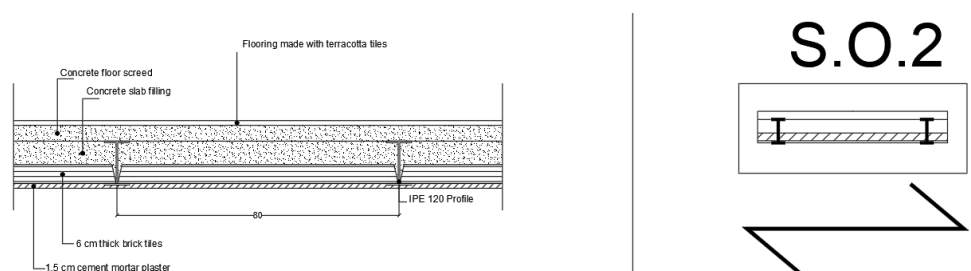
- SO1:



| Description | Thickness [m] | Specific weight [kN/m] | Specific weight [kN/m ³] | Weight [kN/m ²] |
|---|---------------|------------------------|--------------------------------------|-----------------------------|
| IPE 140 Profile (i=80cm) | - | 0,129 | - | 0,161 |
| Brick | - | - | - | 0,756 |
| Filling with inconsistent material | 0,1 | - | 8 | 0,8 |
| Structural permanent load G1 | | | | 1,72 |
| Flooring made with terracotta tiles | - | - | - | 0,8 |
| Cement mortar plaster | 0,015 | - | - | 0,3 |
| Interior partitions | - | - | - | 1,2 |
| Non-structural permanent load G2 | | | | 2,3 |
| Variable load Cat. A Q | | | | 2 |

Table 3. Load analysis SO1

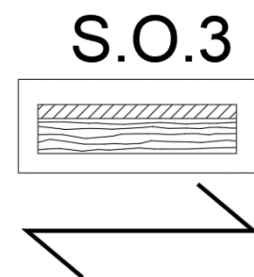
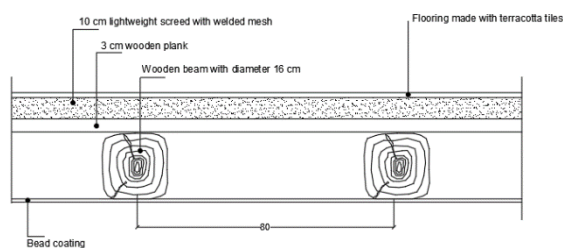
- SO2:



| Description | Thickness [m] | Specific weight [kN/m] | Specific weight [kN/m ³] | Weight [kN/m ²] |
|---|---------------|------------------------|--------------------------------------|-----------------------------|
| IPE 120 Profile (i=80cm) | - | 0,104 | - | 0,13 |
| Thick brick tiles | 0,06 | - | - | 0,39 |
| Concrete slab filling | 0,06 | - | 23 | 1,38 |
| Structural permanent load G1 | | | | 1,9 |
| Concrete floor screed | 0,04 | - | 13 | 0,52 |
| Cement mortar plaster | 0,015 | - | - | 0,3 |
| Interior partitions | - | - | - | 1,2 |
| Non-structural permanent load G2 | | | | 2,02 |
| Variable load Cat. A Q | | | | 2 |

Table 4. Load analysis SO2

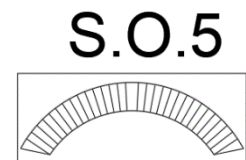
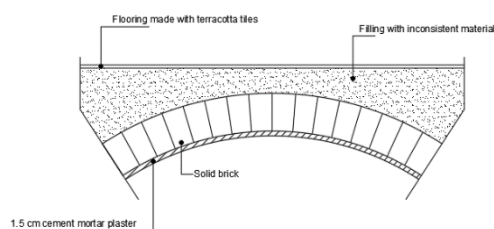
- SO3:



| Description | Thickness [m] | Specific weight [kN/m] | Specific weight [kN/m ³] | Weight [kN/m ²] |
|--|---------------|------------------------|--------------------------------------|-----------------------------|
| Wooden beam with diameter 16 cm (i=80cm) | - | 0,2048 | 8 | 0,256 |
| Wooden plank | 0,03 | - | 8 | 0,18 |
| Lightweight screed with welded mesh | 0,1 | - | 14 | 1,4 |
| Structural permanent load G1 | | | | 1,836 |
| Flooring made with terracotta tiles | - | - | - | 0,4 |
| Cement mortar plaster | 0,015 | - | - | 0,3 |
| Interior partitions | - | - | - | 1,2 |
| Non-structural permanent load G2 | | | | 1,9 |
| Variable load Cat. A Q | | | | 2 |

Table 5. Load analysis SO3

- SO5:

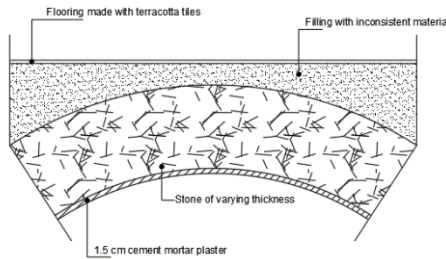


| Description | Thickness [m] | Specific weight [kN/m] | Specific weight [kN/m ³] | Weight [kN/m ²] |
|-------------------------------------|---------------|------------------------|--------------------------------------|-----------------------------|
| Solid brick | 0,12 | - | - | 2,16 |
| Structural permanent load G1 | | | | 2,16 |

| | | | | |
|---|-------|---|----|-------------|
| Filling with inconsistent material | 0,22 | - | 22 | 6,38 |
| Flooring made with terracotta tiles | - | - | - | 0,4 |
| Cement mortar plaster | 0,015 | - | - | 0,3 |
| Interior partitions | - | - | - | 1,2 |
| Non-structural permanent load G2 | | | | 3,66 |
| Variable load Cat. A Q | | | | 2 |

Table 6. Load analysis SO5

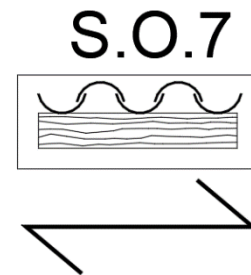
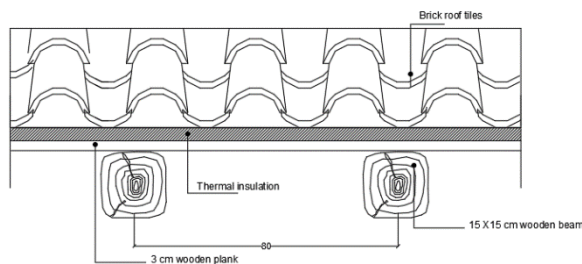
• SO6:



| Description | Thickness [m] | Specific weight [kN/m] | Specific weight [kN/m ³] | Weight [kN/m ²] |
|---|---------------|------------------------|--------------------------------------|-----------------------------|
| Stone | 0,2 | - | 22 | 4,4 |
| Structural permanent load G1 | | | | 4,4 |
| Filling with inconsistent material | 0,16 | - | 22 | 3,52 |
| Flooring made with terracotta tiles | - | - | - | 0,4 |
| Cement mortar plaster | 0,015 | - | - | 0,3 |
| Interior partitions | - | - | - | 1,2 |
| Non-structural permanent load G2 | | | | 5,35 |
| Variable load Cat. A Q | | | | 2 |

Table 7. Load analysis SO6

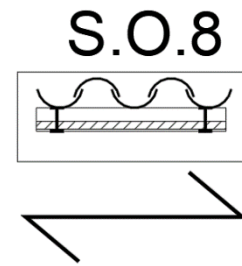
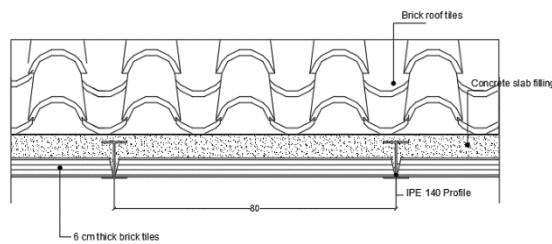
• SO7:



| Description | Thickness [m] | Specific weight [kN/m] | Specific weight [kN/m ³] | Weight [kN/m ²] |
|--|---------------|------------------------|--------------------------------------|-----------------------------|
| Wooden beam with diameter 15 cm (i=80cm) | - | 0,18 | 8 | 0,225 |
| Wooden plank | 0,03 | - | 8 | 0,18 |
| Structural permanent load G1 | | | | 0,405 |
| Thermal insulation | - | - | - | 0,16 |
| Brick roof tiles | - | - | - | 0,8 |
| Non-structural permanent load G2 | | | | 0,96 |
| Variable load Cat. H Q | | | | 0,5 |

Table 8. Load analysis SO7

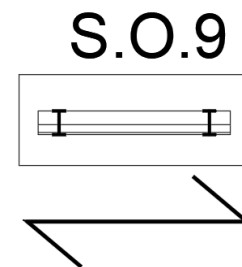
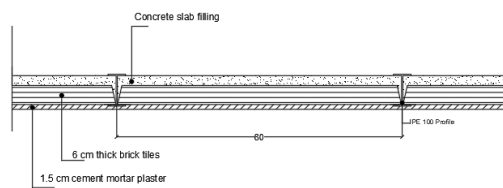
- SO8:



| Description | Thickness [m] | Specific weight [kN/m] | Specific weight [kN/m ³] | Weight [kN/m ²] |
|---|---------------|------------------------|--------------------------------------|-----------------------------|
| IPE 140 Profile (i=80cm) | - | 0,129 | - | 0,16125 |
| Thick brick tiles | 0,06 | - | - | 0,39 |
| Concrete slab filling | 0,08 | - | 23 | 1,84 |
| Structural permanent load G1 | | | | 0,55125 |
| Brick roof tiles | - | - | - | 0,8 |
| Non-structural permanent load G2 | | | | 0,8 |
| Variable load Cat. H Q | | | | 0,5 |

Table 9. Load analysis SO8

- SO9:



| Description | Thickness [m] | Specific weight [kN/m] | Specific weight [kN/m ³] | Weight [kN/m ²] |
|---|---------------|------------------------|--------------------------------------|-----------------------------|
| IPE 100 Profile (i=80cm) | - | 0,081 | - | 0,10125 |
| Thick brick tiles | 0,06 | - | - | 0,39 |
| Structural permanent load G1 | | | | 0,49125 |
| Concrete slab filling | 0,04 | - | 22 | 0,88 |
| Cement mortar plaster | 0,015 | - | - | 0,3 |
| Interior partitions | - | - | - | 1,2 |
| Non-structural permanent load G2 | | | | 2,38 |
| Variable load Cat. H Q | | | | 0,5 |

Table 10. Load analysis SO9

5.3.2. Snow action

The snow load on covers shall be assessed as follows:

$$q_s = q_{sk} \cdot \mu_i \cdot C_E \cdot C_t \quad (5.2)$$

Where:

- q_{sk} is the reference value of the ground snow load calculated as follows:

$$q_{sk} = 0,51 \left[1 + \left(\frac{a_s}{481} \right)^2 \right] = 0,51 \left[1 + \left(\frac{740}{481} \right)^2 \right] = 1,72 \text{ kN/m}^2$$

- μ_i is the coefficient of shape of the roof as a function of the inclination of the roof. In the present case the inclination is less than 30° . Therefore, $\mu_i=0.8$.
- C_E is the exposure coefficient. In the present case the topography is normal and $C_E=1$;
- C_T is the thermal coefficient placed cautiously equal to 1.

Therefore, the snow load is equal to:

$$q_s = q_{sk} \cdot \mu_i \cdot C_E \cdot C_t = 1,72 \cdot 0,8 \cdot 1 \cdot 1 = 1,37 \text{ kN/m}^2$$

5.3.3. Seismic action

The seismic action was evaluated according to the NTC18 and as described above in Ch. 2.1.

The design seismic action was calculated using the OPENSIGNAL software developed by Cimellaro and Marasco (2014). With this software it was possible to determine the design spectra and the values of the reference seismic parameters for the different Limit States. The following design parameters were used:

- | | | |
|--------------------------------|---------|---------|
| • Longitude: | 13,4006 | |
| • Latitude: | 42,3509 | |
| • Limit State: | SLV-SLC | SLO-SLD |
| • Behaviour factor q: | 1,5 | 1 |
| • Nominal design life, V_N : | 50 | |
| • Coefficient of use, C_U : | 1 | |
| • Soil category: | C | |

- Topographical conditions: T1
- Viscous damping, ξ : 5%

The following are the values of the a_g , F_0 and T_C^* parameters associated with each Limit State:

| Limit State | T_R [years] | a_g [g] | F_0 | T_C^* [s] |
|-------------|---------------|-----------|-------|-------------|
| SLO | 30 | 0,079 | 2,395 | 0,273 |
| SLD | 50 | 0,104 | 2,330 | 0,282 |
| SLV | 475 | 0,261 | 2,365 | 0,347 |
| SLC | 975 | 0,334 | 2,401 | 0,364 |

Table 11. Seismic parameters for each Limit State

The following are the design spectra associated with each Limit State:

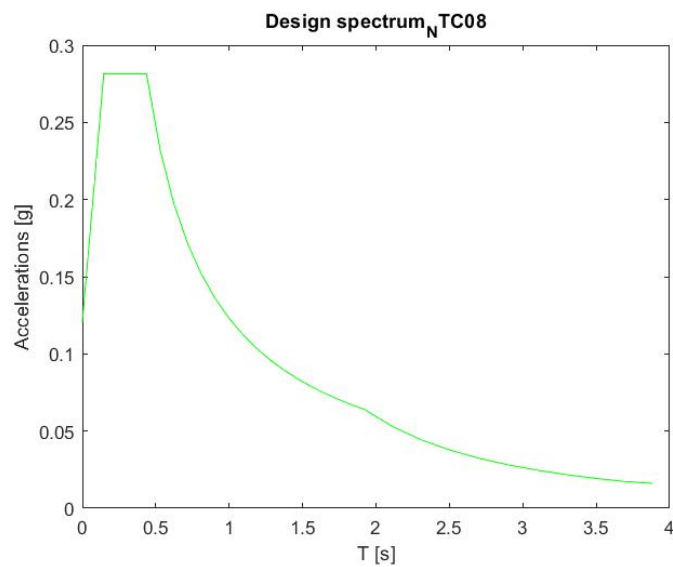


Figure 46. Design Spectrum SLO

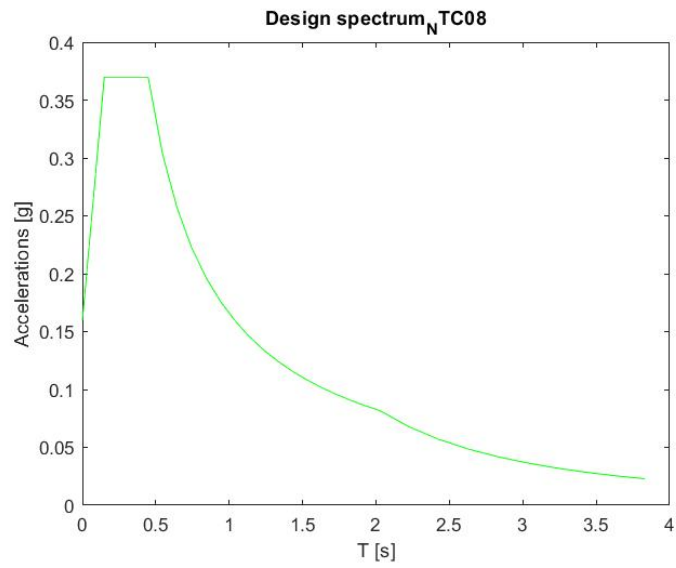


Figure 47. Design Spectrum SLD

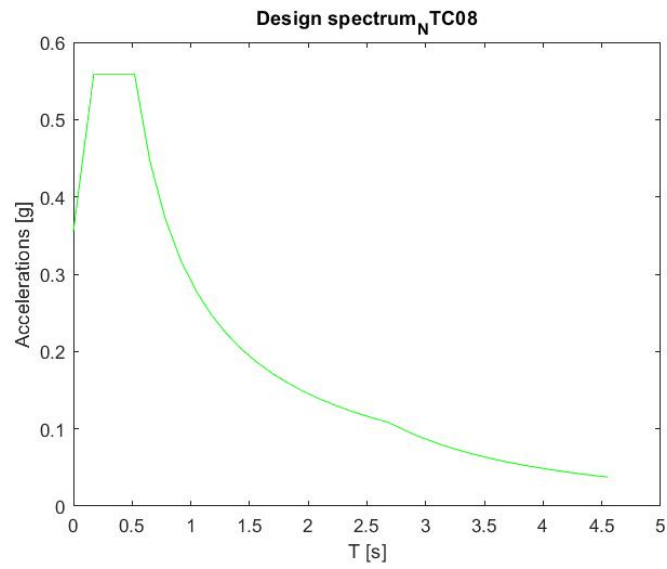


Figure 48. Design Spectrum SLV

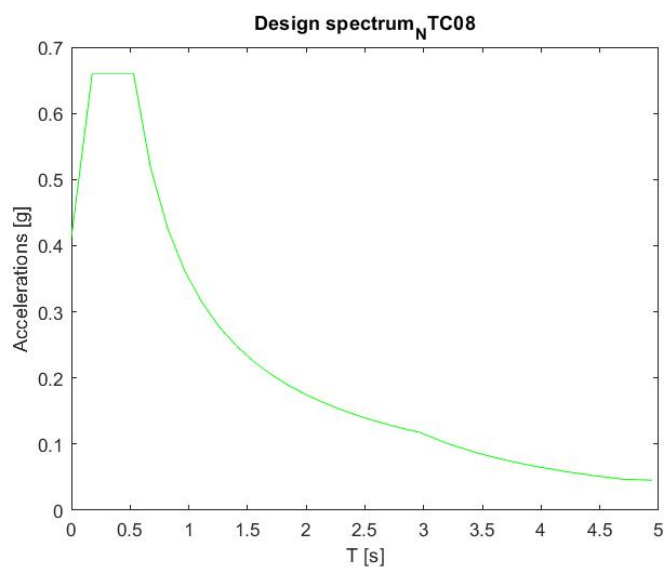


Figure 49. Design Spectrum SLC

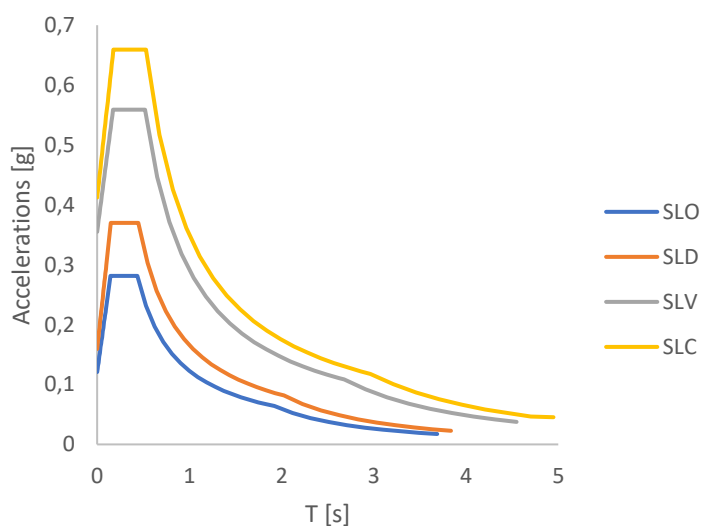


Figure 50. Design Spectrum

5.4. Combination of actions

The actions described above have been combined with each other through the following "Seismic Combination" defined in NTC18.

$$E + G_1 + G_2 + P + \psi_{21} \cdot Q_{k1} + \psi_{22} \cdot Q_{k2} + \dots \quad (5.3)$$

Where E represents the seismic action for the boundary state being examined.

The effects of seismic action are assessed taking into account the masses associated with the following gravitational loads:

$$G_1 + G_2 + \sum_j \psi_{2j} \cdot Q_{kj} \quad (5.4)$$

The values of the coefficients ψ_{2j} are given in Table 2.5.I of NTC18:

Tab. 2.5.I – Valori dei coefficienti di combinazione

| Categoria/Azione variabile | Ψ_{0j} | Ψ_{1j} | Ψ_{2j} |
|---|----------------------------|-------------|-------------|
| Categoria A - Ambienti ad uso residenziale | 0,7 | 0,5 | 0,3 |
| Categoria B - Uffici | 0,7 | 0,5 | 0,3 |
| Categoria C - Ambienti suscettibili di affollamento | 0,7 | 0,7 | 0,6 |
| Categoria D - Ambienti ad uso commerciale | 0,7 | 0,7 | 0,6 |
| Categoria E - Aree per immagazzinamento, uso commerciale e uso industriale Biblioteche, archivi, magazzini e ambienti ad uso industriale | 1,0 | 0,9 | 0,8 |
| Categoria F - Rimesse, parcheggi ed aree per il traffico di veicoli (per autoveicoli di peso ≤ 30 kN) | 0,7 | 0,7 | 0,6 |
| Categoria G - Rimesse, parcheggi ed aree per il traffico di veicoli (per autoveicoli di peso > 30 kN) | 0,7 | 0,5 | 0,3 |
| Categoria H - Coperture accessibili per sola manutenzione | 0,0 | 0,0 | 0,0 |
| Categoria I - Coperture praticabili | da valutarsi caso per caso | | |
| Categoria K - Coperture per usi speciali (impianti, eliporti, ...) | da valutarsi caso per caso | | |
| Vento | 0,6 | 0,2 | 0,0 |
| Neve (a quota ≤ 1000 m s.l.m.) | 0,5 | 0,2 | 0,0 |
| Neve (a quota > 1000 m s.l.m.) | 0,7 | 0,5 | 0,2 |
| Variazioni termiche | 0,6 | 0,5 | 0,0 |

5.5. Hinge properties

In the pushover analysis the post-elastic behaviour of the structure was modeled through the use of plastic hinges.

According to the indications of the Circular 21/01/2019 of the NTC18, to describe these plastic hinges has been used a bilinear shear-displacement model, in which the resistance is calculated as the least among those related to the different possible breaking mechanisms. The displacement capability is assessed accordingly through a limiting angular deformation of the element.

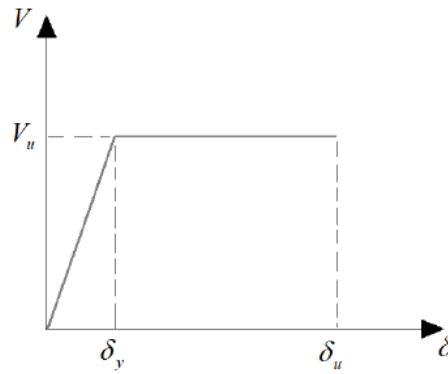


Figure 51. Bilinear shear-displacement model

Where:

- V_u is the ultimate shear equal to: $V_u = \min(V_p; V_t)$;
- δ_y is the yield displacement equal to: $\delta_y = \frac{V_u}{E_m}$;
- δ_u is the ultimate displacement equal to: $\delta_u = \theta_u \cdot (H_i - H_j)$;

These values are different for piers and spandrels . In particular, for piers the following relationships are used:

$$V_p = \frac{1}{H_0} \cdot \left(l^2 \cdot t \cdot \frac{\sigma_0}{2} \right) \cdot \left(1 - \frac{\sigma_0}{0,85 \cdot f_d} \right) \quad (5.5)$$

$$\theta_{u,\text{lim}} = 0,01$$

$$V_t = \begin{cases} l \cdot t \cdot \frac{1,5 \cdot \tau_{0,d}}{b} \cdot \left(1 + \frac{\sigma_0}{0,85 \cdot \tau_{0,d}} \right) & \text{Irregular texture} \\ \left(\frac{l \cdot t}{b} \right) \cdot \left(\frac{f_{v0,d} + \mu \cdot \sigma_0}{1 + \mu \cdot \phi} \right) & \text{Regular texture} \end{cases} \quad (5.6)$$

$$\theta_{u,\text{lim}} = \begin{cases} 0,004 & \text{perforated blocks} \\ 0,005 & \text{other cases} \end{cases}$$

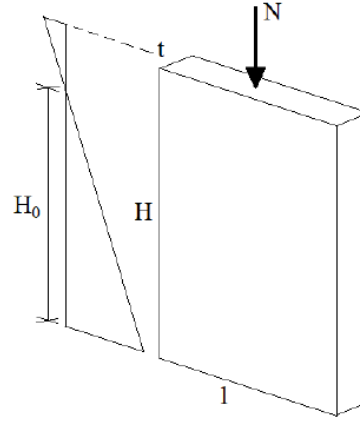


Figure 52. Pier

For spandrels the following relationships are used:

$$V_p = \frac{2}{B} \cdot \left(H_p \cdot \frac{h}{2} \right) \cdot \left(1 - \frac{H_p}{0,85 \cdot f_d \cdot h \cdot t} \right) \quad (5.7)$$

$$V_t = \begin{cases} \left[B \cdot t \cdot \frac{1,5 \cdot \tau_{0,d}}{b} \cdot \left(1 + \frac{\sigma_0}{1,5 \cdot \tau_{0,d}} \right) \right] & \text{Irregular texture} \\ \left[\left(\frac{B \cdot t}{b} \right) \cdot \left(\frac{f_{v0,d} + \mu \cdot \sigma_0}{1 + \mu \cdot \phi} \right) \right] & \text{Regular texture} \end{cases} \quad (5.8)$$

$$\theta_{u, \text{lim}} = \begin{cases} 0,02 & \text{in the presence of elements resistant to traction} \\ 0,0015 & \text{other cases} \end{cases} \quad (5.9)$$

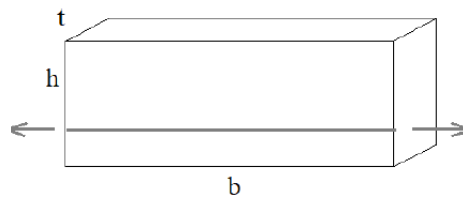


Figure 53. Spandrel

Through the use of a MATLAB script it has been possible to insert inside SAP2000 the respective plastic hinge for every pier and spandrel evaluating these effects:

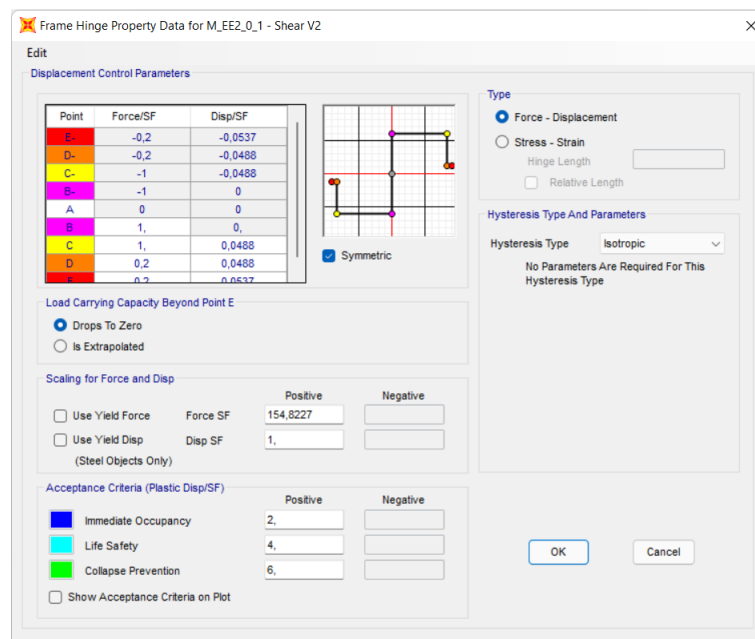


Figure 54. Define Hinge Properties SAP2000

5.6. Modeling “Building C”

As described above, Building C has a wall in common with the case study building. Therefore, it does not cause a hammering effect on the structure.

The common wall will be subject to the loads due to the floors of the reference building, but also to the loads due to the floors of Building C. For this reason, the interaction between the two buildings has been modeled with the insertion of additional masses at the height of the floor of Building C. We remember, in fact, that the floor has an offset of about 80 cm compared to the floor of the case study.

These additional masses were calculated by assuming the same stratigraphy of the floors of the reference building and calculating the area of influence of the common wall.

In particular, the following masses have been calculated:

| Level | Offset [m] | Area [m ²] | Load [kN/m ²] | Weight [kN] | Weight [kg] |
|---------|------------|------------------------|---------------------------|-------------|-------------|
| Level 0 | 0,8 | 13,50 | 5,74 | 77,49 | 7896,23 |
| Level 1 | 0,8 | 13,50 | 5,74 | 77,49 | 7896,23 |
| Level 2 | 0,8 | 13,50 | 5,74 | 77,49 | 7896,23 |

| | | | | | |
|---------|-----|-------|------|-------|---------|
| Level 3 | 0,8 | 13,50 | 3,37 | 45,50 | 4635,94 |
|---------|-----|-------|------|-------|---------|

Table 12. Additional masses "Building C"

5.7. Calculation of pounding effect

To consider the effect of the hammering between Building A and Building D was considered the linear elastic model proposed by Maison and Kasai (1990) (1992). In particular, this model introduces a spring with a stiffness that simulates the impact stiffness of the colliding structures. This spring is activated only when contact between structures occurs:

$$F(t) = \begin{cases} k\delta(t) & \delta(t) > 0 \\ 0 & \delta(t) \leq 0 \end{cases}$$

$$\delta(t) = u_1(t) - u_2(t) - d \quad (5.10)$$

It was necessary to determine the displacements of the two colliding buildings. The method based on displacement amplification factors proposed by Miranda (1999) was used. For Building D the following parameters were considered:

- $w_{max} = 944,16 \text{ kN}$
- $H = 14 \text{ m}$
- $\alpha_0 = 0,70$
- *Load type*: uniform
- $\beta_1 = 1,342$
- $\beta_3 = 1,096$
- $T = 0,543 \text{ s}$

In this way it has been possible to define the value of the maximum roof displacement which is equal to:

$$u_{top} = \beta_1 \beta_3 S_d = 0,058 \text{ m}$$

In addition, the following distribution of lateral displacements was obtained:

| z [m] | $u(z)$ [m] |
|---------|------------|
| 3,5 | 0,006419 |
| 7 | 0,021176 |
| 10,5 | 0,03931 |
| 14 | 0,05813 |

Table 13. Lateral displacements "Building D"

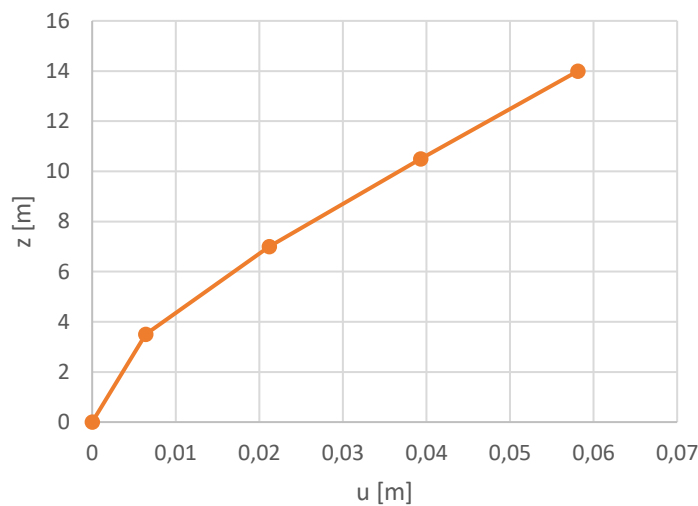


Figure 55. Lateral displacements "Building D"

The same procedure to estimate the maximum roof displacement was also carried out for Building A although in this case more information was available to run more detailed models. It was decided to use this method in order to define lateral displacements with the same degree of error. Nevertheless, the basic period and the pattern of normalised height displacements were used through modal analysis. Therefore, for Building A the following parameters were considered:

- $\beta_1 = 1,203$
- $\beta_3 = 1,050$
- $T = 0,340$ s

In this way it has been possible to define the value of the maximum roof displacement which is equal to:

$$u_{top} = \beta_1 \beta_3 S_d = 0,020 \text{ m}$$

In addition, the following distribution of lateral displacements was obtained:

| z [m] | u(z) [m] |
|-------|----------|
| 4,88 | 0,004739 |
| 8,54 | 0,012794 |
| 11,96 | 0,018993 |
| 13,41 | 0,020318 |

Table 14. Lateral displacements "Building A"

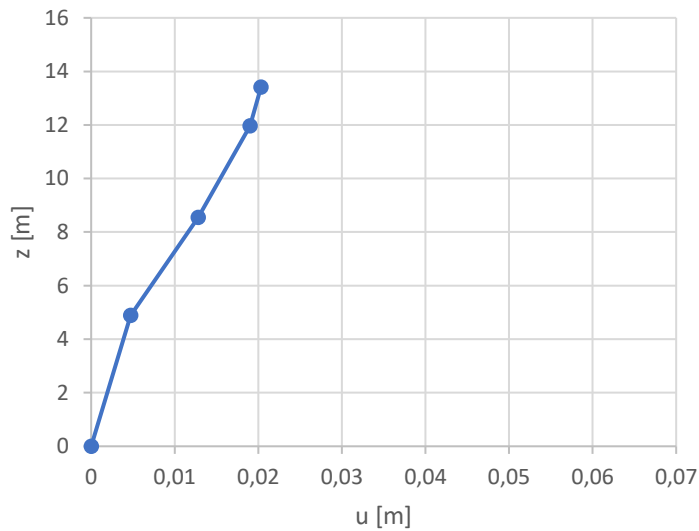


Figure 56. Lateral displacements "Building A"

In order to compare the displacements of the two buildings it was necessary to determine the displacements of Building A at the height of the displacements of Building D. This operation was carried out through a simple linear interpolation of the described results previously. In this way the following displacements have been obtained:

| z [m] | u(z) [m] |
|-------|----------|
| 3,5 | 0,003399 |
| 7 | 0,009405 |

| | |
|------|----------|
| 10,5 | 0,016347 |
| 14 | 0 |

Table 15. Lateral displacements "Building A"

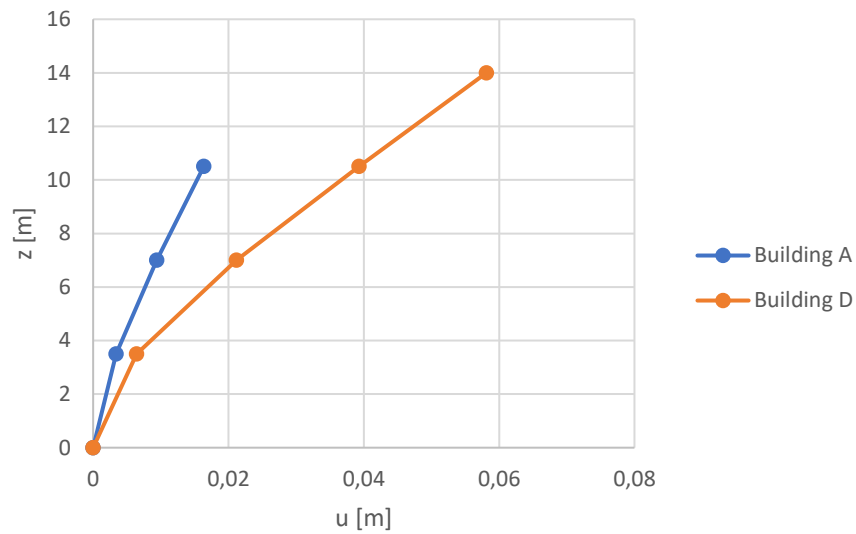


Figure 57. Lateral displacements "Building A" and "Building D"

Then it was possible to define the linear elastic model that describes the pounding effect using a spring stiffness of $k = 491907,4$ kN/m. This value was determined by the following formula proposed by Xu, Xu et al. (2016) according to the fundamental periods of the two collident structures:

$$k = \frac{m_2}{m_1 + m_2} k_1 e^{\frac{2(\ln e)}{\pi} \arcsin \frac{\pi}{\sqrt{\pi^2 + (\ln e)^2}}} \quad T_1 \leq T_2$$

$$k = \frac{m_1}{m_1 + m_2} k_2 e^{\frac{2(\ln e)}{\pi} \arcsin \frac{\pi}{\sqrt{\pi^2 + (\ln e)^2}}} \quad T_1 > T_2 \quad (5.11)$$

In particular, the following parameters were used:

- $T_1 = 0,34$ s
- $T_2 = 0,54$ s
- $e = 0,69$
- $m_1 = 24809,66$ kN

- $m_2 = 17469$ kN
- $k_I = 1048129$ kN/m

Determined the value of the stiffness of impact, the maximum impact forces on the floor were calculated considering the displacements of Building A obtained with the modal analysis and the displacements of Building D obtained with the method of Miranda (1999).

The results are as follows:

| z [m] | $u(z)_D$ [m] | $u(z)_A$ [m] | δ [m] | F [kN] | F_{norm} [-] |
|---------|--------------|--------------|--------------|-----------|----------------|
| 0 | 0,0000 | 0,0000 | 0,0000 | 0,00 | 0,000 |
| 3,5 | 0,0064 | 0,0032 | -0,0032 | -1563,08 | 0,137 |
| 7 | 0,0212 | 0,0094 | -0,0118 | -5791,67 | 0,507 |
| 10,5 | 0,0393 | 0,0161 | -0,0232 | -11415,92 | 1,000 |
| 14 | 0,0581 | - | - | - | - |

Table 16. Maximum impact forces

It is pointed out that in reality the pounding forces are dynamic forces. The approximation of these forces in static forces with the maximum value allows to study the hammering and the vulnerability of the building of interest in favour of security.

Within the SAP model a new Load Pattern has been created based on the distribution of previously calculated F_{norm} . Then, a pushover analysis is performed in which the initial conditions are due to both vertical loads acting on the structure according to the equation ... that by the effect of these horizontal forces.

5.8. Calculation of torsional effect

The extended N2 Method proposed by Fajfar, Marušić et al. (2005) was used to consider the torsional effect. As explained above, this method is based on combining the results of a pushover analysis on a 3D model of the structure with the results of a linear dynamic analysis. In fact, the pushover analysis aims to control the distribution of the target displacement along the

height of the structure, while linear dynamic analysis controls the distribution of lateral displacements caused by the torsional effect.

Therefore, the displacements obtained from the pushover analysis are amplified by a corrective coefficient determined by the ratio of the normalized displacement obtained from the modal analysis, i.e. the displacement of a specific point in the plane divided by the displacement of the center of mass, and that obtained by the analysis pushover.

The following steps of the extended N2 method are performed:

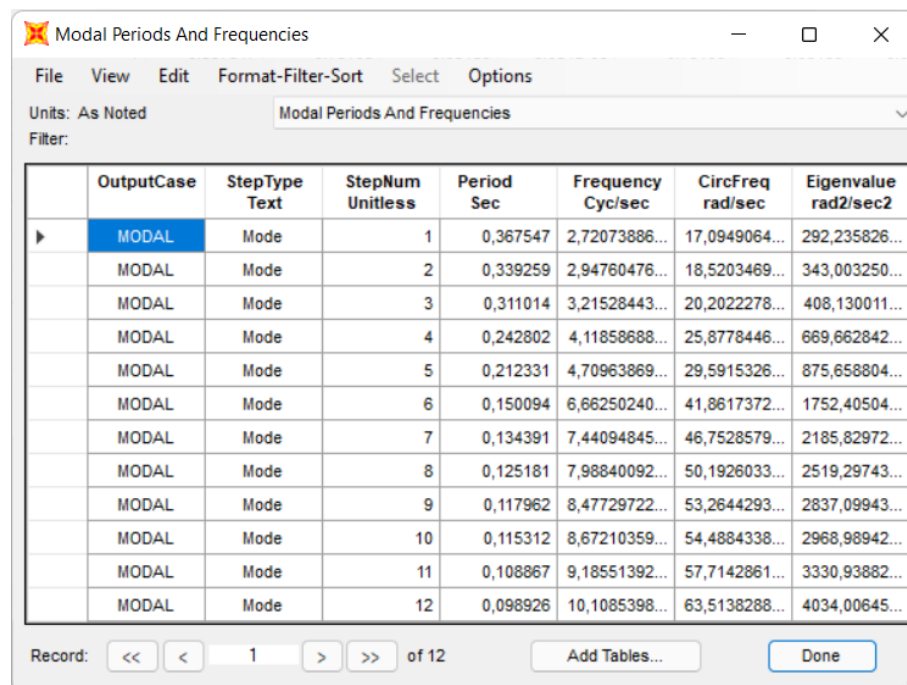
1. Perform pushover analysis in both main directions using a 3D model. A load distribution corresponding to an acceleration pattern proportional to the shape of the fundamental way of vibrating in the considered direction shall be applied to the mass centres. The target displacement (CM displacement demand at roof level) is then determined for each of the two horizontal directions;
2. Perform linear modal analysis of the 3D model in the two horizontal directions and the results were combined according to the SRSS combination rule;
3. Determination of the corrective factor to be applied to the pushover analysis. This factor is determined by the ratio of the normalized roof displacement, i.e. the displacement of a specific point in the plane divided by the displacement of the centre of mass, to that obtained by the pushover analysis;
4. Application of the correction factor to the results obtained from the pushover analysis. In this way, the results obtained are influenced both by the pushover analysis that does not take into account the torsional effect and linear dynamic analysis.

6. Results and comparisons

This section shows the results of the various analyses carried out and a comparison between them.

6.1. Results of modal analysis

The following modes of vibration of the structure under analysis have been calculated with the relative frequency and period values:



| | OutputCase | StepType Text | StepNum Unitless | Period Sec | Frequency Cyc/sec | CircFreq rad/sec | Eigenvalue rad2/sec2 |
|---|------------|---------------|------------------|------------|-------------------|------------------|----------------------|
| ▶ | MODAL | Mode | 1 | 0,367547 | 2,72073886... | 17,0949064... | 292,235826... |
| | MODAL | Mode | 2 | 0,339259 | 2,94760476... | 18,5203469... | 343,003250... |
| | MODAL | Mode | 3 | 0,311014 | 3,21528443... | 20,2022278... | 408,130011... |
| | MODAL | Mode | 4 | 0,242802 | 4,11858688... | 25,8778446... | 669,662842... |
| | MODAL | Mode | 5 | 0,212331 | 4,70963869... | 29,5915326... | 875,658804... |
| | MODAL | Mode | 6 | 0,150094 | 6,66250240... | 41,8617372... | 1752,40504... |
| | MODAL | Mode | 7 | 0,134391 | 7,44094845... | 46,7528579... | 2185,82972... |
| | MODAL | Mode | 8 | 0,125181 | 7,98840092... | 50,1926033... | 2519,29743... |
| | MODAL | Mode | 9 | 0,117962 | 8,47729722... | 53,2644293... | 2837,09943... |
| | MODAL | Mode | 10 | 0,115312 | 8,67210359... | 54,4884338... | 2968,98942... |
| | MODAL | Mode | 11 | 0,108867 | 9,18551392... | 57,7142861... | 3330,93882... |
| | MODAL | Mode | 12 | 0,098926 | 10,1085398... | 63,5138288... | 4034,00645... |

Figure 58. Modal periods and frequencies

For each mode of vibration it is possible to define a participation factor, this represents the degree of participation of the i-th vibrating mode to the vibration of the system:

| | OutputCase | StepType Text | StepNum Unitless | Period Sec | UX KN-m | UY KN-m | UZ KN-m | RX KN-m | RY KN-m | RZ KN-m | ModalMass KN-m-s ² | ModalStiff KN-m |
|---|------------|---------------|------------------|------------|------------|------------|------------|------------|-------------|-------------|-------------------------------|-----------------|
| ▶ | MODAL | Mode | 1 | 0,367547 | -40,49932 | 10,690538 | 0,367122 | -35,909954 | -128,07418 | -86,183338 | 1 | 292,23583 |
| | MODAL | Mode | 2 | 0,339259 | -7,647341 | -35,055398 | -0,746568 | 141,130378 | -21,804528 | -178,584063 | 1 | 343,00325 |
| | MODAL | Mode | 3 | 0,311014 | -10,607287 | -14,669219 | 0,024171 | 40,675161 | -32,858493 | 394,460056 | 1 | 408,13001 |
| | MODAL | Mode | 4 | 0,242802 | -0,788636 | 0,605569 | 0,183131 | -7,160076 | -0,370562 | 78,810532 | 1 | 669,66284 |
| | MODAL | Mode | 5 | 0,212331 | -0,040482 | 1,695726 | 0,027549 | 8,074765 | -0,052757 | 18,354064 | 1 | 875,6588 |
| | MODAL | Mode | 6 | 0,150094 | 16,447877 | -4,574631 | 0,647016 | -30,456815 | -165,78232 | -24,266094 | 1 | 1752,40504 |
| | MODAL | Mode | 7 | 0,134391 | -4,136728 | -16,800739 | -0,690594 | -98,257871 | 42,979236 | -124,105206 | 1 | 2185,82973 |
| | MODAL | Mode | 8 | 0,125181 | 2,025525 | -10,536608 | -0,179814 | -63,503686 | -26,995347 | 95,638224 | 1 | 2519,29743 |
| | MODAL | Mode | 9 | 0,117962 | -1,446686 | 1,463846 | 0,091917 | 12,528801 | 12,919999 | -25,089856 | 1 | 2837,09944 |
| | MODAL | Mode | 10 | 0,115312 | 3,406656 | 6,952991 | 1,76357 | 63,191991 | -17,997762 | -101,012103 | 1 | 2968,98942 |
| | MODAL | Mode | 11 | 0,108867 | 3,629852 | 1,69724 | 0,367738 | 24,672337 | 28,703881 | -93,759286 | 1 | 3330,93882 |
| | MODAL | Mode | 12 | 0,098926 | -0,036571 | 2,959531 | -21,205545 | -56,169299 | -236,664514 | -28,76812 | 1 | 4034,00646 |

Figure 59. Modal participation factors

Then, it was possible to calculate the actual modal mass for each mode of vibration:

| | OutputCase | StepType Text | StepNum Unitless | Period Sec | UX Unitless | UY Unitless | UZ Unitless | RX Unitless | RY Unitless | RZ Unitless |
|---|------------|---------------|------------------|------------|-------------|-------------|-------------|-------------|-------------|-------------|
| ▶ | MODAL | Mode | 1 | 0,367547 | 0,73103 | 0,05159 | 6,084E-05 | 0,01426 | 0,06488 | 0,02761 |
| | MODAL | Mode | 2 | 0,339259 | 0,02607 | 0,55472 | 0,00025 | 0,22032 | 0,00188 | 0,11857 |
| | MODAL | Mode | 3 | 0,311014 | 0,05015 | 0,09713 | 2,637E-07 | 0,0183 | 0,00427 | 0,57848 |
| | MODAL | Mode | 4 | 0,242802 | 0,00028 | 0,00017 | 1,514E-05 | 0,00057 | 5,431E-07 | 0,02309 |
| | MODAL | Mode | 5 | 0,212331 | 7,304E-07 | 0,0013 | 3,426E-07 | 0,00072 | 1,101E-08 | 0,00125 |
| | MODAL | Mode | 6 | 0,150094 | 0,12058 | 0,00945 | 0,00019 | 0,01026 | 0,1087 | 0,00219 |
| | MODAL | Mode | 7 | 0,134391 | 0,00763 | 0,12741 | 0,00022 | 0,10679 | 0,00731 | 0,05726 |
| | MODAL | Mode | 8 | 0,125181 | 0,00183 | 0,05011 | 1,46E-05 | 0,04461 | 0,00288 | 0,03401 |
| | MODAL | Mode | 9 | 0,117962 | 0,00093 | 0,00097 | 3,814E-06 | 0,00174 | 0,00066 | 0,00234 |
| | MODAL | Mode | 10 | 0,115312 | 0,00517 | 0,02182 | 0,0014 | 0,04417 | 0,00128 | 0,03793 |
| | MODAL | Mode | 11 | 0,108867 | 0,00587 | 0,0013 | 6,104E-05 | 0,00673 | 0,00326 | 0,03268 |
| | MODAL | Mode | 12 | 0,098926 | 5,961E-07 | 0,00395 | 0,20298 | 0,0349 | 0,22153 | 0,00308 |

Figure 60. Modal participating mass ratios

From this analysis it was possible to identify the fundamental modes of vibration in the two main directions, with their respective periods.

In particular, for direction X:

- Fundamental mode: 1
- Period: 0,368 s
- Effective modal mass: 73,10%

For direction X:

- Fundamental mode: 2
- Period: 0,340 s
- Effective modal mass: 55,47%

In addition, it can be noted that both fundamental modes do not have a high effective modal mass. This is due precisely to the geometry of the structure which, being irregular, has no modes of vibrating purely translations. In this case, therefore, the higher modes have a significant effect on the analysis.

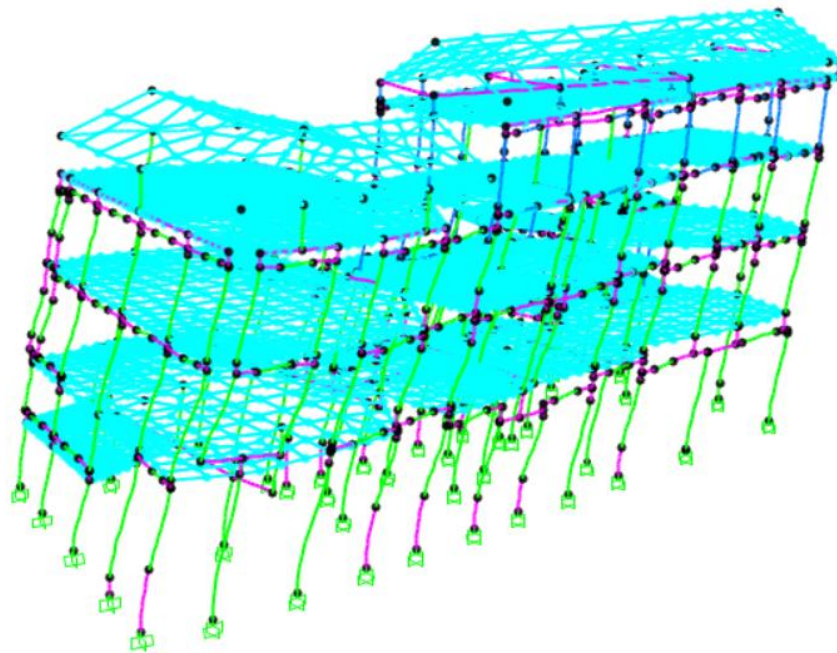


Figure 61. Deformed shape Mode 1

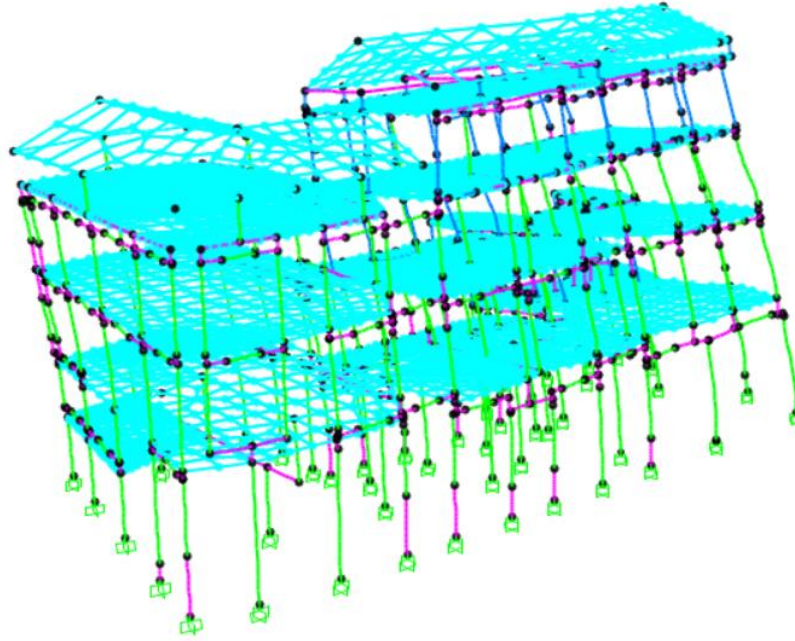


Figure 62. Deformed shape Mode 2

6.2. Results pushover analysis isolated building

Define the plastic hinges as described in the previous chapter and performed the modal analysis, it has been possible to perform a pushover analysis considering a distribution of forces corresponding to a trend of accelerations proportional to the shape of the fundamental mode in the direction considered. This analysis was carried out in both main directions. Thus, the Pushover_x is proportional to the 1 mode of vibrating, while the Pushover_y is proportional to the 2 mode of vibrating. In addition, in this case no account was taken of the torsional effects and the pounding effect. The only effect considered is the presence of Building C. This effect has been modeled considering additional masses at the height of the floors of Building C.

Below are the capacity curves in the two main directions X and Y:

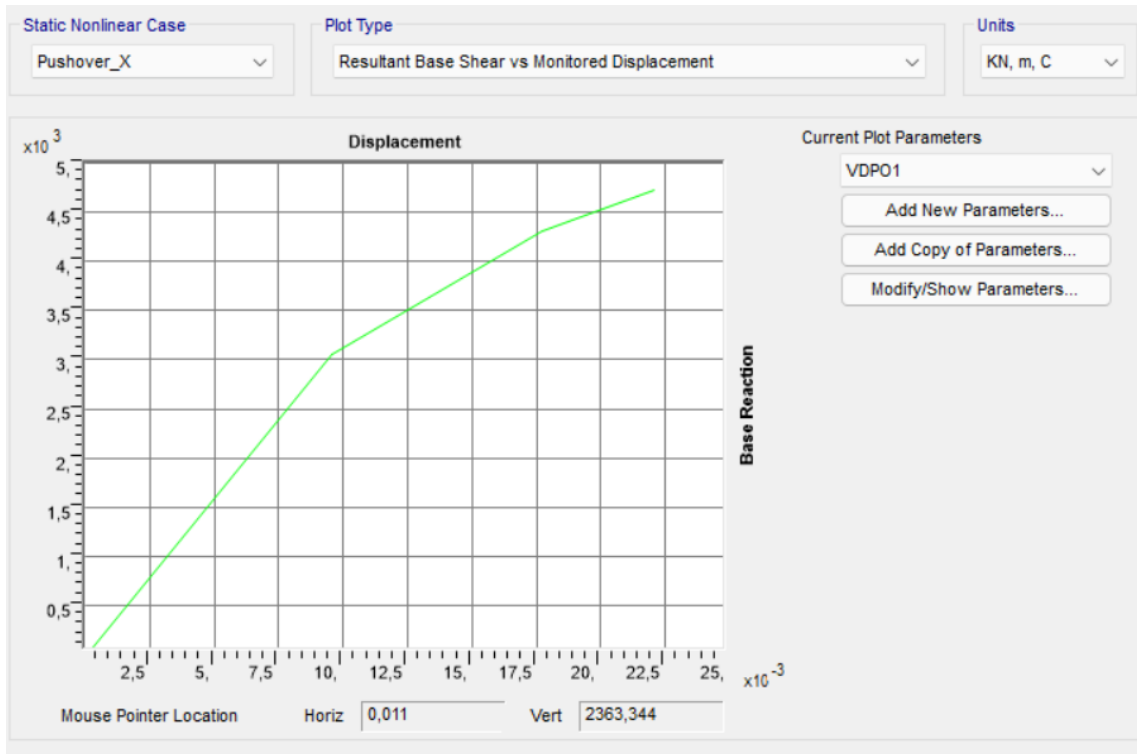


Figure 63. Capacity curve Pushover_X

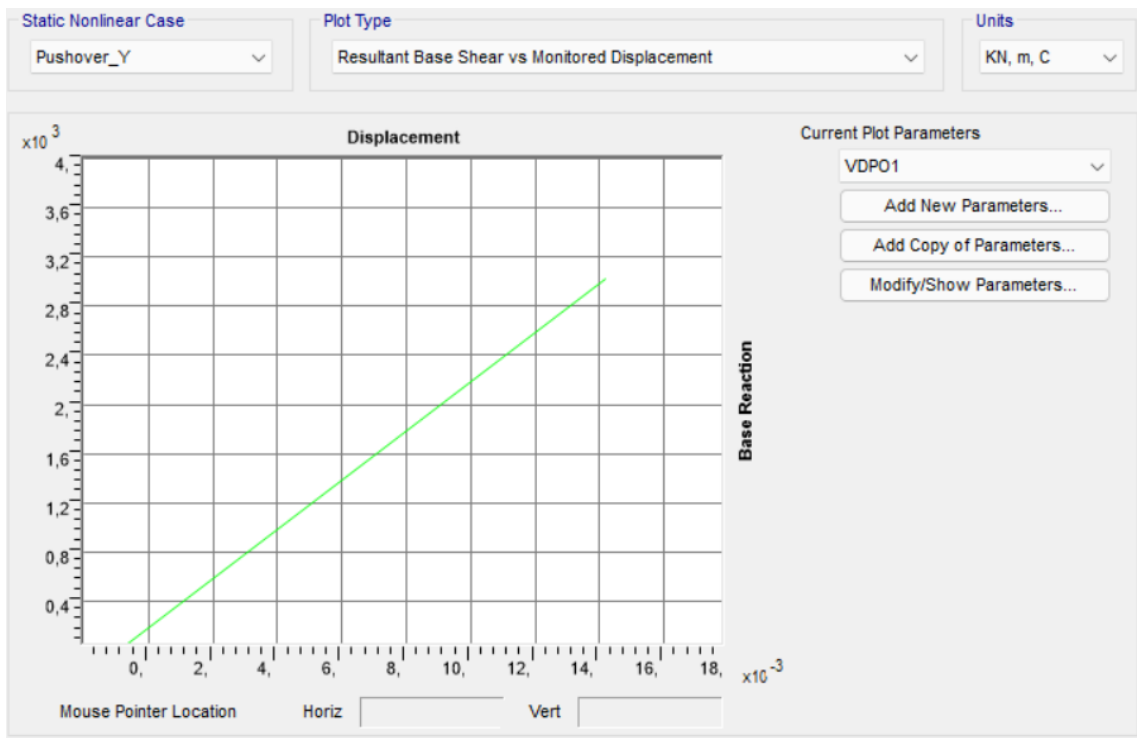


Figure 64. Capacity curve Pushover_Y

It is possible to notice that the capacity curve along the X-direction is elasto-plastic, while the capacity curve along the Y-direction is almost exclusively elastic. This situation is due to the torsional effect that the structure undergoes. In fact, the second mode of vibrating has a higher

percentage of torsional participant mass than the first mode of vibrating. The torsion having a fragile behaviour involves an instantaneous collapse of the structure once the elastic behavior is overcome.

For completeness, plastic hinges were analyzed during the different loading phases.

These analyses are given below with regard to the following steps:

- Start loading;
- End loading.

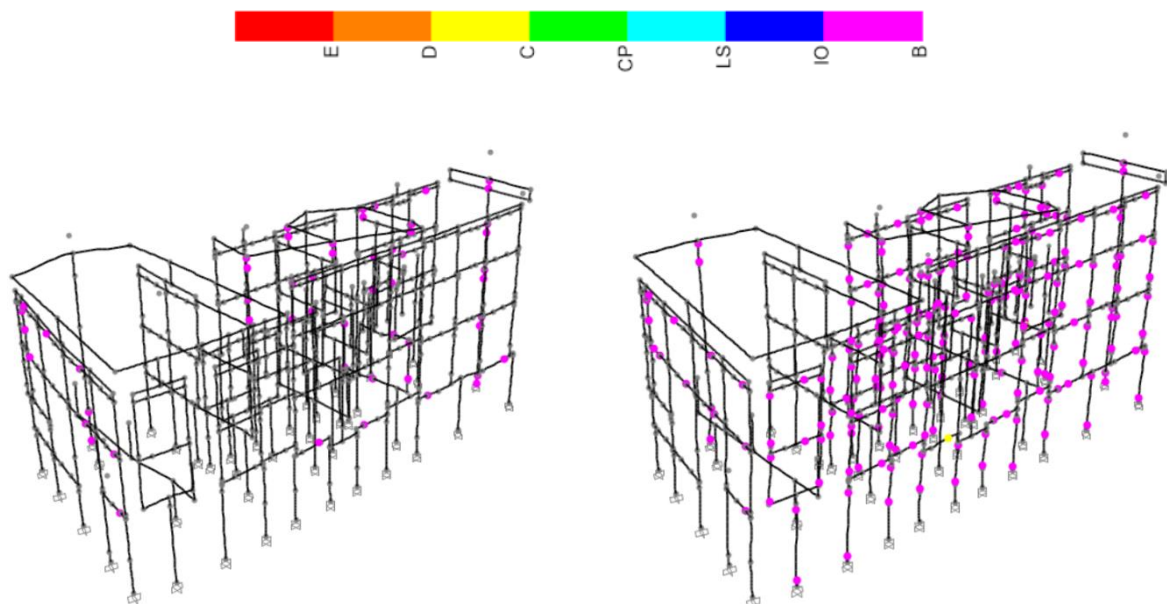


Figure 65. Hinge analysis Pushover_X

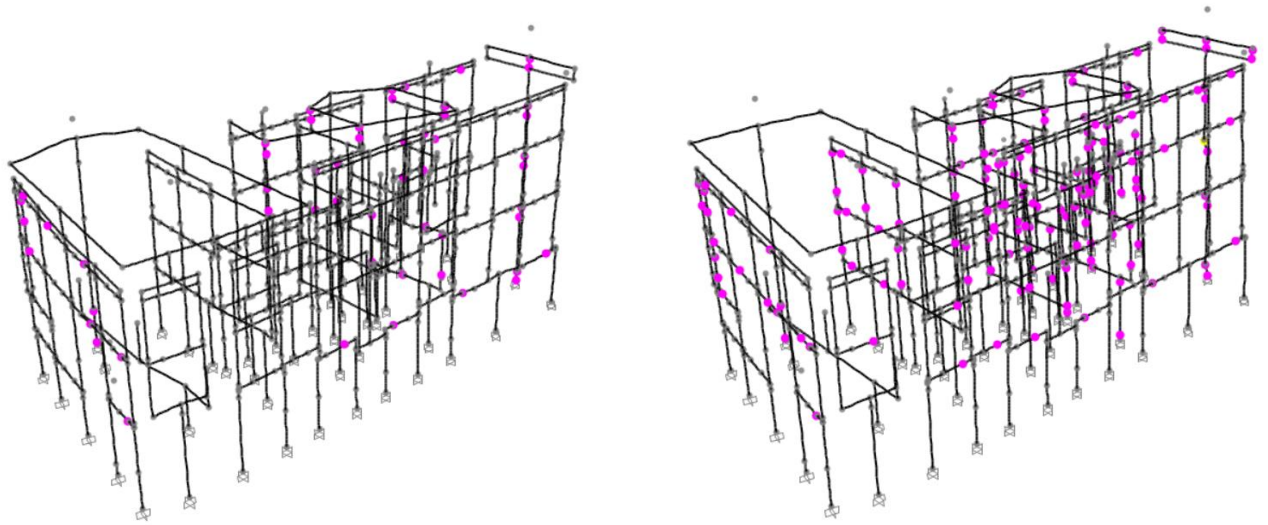


Figure 66. Hinge analysis Pushover_Y

Subsequently, the following characteristics of the equivalent elasto-plastic SDOF system were calculated and performance checks carried out.

- In direction X:

| m^* [kNs ² /m] | γ [-] | k^* [kN/m] | T^* [s] | $S_a(T^*)$ [g] |
|--------------------------------|--------------------|-----------------------|----------------|-------------------|
| 1216,3 | 1,348 | 319917,7 | 0,387 | 0,659 |
| F_y^* [kN] | F_{bu}^* [kN] | $0,6F_{bu}^*$ [kN] | d_y^* [m] | d_u^* [m] |
| 3042,208 | 3505,7 | 2103,4 | 0,01 | 0,016 |

Table 17. Characteristics of equivalent elasto-plastic SDOF_X

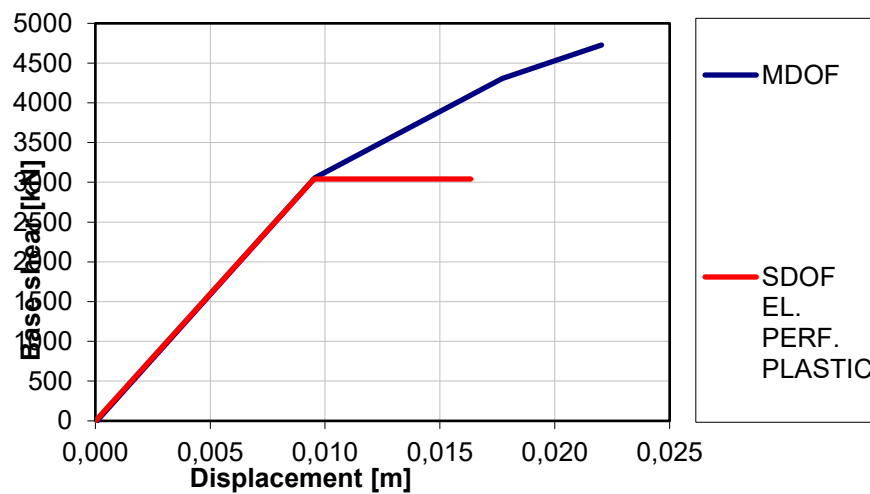


Figure 67. Equivalent elasto-plastic SDOF_X

| SLD | | | SLV | | | SLC | | |
|-------|-------|-------|-------|-------|-------|-------|-------|-------|
| q* | d*max | dmax | q* | d*max | dmax | q* | d*max | dmax |
| [-] | [m] | [m] | [-] | [m] | [m] | [-] | [m] | [m] |
| 1,451 | 0,014 | 0,020 | 2,192 | 0,025 | 0,033 | 2,586 | 0,030 | 0,041 |

Table 18. Performance checks_X

- In direction Y:

| m* | Γ | k* | T* | S _a (T*) |
|-----------------------|-------------------|----------------------|------------------|---------------------|
| [kNs ² /m] | [-] | [kN/m] | [s] | [g] |
| 966,2 | 1,272 | 212818,9 | 0,423 | 0,659 |
| F _y * | F _{bu} * | 0,6F _{bu} * | d _y * | d _u * |
| [kN] | [kN] | [kN] | [m] | [m] |
| 2372,608 | 2371,7 | 1423 | 0,011 | 0,012 |

Table 19. Characteristics of equivalent elasto-plastic SDOF_Y

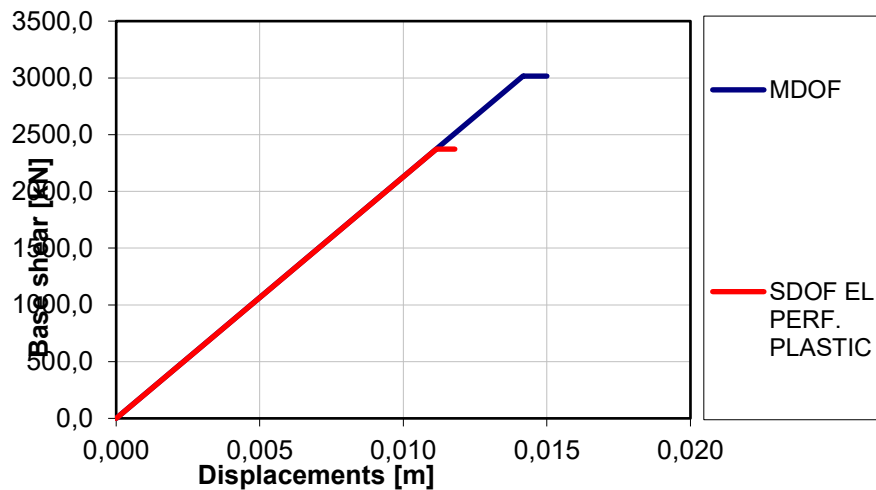


Figure 68. Equivalent elasto-plastic SDOF_Y

| SLD | | | SLV | | | SLC | | |
|-------|-------|-------|-------|-------|-------|-------|-------|-------|
| q* | d*max | dmax | q* | d*max | dmax | q* | d*max | dmax |
| [-] | [m] | [m] | [-] | [m] | [m] | [-] | [m] | [m] |
| 1,478 | 0,017 | 0,021 | 2,233 | 0,028 | 0,036 | 2,634 | 0,034 | 0,043 |

Table 20. Performance checks_Y

6.3. Calculation of isolated building vulnerability index

The seismic vulnerability index, as already described in Chap. 2, represents the security assessment of the building of interest. It is defined as the relationship between the maximum seismic action bearable by the structure and the maximum seismic action that would be used in the design of a new construction on the same soil and with the same characteristics.

In the case analysed, this index was calculated as the ratio of capacity to demand in terms of displacement. In particular, the following results were obtained:

- In direction X:

| SLD | | | SLV | | | SLC | | |
|------------------------|------------------------|-----------------------|------------------------|------------------------|-----------------------|------------------------|------------------------|-----------------------|
| d _c [mm] | d _d [mm] | ζ _E [-] | d _c [mm] | d _d [mm] | ζ _E [-] | d _c [mm] | d _d [mm] | ζ _E [-] |
| 9,559 | 19,504 | 0,490 | 9,559 | 33,351 | 0,287 | 9,559 | 40,617 | 0,235 |

Table 21. Isolated building vulnerability index_X

- In direction Y:

| SLD | | | SLV | | | SLC | | |
|------------------------|------------------------|-----------------------|------------------------|------------------------|-----------------------|------------------------|------------------------|-----------------------|
| d _c [mm] | d _d [mm] | ζ _E [-] | d _c [mm] | d _d [mm] | ζ _E [-] | d _c [mm] | d _d [mm] | ζ _E [-] |
| 14,176 | 21,343 | 0,664 | 14,176 | 35,660 | 0,398 | 14,176 | 43,155 | 0,328 |

Table 22. Isolated building vulnerability index_Y

Comparing the results in the two directions it is possible to notice that the vulnerability index in the X direction is lower than in the Y direction. This is due to the fact that the only effects that come into play are the additional masses in direction X due to the presence of the adjacent Building C with the wall in common with the reference building. This results in an unstable effect only along the X-direction.

Nevertheless, from these results it is possible to note the need for local interventions or seismic improvement to increase the vulnerability index.

6.4. Results pushover analysis building in aggregate

The following are the results of the building's pushover analysis in aggregate. In addition to the effect of Building C previously considered, the pounding effect caused by Building D and the torsional effect were also considered. In particular, as already described in Chap.5, the pounding effect was considered by calculating a distribution of impact forces along the height of the building. This distribution was combined with the vertical loads acting on the structure and subsequently a pushover analysis was carried out considering this combination as initial loads.

Instead, the torsional effect was considered by applying a correction coefficient to the results of the modal analysis. This coefficient, as already described in Cap.5, has been calculated by the ratio between the normalized displacement obtained from the modal analysis and the normalized displacement obtained from the pushover analysis.

The following are the values of the normalised displacements obtained with modal analysis and pushover analysis and the values of the corrective coefficients to be applied to the X and Y pushover analysis:

| $d_{\text{norm,modal}}$ [-] | $d_{\text{norm,pushX}}$ [-] | $d_{\text{norm,pushY}}$ [-] |
|--------------------------------|--------------------------------|--------------------------------|
| 1,215 | 1 | 1 |

Table 23. Normalised displacements

| C_X [-] | C_Y [-] |
|--------------|--------------|
| 1,215 | 1,215 |

Table 24. Corrective coefficients torsional effects

Below are the capacity curves in the two main directions X and Y:

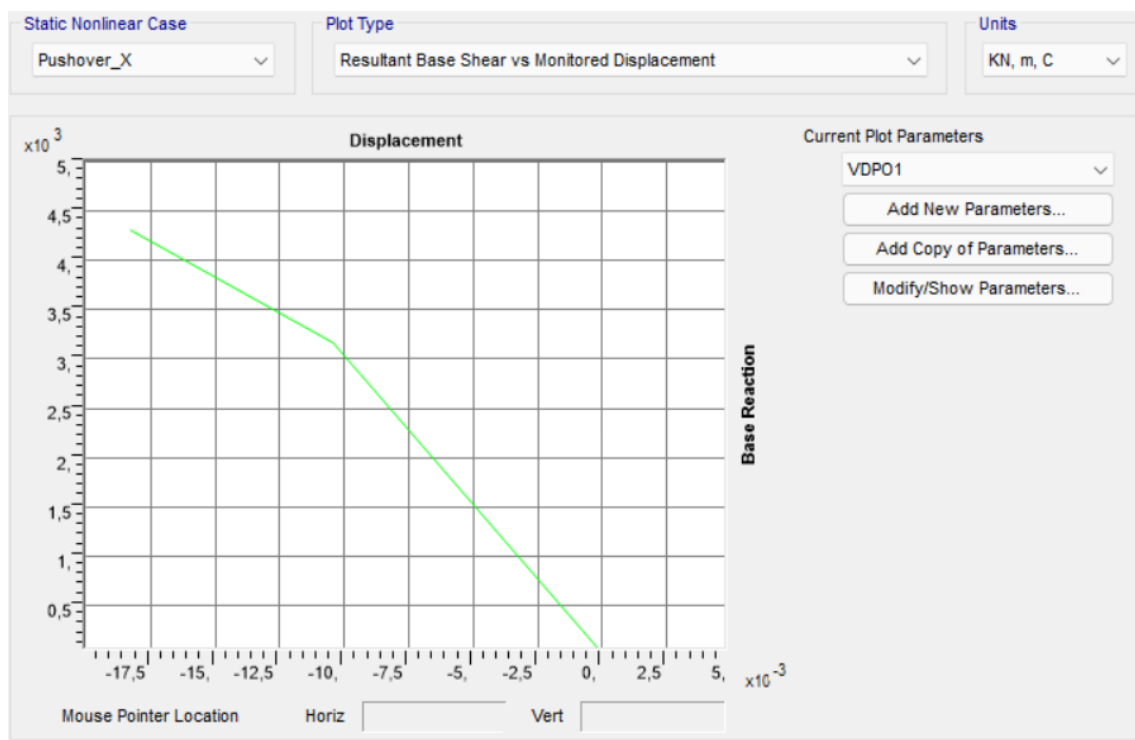


Figure 69. Capacity curve Pushover_X

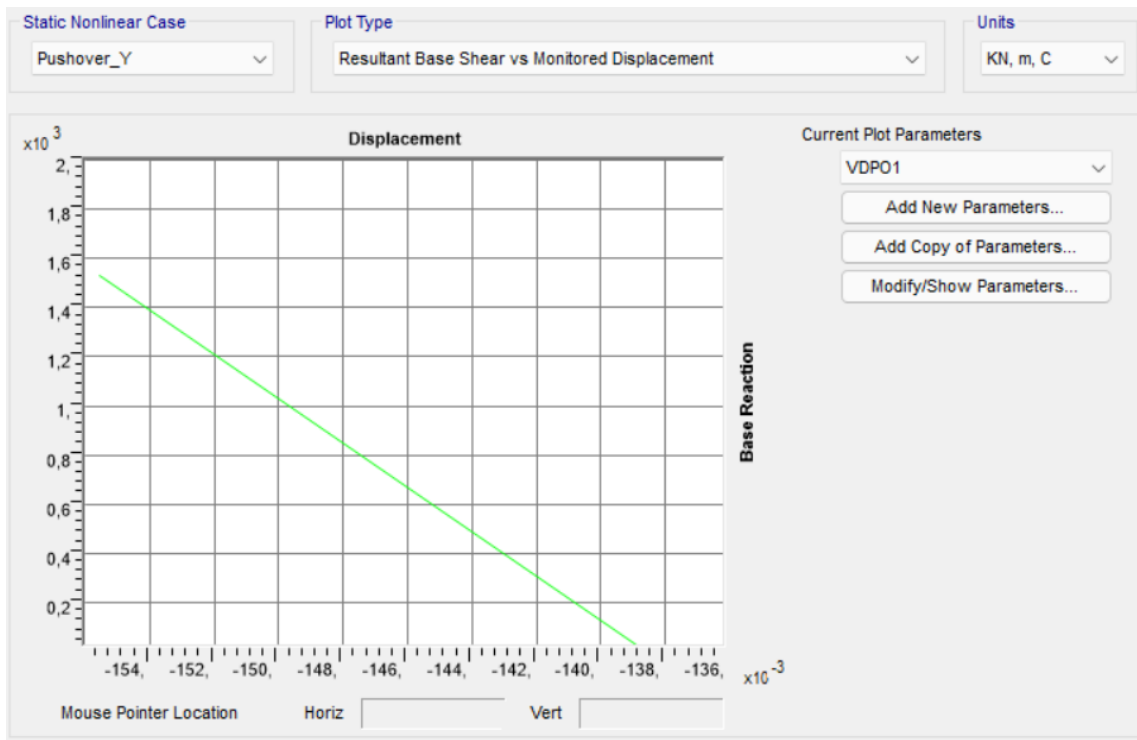


Figure 70. Capacity curve Pushover_Y

Also in this case, it's possible to notice that the capacity curve along the X-direction is elasto-plastic, while the capacity curve along the Y-direction is almost exclusively elastic due to the higher torsional participant mass of the second mode of vibrating. The torsion having a fragile behaviour involves an instantaneous collapse of the structure once the elastic behavior is overcome.

For completeness, plastic hinges were analyzed during the different loading phases.

These analyses are given below with regard to the following steps:

- Start loading;
- End loading.



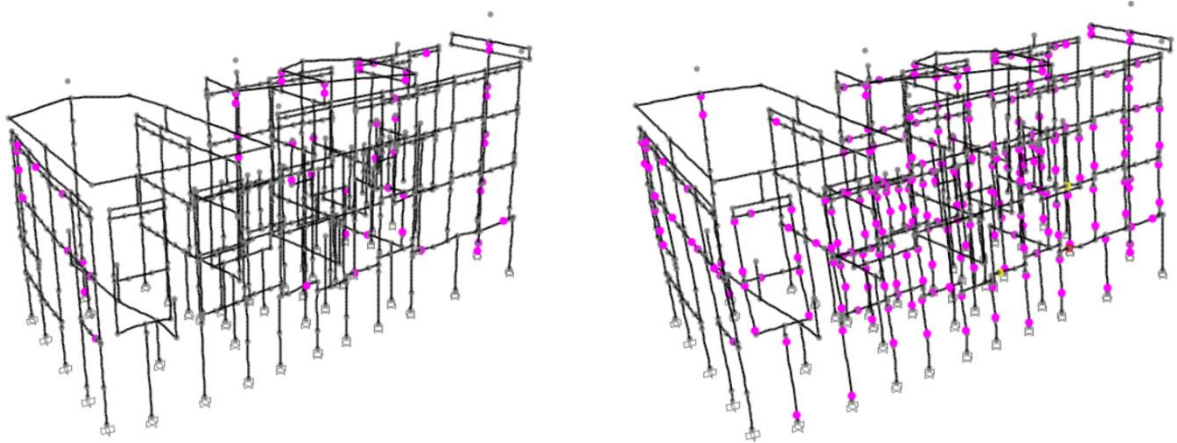


Figure 71. Hinge analysis Pushover_X

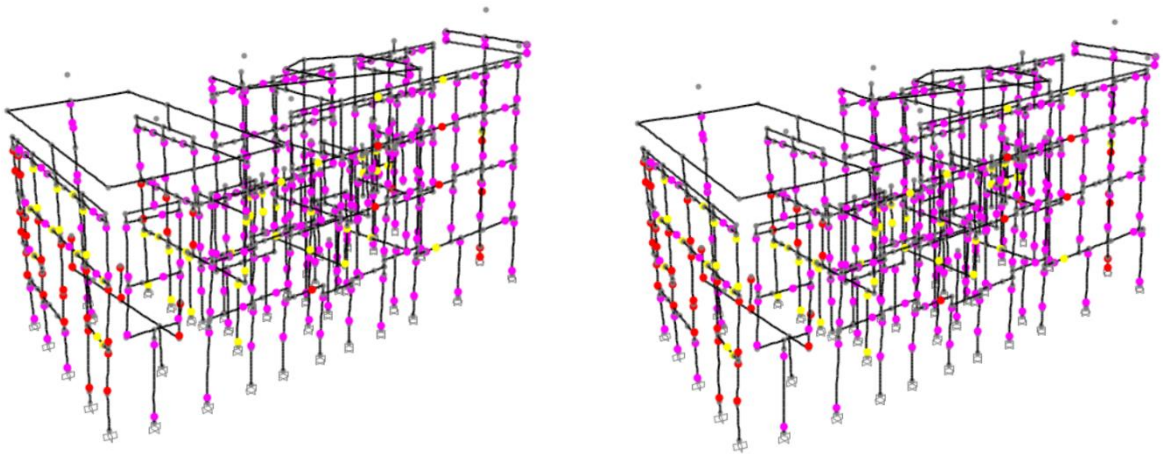


Figure 72. Hinge analysis Pushover_Y

From these images and from the curves of capacity it is possible to notice that in direction X the behaviour remains almost equal, while in direction Y there is a remarkable capacity drop. This is due to the pounding effect which acts mainly along the Y axis.

Subsequently, the following characteristics of the equivalent elasto-plastic SDOF system were calculated and performance checks carried out.

- In direction X:

| m^* [kNs ² /m] | Γ [-] | k^* [kN/m] | T^* [s] | $S_a(T^*)$ [g] |
|--------------------------------|-----------------|-----------------|--------------|-------------------|
| 1216,5 | 1,349 | 304236,5 | 0,397 | 0,659 |
| F_y^* | F_{bu}^* | $0,6F_{bu}^*$ | d_y^* | d_u^* |

| | | | | |
|----------|------|------|-------|-------|
| [kN] | [kN] | [kN] | [m] | [m] |
| 2844,587 | 3200 | 1920 | 0,009 | 0,014 |

Table 25. Characteristics of equivalent elasto-plastic SDOF_X

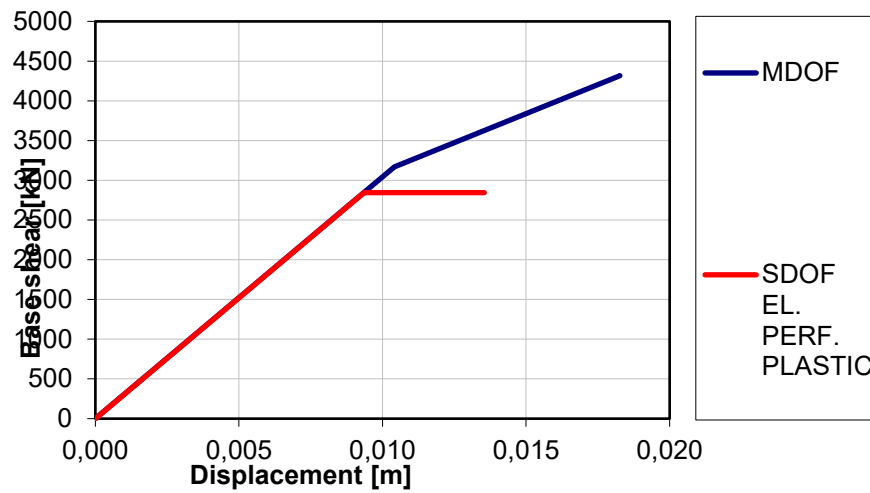


Figure 73. Equivalent elasto-plastic SDOF_X

| SLD | | | SLV | | | SLC | | |
|-------|-------|-------|-------|-------|-------|-------|-------|-------|
| q* | d*max | dmax | q* | d*max | dmax | q* | d*max | dmax |
| [-] | [m] | [m] | [-] | [m] | [m] | [-] | [m] | [m] |
| 1,552 | 0,015 | 0,020 | 2,345 | 0,026 | 0,035 | 2,766 | 0,031 | 0,042 |

Table 26. Performance checks_X

- In direction Y:

| | | | | |
|-----------------------|-------------------|----------------------|------------------|---------------------|
| m* | Γ | k* | T* | S _a (T*) |
| [kNs ² /m] | [-] | [kN/m] | [s] | [g] |
| 966,2 | 1,272 | 90485,6 | 0,649 | 0,542 |
| F _y * | F _{bu} * | 0,6F _{bu} * | d _y * | d _u * |
| [kN] | [kN] | [kN] | [m] | [m] |
| 1203,8 | 1203,8 | 722,3 | 0,013 | 0,014 |

Table 27. Characteristics of equivalent elasto-plastic SDOF_Y

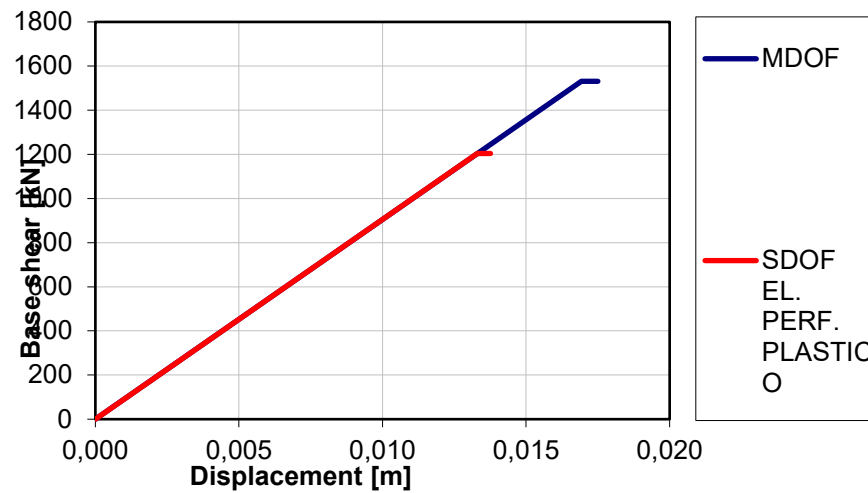


Figure 74. Equivalent elasto-plastic SDOF_Y

| SLD | | | SLV | | | SLC | | |
|-------|-------|-------|-------|-------|-------|-------|-------|-------|
| q* | d*max | dmax | q* | d*max | dmax | q* | d*max | dmax |
| [-] | [m] | [m] | [-] | [m] | [m] | [-] | [m] | [m] |
| 2,010 | 0,027 | 0,034 | 3,539 | 0,047 | 0,060 | 4,270 | 0,057 | 0,072 |

Table 28. Performance check_Y

6.5. Calculation of building in aggregate vulnerability index

In this case, the capacity displacement values obtained from the pushover analysis were deamplified by the correction coefficient to consider the torsional effects.

In particular, the following results were obtained:

- In direction X:

| SLD | | | SLV | | | SLC | | |
|----------------|----------------|----------------|----------------|----------------|----------------|----------------|----------------|----------------|
| d _c | d _d | ζ _E | d _c | d _d | ζ _E | d _c | d _d | ζ _E |
| [mm] | [mm] | [-] | [mm] | [mm] | [-] | [mm] | [mm] | [-] |
| 8,573 | 20,451 | 0,419 | 8,573 | 34,814 | 0,246 | 8,573 | 42,286 | 0,203 |

Table 29. Building in aggregate vulnerability index_X

- In direction Y:

| SLD | | | SLV | | | SLC | | |
|---------------|---------------|------------------|---------------|---------------|------------------|---------------|---------------|------------------|
| d_c [mm] | d_d [mm] | ζ_E [-] | d_c [mm] | d_d [mm] | ζ_E [-] | d_c [mm] | d_d [mm] | ζ_E [-] |
| 13,926 | 34,007 | 0,410 | 13,926 | 59,709 | 0,233 | 13,926 | 72,257 | 0,193 |

Table 30. Building in aggregate vulnerability index_Y

In this case, comparing the results in the two directions it is possible to notice that the vulnerability index in the Y direction is lower than in the X direction. This is due to the fact that the pounding effect acting on the Y axis has been considered. For this reason the reason for the Y-direction analysis is most affected by this effect, while in the X direction it is less. This results in an unstable effect along the Y-direction on building.

6.6. Comparisons

The following paragraph describes the comparisons of the results obtained with the pushover analysis considering the isolated building and the building in aggregate. In addition, the results of vulnerability indices obtained in both cases are also compared.

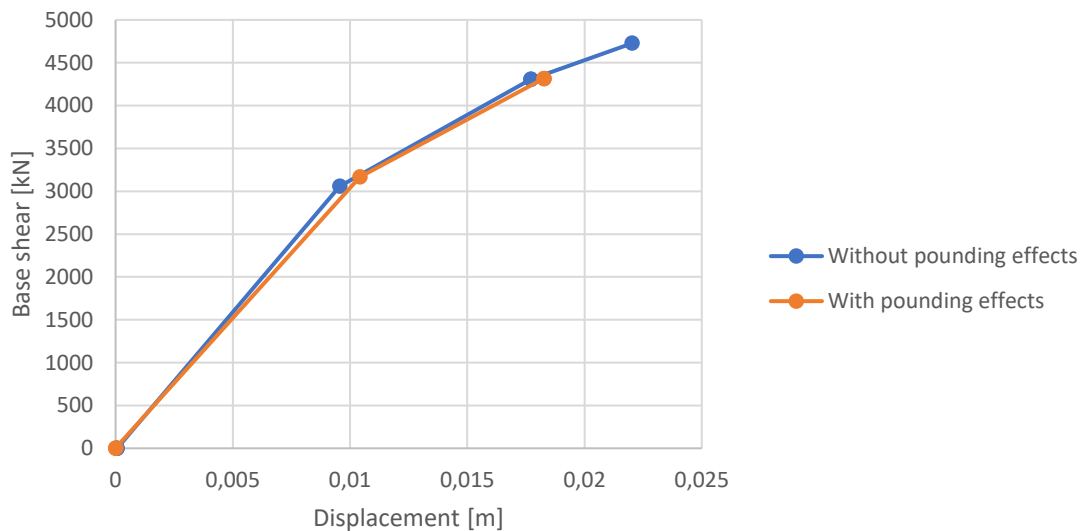


Figure 75. Comparison capacity curves_X

From the comparison of the capacity curves in the X direction, it is possible to notice that the pounding effect causes a small loss of capacity in terms of displacements. This is due to the fact

that the pounding acts mainly along the Y axis. Therefore, along the X axis the structure is less affected by this effect.

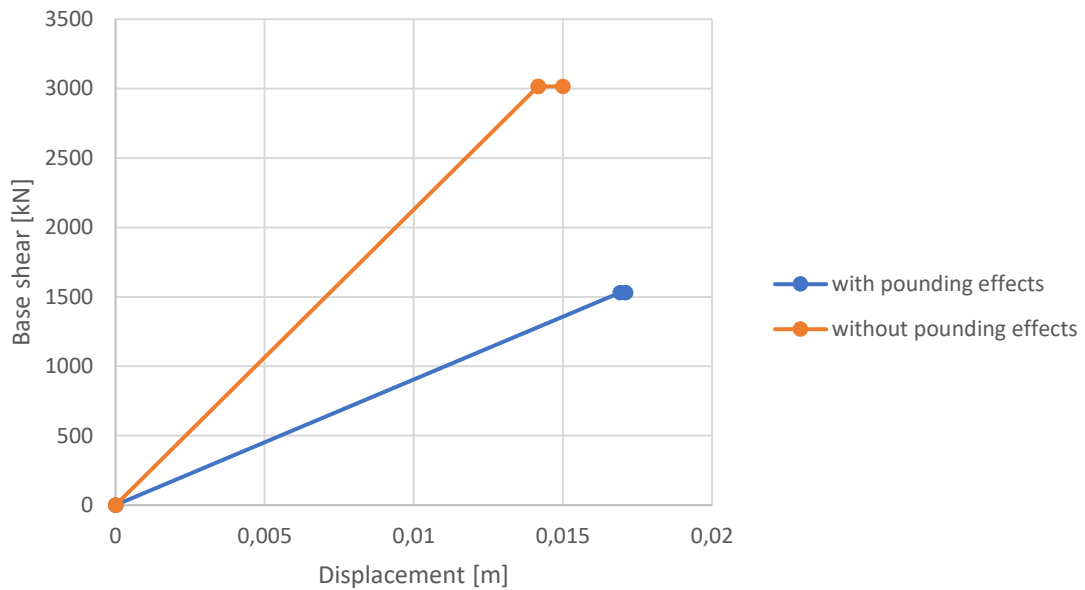


Figure 76. Comparison capacity curves_Y

Instead, by comparing the capacity curves in the Y direction, it is possible to notice a high loss of capacity in terms of resistance due to the pounding effect. Therefore, it can be concluded that in this case, if the pounding effect is not taken into account, the results are overestimated.

Subsequently, a comparison was made between the vulnerability indices obtained considering the isolated building and the building in aggregate. The reduction of these indices are as follows:

- In direction X:

| SLD | | | SLV | | | SLC | | |
|---------------------|------------------|-------------------|---------------------|------------------|-------------------|---------------------|------------------|-------------------|
| $\zeta_{E,without}$ | $\zeta_{E,with}$ | $\zeta_{E,ratio}$ | $\zeta_{E,without}$ | $\zeta_{E,with}$ | $\zeta_{E,ratio}$ | $\zeta_{E,without}$ | $\zeta_{E,with}$ | $\zeta_{E,ratio}$ |
| [-] | [-] | [-] | [-] | [-] | [-] | [-] | [-] | [-] |
| 0,490 | 0,419 | 0,145 | 0,287 | 0,246 | 0,142 | 0,235 | 0,203 | 0,137 |

Table 31. Percentage variation of vulnerability indices_X

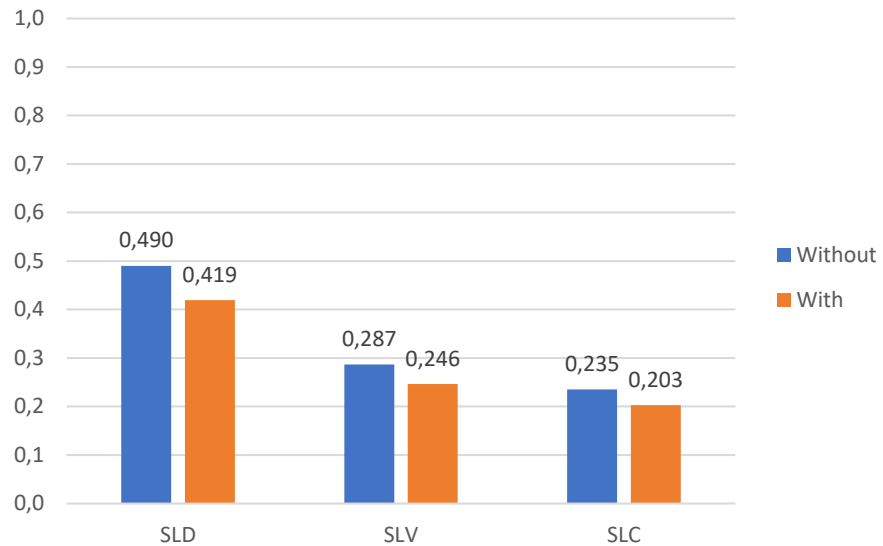


Figure 77. Variation of vulnerability indices_X

- In direction Y:

| SLD | | | SLV | | | SLC | | |
|---------------------|------------------|-------------------|---------------------|------------------|-------------------|---------------------|------------------|-------------------|
| $\zeta_{E,without}$ | $\zeta_{E,with}$ | $\zeta_{E,ratio}$ | $\zeta_{E,without}$ | $\zeta_{E,with}$ | $\zeta_{E,ratio}$ | $\zeta_{E,without}$ | $\zeta_{E,with}$ | $\zeta_{E,ratio}$ |
| [-] | [-] | [-] | [-] | [-] | [-] | [-] | [-] | [-] |
| 0,664 | 0,410 | 0,383 | 0,398 | 0,233 | 0,414 | 0,328 | 0,193 | 0,412 |

Table 32. Percentage variation of vulnerability indices_Y

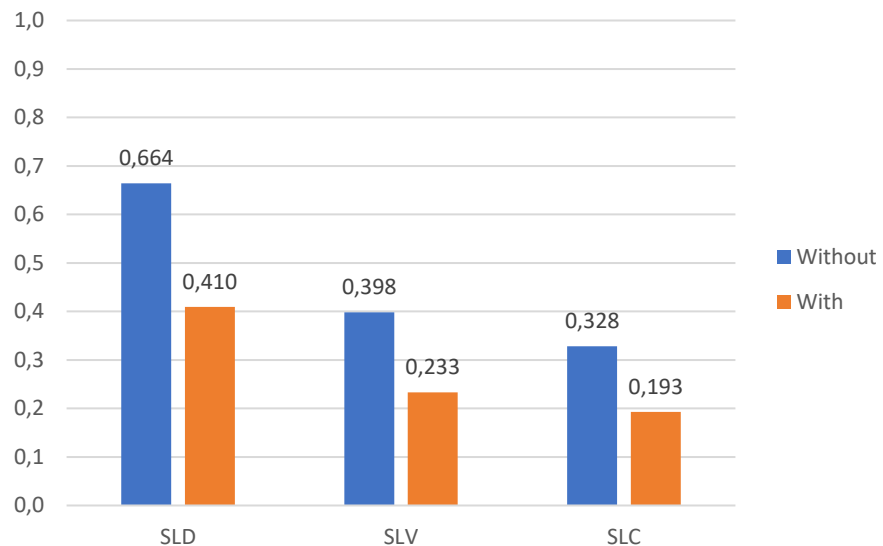


Figure 78. Variation of vulnerability indices_Y

It is possible to notice how the percentage variation of the results is of approximately 14% in direction X and approximately 40% in direction Y. Obviously these two values are not equal because in direction Y the pounding effects and the torsional effects are greater than in

direction X. This is due to the fact that the pounding takes place mainly along the Y axis, while the 2 mode of vibrating has a more torsional participating mass than the first. In both cases, however, not considering the pounding effects and torsional effects would overestimate the capacity of the structure.

7. Conclusions

From the thesis work and the analyses carried out it has emerged that the interactions with the adjacent buildings can drastically modify the seismic response of the single Structural Unit that constitutes the aggregate. The simplified nonlinear static-based method proposed allows to assess the seismic vulnerability of a building in aggregate considering the pounding effects and the torsional effect with a reduced computational effort. In particular, the pounding effect is simulated through a distribution of maximum static forces along the height of the building. These static forces were calculated using the linear elastic model proposed by Maison and Kasai (1990) (1992) which introduces a spring with a stiffness that simulates the impact stiffness of colliding structures. Instead, the torsional effect is calculated through the modified N2 method proposed by Fajfar, Marušić et al. (2005) which determines a corrective coefficient to be applied to the pushover analysis that takes into account the results of the modal analysis.

Therefore, the proposed method is very simple to apply, but has some precautionary approximations. In particular, simulating the dynamic pounding forces in maximum static forces neglects the dynamism of this action. This results in an overestimation of the pounding effect during the loading period because the final loading phase is directly considered.

Possible future works allow to consider further models of simulation of the pounding effect in order to be able to consider also the plastic behaviour and the dissipation of energy during the collision.

From the analysis of the obtained results it is possible to notice how the application of the proposed method involves a reduction of the vulnerability index of the structure of approximately 40%.

In conclusion, it is worth noticing that perform a pushover analysis without considering the pounding effects and torsional effects would have overestimated the capacity of the structure.

8. References

Anagnostopoulos, S. A. (1988). "Pounding of buildings in series during earthquakes." Earthquake engineering & structural dynamics **16**(3): 443-456.

Anagnostopoulos, S. A. and K. V. Spiliopoulos (1992). "An investigation of earthquake induced pounding between adjacent buildings." Earthquake engineering & structural dynamics **21**(4): 289-302.

Azizi-Bondarabadi, H., et al. (2021). "Higher mode effects in pushover analysis of irregular masonry buildings." Journal of Earthquake engineering **25**(8): 1459-1493.

Bento, R., et al. (2010). "Using nonlinear static procedures for seismic assessment of the 3D irregular SPEAR building." Earthquakes and Structures **1**(2): 177-195.

Bosco, M., et al. (2012). "Corrective eccentricities for assessment by the nonlinear static method of 3D structures subjected to bidirectional ground motions." Earthquake engineering & structural dynamics **41**(13): 1751-1773.

Bosco, M., et al. (2013). "Comparison of nonlinear static methods for the assessment of asymmetric buildings." Bulletin of Earthquake Engineering **11**(6): 2287-2308.

Browning, J., et al. (2008). "Global and local seismic drift estimates for RC frames." Engineering Structures **30**(5): 1262-1271.

Chopra, A. K. and R. K. Goel (2002). "A modal pushover analysis procedure for estimating seismic demands for buildings." Earthquake engineering & structural dynamics **31**(3): 561-582.

Chopra, A. K. and R. K. Goel (2004). "A modal pushover analysis procedure to estimate seismic demands for unsymmetric-plan buildings." Earthquake engineering & structural dynamics **33**(8): 903-927.

Cimellaro, G. and S. Marasco (2014). OPENSIGNAL: a software framework for earthquake record processing and selection. Second European conference on earthquake engineering and seismology (2ECSEES), Istanbul, Turkey.

- Cole, G., et al. (2010). "Building pounding state of the art: Identifying structures vulnerable to pounding damage."
- Cole, G., et al. (2011). "An investigation of the effects of mass distribution on pounding structures." Earthquake engineering & structural dynamics **40**(6): 641-659.
- Davis, R. (1992). "Pounding of buildings modelled by an impact oscillator." Earthquake engineering & structural dynamics **21**(3): 253-274.
- Dolce, M. (1989). Schematizzazione e modellazione per azioni nel piano delle Paretti, Ordine degli Ingegneri della Prov. di Potenza.
- Donà, C. and A. De Maria (2011). "Manuale delle murature storiche." Roma, DEI.
- Fajfar, P., et al. (2005). "Torsional effects in the pushover-based seismic analysis of buildings." Journal of Earthquake engineering **9**(06): 831-854.
- Goldsmith, W. (2001). Impact, Courier Corporation.
- Jankowski, R. (2005). "Non-linear viscoelastic modelling of earthquake-induced structural pounding." Earthquake engineering & structural dynamics **34**(6): 595-611.
- Jankowski, R. (2008). "Earthquake-induced pounding between equal height buildings with substantially different dynamic properties." Engineering Structures **30**(10): 2818-2829.
- Jankowski, R. (2010). "Experimental study on earthquake-induced pounding between structural elements made of different building materials." Earthquake engineering & structural dynamics **39**(3): 343-354.
- Jeng, V. and W. Tzeng (2000). "Assessment of seismic pounding hazard for Taipei City." Engineering Structures **22**(5): 459-471.
- Khawwaja, S., et al. (2011). Development of pounding model for adjacent structures in earthquakes. Proceeding of 9th Pacific Conference on Earthquake Engineering.
- Lin, Y.-Y. and E. Miranda (2010). "Estimation of maximum roof displacement demands in regular multistory buildings." Journal of engineering mechanics **136**(1): 1-11.
- Magenes, G. (2000). A method for pushover analysis in seismic assessment of masonry buildings. Proceedings of the 12th world conference on earthquake engineering, Citeseer.
- Mahmoud, S. and R. Jankowski (2011). "Modified linear viscoelastic model of earthquake-induced structural pounding."

Maison, B. F. and K. Kasai (1990). "Analysis for a type of structural pounding." Journal of Structural Engineering **116**(4): 957-977.

Maison, B. F. and K. Kasai (1992). "Dynamics of pounding when two buildings collide." Earthquake engineering & structural dynamics **21**(9): 771-786.

Miranda, E. (1999). "Approximate seismic lateral deformation demands in multistory buildings." Journal of Structural Engineering **125**(4): 417-425.

Moghadam, A. and W. Tso (2000). "3-D pushover analysis for damage assessment of buildings."

Moghadam, A. and W. Tso (2000). Pushover analysis for asymmetric and set-back multi-story buildings. Proceedings of the 12th world conference on earthquake engineering.

Muthukumar, S. and R. DesRoches (2006). "A Hertz contact model with non-linear damping for pounding simulation." Earthquake engineering & structural dynamics **35**(7): 811-828.

Nakamura, Y., et al. (2017). "Applicability of nonlinear static procedures for low-rise unreinforced masonry buildings with flexible diaphragms." Engineering Structures **137**: 1-18.

Pant, D. R., et al. (2010). "Seismic pounding between reinforced concrete buildings: A study using two recently proposed contact element models." Proceedings of the 14ECEE, Ohrid, Macedonia.

Paret, T. F., et al. (1996). Approximate inelastic procedures to identify failure mechanisms from higher mode effects. Proceedings of the eleventh world conference on earthquake engineering.

Polycarpou, P. C., et al. (2014). "An efficient methodology for simulating earthquake-induced 3D pounding of buildings." Earthquake engineering & structural dynamics **43**(7): 985-1003.

Requena, M. and G. Ayala (2000). Evaluation of a simplified method for the determination of the nonlinear seismic response of RC frames. Proceedings of the twelfth world conference on earthquake engineering, Citeseer.

Reyes, J. C. and A. K. Chopra (2011). "Evaluation of three-dimensional modal pushover analysis for unsymmetric-plan buildings subjected to two components of ground motion." Earthquake engineering & structural dynamics **40**(13): 1475-1494.

Reyes, J. C. and A. K. Chopra (2011). "Three-dimensional modal pushover analysis of buildings subjected to two components of ground motion, including its evaluation for tall buildings." Earthquake engineering & structural dynamics **40**(7): 789-806.

trasporti, M. d. i. e. d. (2018). Norme Tecniche per le Costruzioni.

Xu, X., et al. (2016). "A new formula of impact stiffness in linear viscoelastic model for pounding simulation." Shock and Vibration **2016**.

Yaghmaei-Sabegh, S., et al. (2017). "Evaluation of approximate methods for estimating maximum displacement response of MDOF systems." Soil Dynamics and Earthquake Engineering **101**: 125-136.

Yaghmaei-Sabegh, S., et al. (2014). "Nonlinear response estimates of RC frames using linear analysis of SDOF systems." Earthquake engineering & structural dynamics **43**(5): 769-790.

Ye, K., et al. (2009). "A modified Kelvin impact model for pounding simulation of base-isolated building with adjacent structures." Earthquake Engineering and Engineering Vibration **8**(3): 433-446.

Ye, K., et al. (2009). "A note on the Hertz contact model with nonlinear damping for pounding simulation." Earthquake engineering & structural dynamics **38**(9): 1135-1142.

Ringraziamenti

Desidero ringraziare il Prof. Gian Paolo Cimellaro, relatore di questa prova finale, per la sua disponibilità e per l'aiuto datomi durante la stesura dell'elaborato. Lo ringrazio, inoltre, per la sua passione trasmessa durante l'insegnamento. Ringrazio il Prof. Sebastiano Marasco per la sua gentilezza, il suo prezioso aiuto e per i consigli che mi ha dato durante l'intera stesura della tesi.

Un ringraziamento speciale alla mia famiglia. A mio padre, che è stato, è e sarà sempre il mio modello di riferimento. Ti ringrazio per i tuoi preziosi consigli e per tutti gli insegnamenti che mi hai sempre dato. A mia madre, che ringrazio per tutto l'amore che solo una madre sa dare. Ogni volta che ho bisogno di un aiuto ci sei e non smetterò mai di ringraziarti. A mia sorella, che anche se viviamo distanti e sono ormai poche le occasioni per vederci so che ci sarai sempre per me, come io ci sarò sempre per te. A voi che mi avete sempre sostenuto moralmente un semplice grazie non basta.

Ringrazio le mie nonne, per avermi viziato e coccolato e per tutto l'affetto che mi danno ogni volta che ritorno a casa.

A Irene, la Donna migliore che potessi mai incontrare, che mi rende felice e che sa tranquillizzarmi in qualsiasi momento. Mi hai reso un ragazzo forte e sicuro di se stesso, mi hai fatto sempre sentire amato e apprezzato per ciò che veramente sono e soprattutto mi fai sentire il ragazzo più fortunato al mondo ad avere te al mio fianco. Ti ringrazio per tutti i sacrifici che hai fatto per sostenermi e per aiutarmi, per avermi sempre incoraggiato e per essere stata sempre presente in qualsiasi situazione. Grazie. Ti amo.

Ringrazio tutti i miei amici di Torino che mi hanno fatto passare giornate di studio con il sorriso e per il sostegno che mi hanno sempre dato. Vorrei ringraziarvi uno ad uno per essere stati la mia seconda famiglia lontano da casa.

Vorrei ringraziare Gigi, compagno di notti di studio che da 6 anni a questa parte ha condiviso con me paure e successi. Sono sicuro che la nostra amicizia va oltre alla semplice esperienza universitaria e che continueremo a sostenerci a vicenda anche nei prossimi anni.

Ai miei amici di Sulmona e Campo di Giove che, nonostante la lontananza, mi fanno sentire come se non me ne fossi mai andato.

A Miriana, la coinquilina migliore che potessi avere, e a Mimmo, non un semplice coinquilino, ma un vero e proprio fratello. Vi ringrazio per tutte le sere passate a ridere e a confidarmi.

Un ringraziamento speciale va a me stesso, che ho avuto sempre la forza di andare avanti nonostante le difficoltà, che non mi sono mai arreso di fronte agli ostacoli e che ho saputo perseverare per raggiungere i miei obiettivi. Il mio più grande augurio è che la mia tenacia mi porti verso traguardi sempre più alti.